UNIVERSITY OF LINCOLN

# THE EFFECT OF STELLAR FLYBYS ON THE PERTURBATION OF EARTH'S ORBIT.

THOMAS HOBSON

MSC APPLIED MATHEMATICS (BY RESEARCH)

SCHOOL OF MATHEMATICS AND PHYSICS

AUGUST 2020

# THE EFFECT OF STELLAR FLYBYS ON THE PERTURBATION OF EARTH'S ORBIT

Thomas Hobson

A thesis submitted in partial fulfilment of the requirements of the University of Lincoln for the degree of MSc by Research in Applied Mathematics

School of Mathematics and Physics

*Supervisor:*
Dr Phil Sutton

August 2020

# DECLARATION OF AUTHORSHIP

I, Thomas Hobson, declare that this thesis entitled, ‘The Effect of Stellar Flybys on the Perturbations of Earth’s Orbit’ and the work presented in it are my own. I confirm that:

- This work was done wholly or mainly while in candidature for a research degree at the University of Lincoln.
- This work and associated simulations have not been submitted for any other degree at the University of Lincoln or any other institution.
- Where I consulted the published work of others, this is always clearly attributed.
- Where I have quoted work of others, the source is always given. With the exception of such quotations, this thesis is entirely my own work.
- I have acknowledged all main sources of help.

Signed: J. Hobson

Date: 22/08/2020

# ABSTRACT

The effect of stellar flybys on planetary bodies within our solar system is relatively unknown. Research suggests that changes in Earth's orbit can affect the climatic evolution on our planet. These cycles, dubbed the Milankovitch cycles, have been cited as playing a role in the extinction events in Earth's history. There is the potential that long term consecutive stellar flybys could alter the Milankovitch cycles. This may be a contributing factor in the extinction events that are associated with the crossing of the spiral arms. This study presents the effects of 34 flyby scenarios on the Earth's eccentricity and inclination evolution. A number of REBOUND simulations were run over a $15$ Myr period, passing stars of various masses at a variety of encounter distances, locations, and inclinations. The numerical models show that although many cases have little impact on the evolution of Earth's eccentricity and inclination cycles, that coplanar flybys at distances $< 50000$ AU can change these cycles significantly. The results suggest that consecutive close encounters of stars to our solar system can perturb Earth's orbit. Therefore, it is plausible that stellar flybys may influence the Milankovitch cycles and play a role in mass extinction events on Earth.

# ACKNOWLEDGEMENTS

Studying a MSc by Research has been a rollercoaster of emotions, especially studying part-time whilst working. There are so many people who have played a role in getting me to this point and I'd like to thank at least some of them here.

Firstly, thank you to my family and friends for being supportive, and listening to me moan and stress about things which at times didn't make sense to me, let alone to you! Maths isn't everyone's cup of tea so I can only imagine what it was like to have me wittering about stuff was like, so thank you…and sorry.

Next, I'd like to thank Fiona Bissett. Having someone to talk to who has been through the same thing was really helpful. Thank you for answering my questions, helping me figure out what questions I had and who to ask, and mostly for reassuring me that how I was feeling at times was normal and that I would get through it.

Dr Sergey Chulkov, without you I really don't think I would have completed this project. Thank you for your patience and help with sorting out my ICT problems and misunderstandings. And especially given that this support all had to be given remotely because of COVID-19 you were fantastically clear and supportive. I really am indebted to you.

I'd also like to thank Max Bodmer for your support, encouragement and, at times, brutal honesty that kicked me into gear instead of burying my head in the sand. I really needed that so thank you. And thank you for reading through my draft thesis, that must have been painful for you. A thesis filled with mathematics… your favourite!

And finally, Phil. Where do I begin. Thank you for being there whenever I needed you, and for all the suggestions, ideas and direction along the way. You have taught me SO much, both conceptually and in how to research. The opportunity to research in an area that bridges so many fields has been incredible. I really appreciate everything, thank you.

# CONTENTS

# LIST OF FIGURES

# LIST OF TABLES

# CHAPTER 1

# INTRODUCTION

## 1.1 Background

Although it may appear that the orbit of our planet is both stable and static, changes in Earth's orbit have been recognised since as early as 130 BC (Hipparchus, 130 BC). In the 1900's it was suggested that Earth's orbit undergoes cyclic changes on timescales of tens of thousands, to hundreds of thousands of years (Hays et al., 1976). Geological data suggests that these changes are significant enough to alter the Earth's climate, forcing climate cycles on timescales analogous to the orbital periods (Hays et al., 1976). Links between these climatic changes and mass extinction events have been discovered (Bennett, 1990; van Dam, 2006), and demonstrate the significant impact orbital variation has on the planet's biosphere.

Analysis of numerical models suggests that these orbital variation cycles are the result of the perturbative effects of other bodies within our solar system (Kent et al., 2018). Although stellar flybys have been shown to have an effect on the Oort cloud (Mamajek et al., 2015), it is argued that these passes would have little impact on larger bodies such as planets and moons (Berski and Dybczynski, 2016). The frequency of these encounters is approximately 50,000 years (Bailer-Jones et al., 2018), and therefore a potential build-up of small perturbations into more significant changes may be possible (Bailey and Fabrycky, 2019). The effect of multiple stellar encounters on other celestial systems has shown to interrupt Oort planet generation (Bailey and Fabrycky, 2019), however these are significantly closer than the encounter distances suggested from the analysis of data sent back from the Gaia space observatory; the *Gaia* DR2 data (Bailer-Jones et al., 2018). The factors that drive orbital evolutions are explored and used to present a study into the effects that stellar flybys have on Earth's orbit.

## 1.2 Orbital Mechanics

When considering the orbits of celestial bodies, it is conventional to consider the bodies in a Kepler orbit (Curtis, 2020). A Kepler orbit is an idealised orbital motion between two bodies, where perturbing factors such as the gravitational pull of other bodies, solar radiation and atmospheric drag are not factors (Curtis, 2020). It is often assumed that the mass of the first body (the primary) is substantially larger than that of the second, and therefore the second body will orbit around a barycentre (the centre of mass in the system) contained within the first body (Curtis, 2020). However, in some cases, the second body is not bounded to the body it is orbiting. This means that although the second body's path is affected by the gravitational pull of the primary, the pull is not strong enough to keep the body around the primary. The second body will therefore escape the gravitational pull. The diagrams below show an example of a bounded Keplerian system (figure 1) and an unbounded Keplerian system (figure 2):

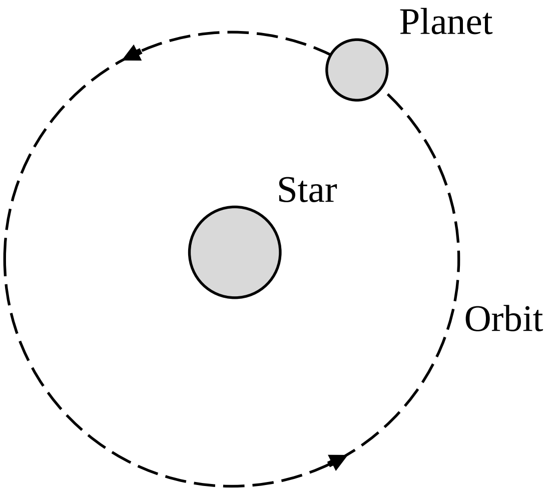


*Figure 1: A diagram of a simple bounded Keplerian system between a planet and a star.*

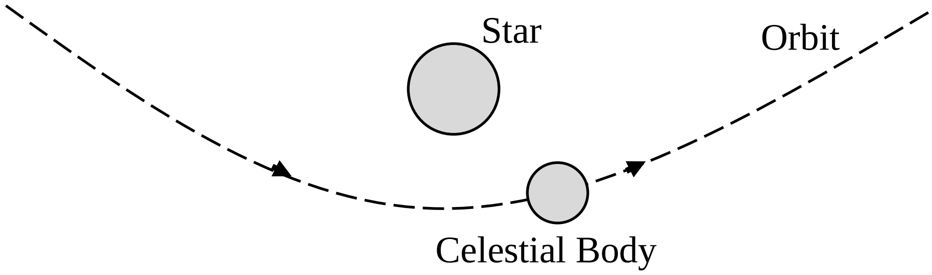


*Figure 2: A diagram of a simple unbounded Keplerian system between a celestial body and a star.*

For such scenarios where the second body's mass is significantly smaller than the primaries, a Newtonian approach is appropriate. However, in cases where the masses are sufficiently large enough, for example a binary system, additional corrections must be implemented (Curtis, 2020).

Newtonian mechanics suggests that the motion of the second body relative to that of the first can be expressed by the '*two body equation of relative motion*' (Curtis, 2020):

$$\ddot{\boldsymbol{r}} = -\mu\frac{\boldsymbol{r}}{r^3} \qquad \textit{Equation 1}$$

where $\ddot{\boldsymbol{r}}$ is the relative acceleration vector, $\boldsymbol{r}$ is the relative position vector, $r$ is the distance between the bodies and $\mu$ is the reduced mass of the system such that:

$$\mu = \frac{m_1 m_2}{m_1 + m_2} \qquad \textit{Equation 2}$$

where $m_1$ is the mass of the first body and $m_2$ is the mass of the second.

In reality, the orbital path of a bounded smaller body is not circular (as depicted in figure 1), instead it follows an ellipse. The amount that the planet's orbit differs from a circle is known as the eccentricity of the orbit (Curtis, 2020).

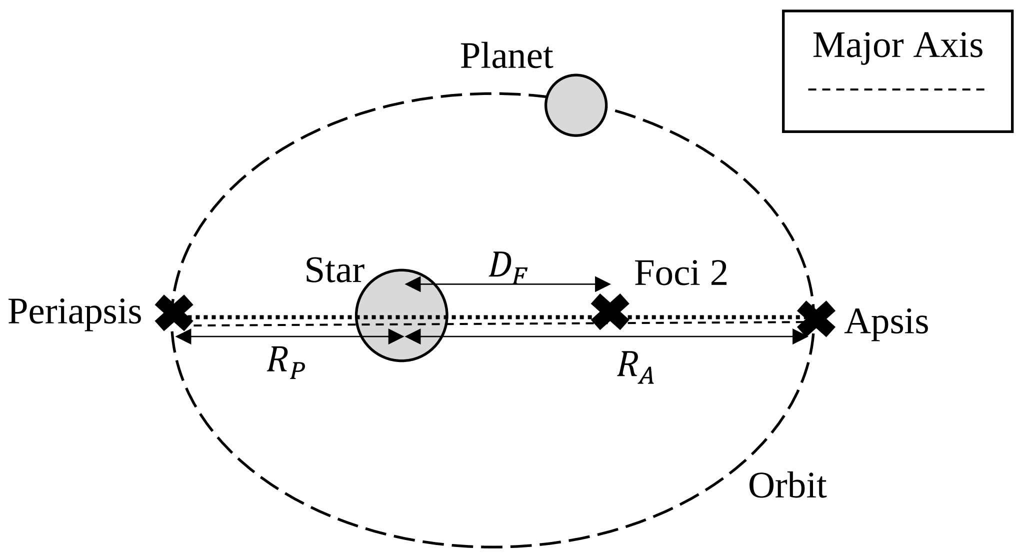


*Figure 3: A diagram of an elliptical bounded Keplerian orbit between a planet and a star.*

Kepler's laws of planetary motion state that:

1. The primary is located at one of the foci of the ellipse (see figure 3) (Kepler, 1609; Curtis, 2020).
2. The area covered by a line segment between the Sun and a planet is equal for equal time intervals (Kepler, 1609; Curtis, 2020).
3. The ratio of the orbital period of a planet squared, to the length of the semi-major axis (half of the major axis) cubed is equal for all planets in the system (Kepler, 1618; Curtis, 2020).

In 1687, Newton determined that Kepler's laws could be derived from his own Laws of Motion (Newton, 1687). They are still used frequently in many celestial modelling scenarios, such as determining satellite orbits (Hyde and Bargellini, 2002).

The point on the orbit that is farthest away from the primary is known as the apsis, with the closest point being the periapsis (Curtis, 2020). The distance from the primary to the apsis is denoted as $R_A$, and the distance to the periapsis as $R_P$, with the line that connects these two points being named the major axis (Curtis, 2020). Conventionally, the length of the semi-major axis, $a$, is given (Curtis, 2020). As the major axis is the distance between the apsis and the periapsis, it can be derived that:

$$2a = R_P + R_A$$

*Equation 3*

By comparing how much of the major axis is the distance between the foci of the ellipse, $D_F$, it can be determined how much the orbit tends away from a circle (Curtis, 2020). Therefore, it follows that the eccentricity, $e$, is given by:

$$e = \frac{D_F}{2a}$$

*Equation 4*

The distance from either focus to the nearest point on the orbit must be equal, as a result of the ellipse's symmetry (Curtis, 2020). Therefore, given that the distance from the primary (located at one focus) to the periapsis is $R_P$, it follows that:

$$D_F = 2a - 2R_P$$

*Equation 5*

Substituting in Equation 3:

$$D_F = R_A - R_P$$

*Equation 6*

Substituting Equation 3 and Equation 6 into Equation 4:

$$e = \frac{R_A - R_P}{R_P + R_A} \qquad \textit{Equation 7}$$

Considering the least elliptical orbit (i.e. a circular orbit) a minimum value for $e$ can be calculated. In a circle there is only one focus, therefore, there is no distance between foci:

$$D_F = 0 \qquad \textit{Equation 8}$$

Substituting this into Equation 4:

$$e = \frac{0}{2a} \qquad \textit{Equation 9}$$

$$e = 0 \qquad \textit{Equation 10}$$

Thus, the minimum value of eccentricity is 0. As the circle is extended into an ellipse the foci would begin to separate. This would continue until the foci are on the ellipse itself, turning the ellipse into a straight line (see figure 3).

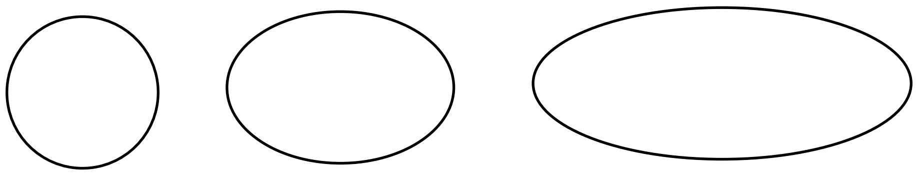

*Figure 4: A diagram showing the effect of increasing the value of* e.

In this straight line, the distance between the foci is the same as the major axis, therefore for an ellipse, the distance between the foci must remain below the length of the major axis, thus:

$$D_F < 2a \qquad \textit{Equation 11}$$

Substituting this into Equation 4:

$$e < \frac{2a}{2a} \qquad \text{where } a > 0$$

$$e < 1 \qquad \textit{Equation 12}$$

Therefore, for an elliptical orbit, $0 \leq e < 1$, the closer the eccentricity value is to 0, the more circular the orbit, the closer to 1, the more elliptical the orbit (Curtis, 2020).

When $e = 1$, the orbit becomes unbounded, following a parabolic flight path (Canuto, 2018; Curtis, 2020). Beyond this where $e > 1$ the orbit remains unbounded; however it follows a hyperbolic trajectory. In both of these cases, the length of the semi-major axis can no longer be calculated in the same way. The value of the apsis tends towards infinity because it is unbounded to the primary, and only the periapsis value is obtainable. The value for the semi-major axis becomes the distance from the periapsis, to the point at which the asymptotes of legs of the curve meet. This value does exist in a hyperbolic orbit, however in a parabolic orbit, this does not exist as the legs of the curve tend towards parallelism.

A body's orbit can be defined by either Cartesian co-ordinates, such as position and velocity, or by orbital elements. These elements form a map of the body's current position, as well as the path the body has/will travel in a Kepler orbit (Curtis, 2020). Two of these are mentioned previously; the semi-major axis, and the eccentricity. Below is a diagram of the remaining four orbital elements (N.B. '*' are included for explanative purposes and are not orbital elements).

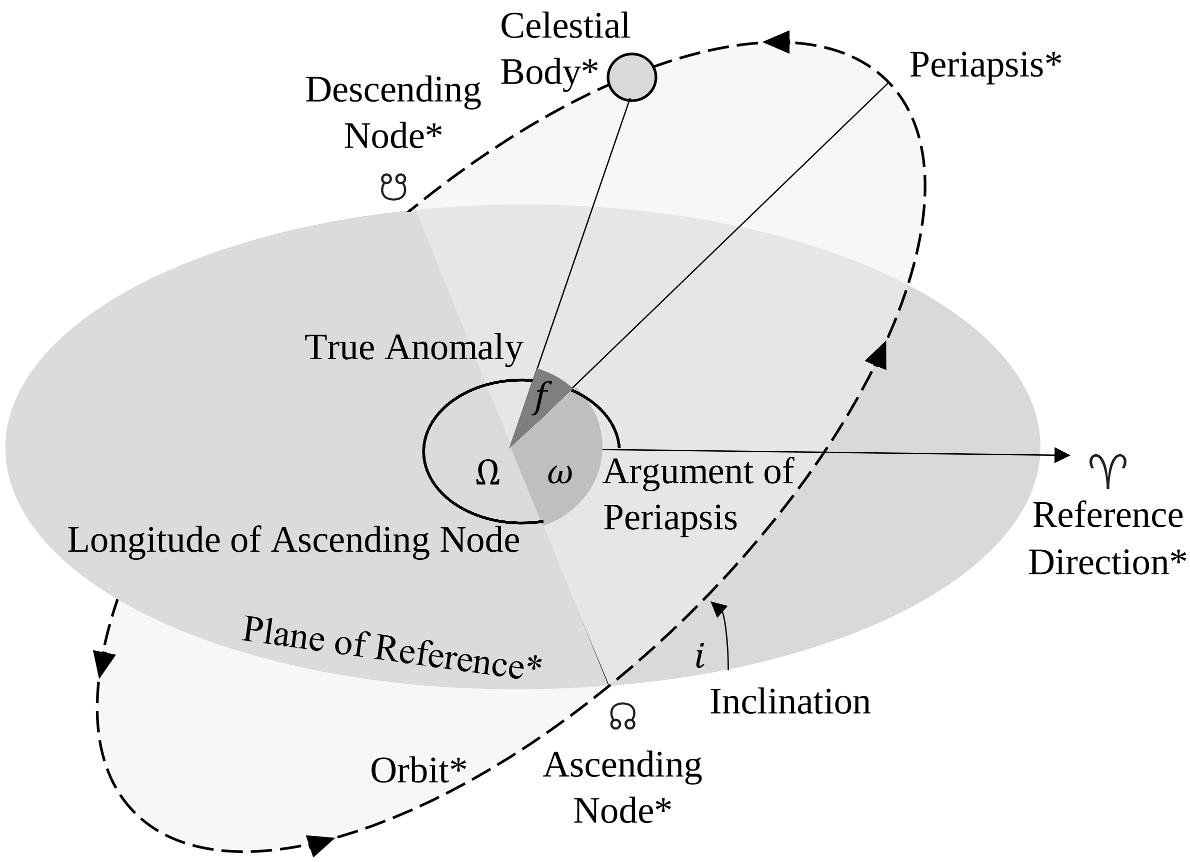


*Figure 5: A diagram showing orbital elements in relation to the path of a celestial body* (Curtis, 2020)

The four elements above are all angular elements and therefore require a reference plane and reference direction, ♈ (Curtis, 2020). The plane and direction can be chosen arbitrarily, however must remain the same for all elements and bodies in the system (Curtis, 2020). When considering the solar system, it is conventional to consider the reference plane as the plane of the Sun-Earth Keplerian orbit. Once a reference plane is established the remaining four elements are defined in the following way:

**Inclination** ($\boldsymbol{i}$)– the angle made between the reference plane and the ascending node, ☊. The ascending node is the point at which the reference plane and body's orbit intersect, with the body moving from this point above (to the north of) the reference plane (Curtis, 2020).

**Argument of Periapsis** ($\boldsymbol{\omega}$) – the angle made between the periapsis and the ascending node. It is measured in the direction the body is moving and is the orientation of the ellipse relative to the reference frame (Curtis, 2020).

**True anomaly** ($\boldsymbol{f}$) – the angle made between the periapsis and current position of the body, measured counter-clockwise and is the position of the body on its orbital path (Curtis, 2020).

**Longitude of the Ascending Node** ($\boldsymbol{\Omega}$) – the angle made between the reference direction and the ascending node (Curtis, 2020).

## 1.3 Perturbation Theory

Perturbation theory suggests that the orbital path of a body can be distorted from the expected path as the result of a variety of causes (Gurfil, 2006; Curtis, 2020). These causes may include the gravitational influences of bodies in the system other than those included in the bodies Kepler orbit, the release of material and gases during the flight path causing drag, and the oblateness (how flattened the planets spheroid shape is) of the body (Gurfil, 2006). The perturbation of an orbit can be thought of as adding a perturbation term, $\boldsymbol{p}$, to the equation of relative motion (Curtis, 2020):

$$\ddot{\boldsymbol{r}} = -\mu \frac{\boldsymbol{r}}{r^3} + \boldsymbol{p}$$

*Equation 13*

where $\boldsymbol{p}$ is the vector formed from the effect of all perturbations on the system.

# 1.4 The $N$-Body Problem

In the classical two-body problem discussed by Kepler and Newton (Kepler, 1609; Newton, 1687) an analytical solution can be derived by splitting the system into a pair of one-body problems (Curtis, 2020). This assumes that no other forces act on the bodies, and that the bodies orbit a shared centre of mass; the barycentre (Curtis, 2020). However, when more bodies and/or forces are added the system becomes chaotic, and an analytical solution becomes unachievable in most cases (Curtis, 2020). The restricted three-body problem, a system where one body has negligible mass compared to the other two bodies, does have an analytical solution, but no general solution for a three-body system has been developed (Curtis, 2020). To solve $N$-body systems, numerical approaches are adopted, finding approximations to the movements within the system (Curtis, 2020).

## 1.4.1 Numerical Integration

Numerical integration applies algorithmic processes to provide numerical solutions to ordinary differential equations (ODEs) of the form (Iyengar and Jain, 2009):

$$y'(t) = f\big(t, y(t)\big) \qquad \textit{Equation 14}$$

given a set of initial values:

$$y(t_0) = y_0 \qquad \textit{Equation 15}$$

The term 'numerical integrator' refers to a family of algorithms including the Newton-Raphson Method, the Euler Method and Runge-Kutta Methods (Iyengar and Jain, 2009). These numerical integrators have an 'order' which is the measure of how well the approximation made by the integrator matches the actual solutions (Iyengar and Jain, 2009). Numerical integrators are often used in solving $N$-body simulations, as the equation for the acceleration of any body in the system as derived from Newton's second law (Newton, 1687) is a second order differential equation.

## 1.4.2 Newtonian Mechanics

Newton's second law (Newton, 1687) states that:

$$\boldsymbol{F} = m\boldsymbol{a} \qquad \textit{Equation 16}$$

where $\boldsymbol{F}$ is the force acting on the body, $m$ is the mass of the body and $\boldsymbol{a}$ is the acceleration of the body.

Newton's law of gravity (Newton, 1687), states that the gravitational force exerted by one body, $j$, on another, $i$, is given by the equation:

$$\boldsymbol{F}_{ij} = \frac{Gm_i m_j(\boldsymbol{q}_j - \boldsymbol{q}_i)}{\|\boldsymbol{q}_j - \boldsymbol{q}_i\|^3} \qquad \textit{Equation 17}$$

where $\boldsymbol{F}_{ij}$ is the force acting on the body $i$, $G$ is the gravitational constant, $m_i$ is the mass of body $i$, $m_j$ is the mass of body $j$, $\boldsymbol{q}_i$ is the position of body $i$ and $\boldsymbol{q}_j$ is the position of body $j$.

From these equations it can be derived that:

$$m_i\boldsymbol{a}_i = \frac{Gm_i m_j(\boldsymbol{q}_j - \boldsymbol{q}_i)}{\|\boldsymbol{q}_j - \boldsymbol{q}_i\|^3} \qquad \textit{Equation 18}$$

As $\boldsymbol{a}_i = \frac{d^2\boldsymbol{q}_i}{dt^2}$:

$$m_i\ddot{\boldsymbol{q}}_i = \frac{Gm_i m_j(\boldsymbol{q}_j - \boldsymbol{q}_i)}{\|\boldsymbol{q}_j - \boldsymbol{q}_i\|^3} \qquad \textit{Equation 19}$$

Dividing through by $m_i$:

$$\ddot{\boldsymbol{q}}_i = \frac{Gm_j(\boldsymbol{q}_j - \boldsymbol{q}_i)}{\|\boldsymbol{q}_j - \boldsymbol{q}_i\|^3} \qquad \textit{Equation 20}$$

This equation describes the acceleration of a body, based on the gravity exerted by another. Given that there are $N$-bodies exerting a gravitational force on the body, we derive that:

$$\ddot{\boldsymbol{q}}_i = \sum_{\substack{j=1 \\ j\neq i}}^{\boldsymbol{N}} \frac{Gm_j(\boldsymbol{q}_j - \boldsymbol{q}_i)}{\|\boldsymbol{q}_j - \boldsymbol{q}_i\|^3} \qquad \textit{Equation 21}$$

This equation describes the motion of a body in an $N$-body system. Solving the above equation with respect to all $N$-bodies in the system will describe the evolution of the system under the influence of gravity.

### 1.4.3 Hamiltonian Mechanics

Hamiltonian mechanics is a rederivation of Lagrangian mechanics, which itself comes from, and is equivalent to, Newtons laws of motion (Hamilton, 1833; Calkin, 1996 ). The Hamiltonian equations of motion for an $N$-body system are:

$$\frac{d\boldsymbol{p}_i}{dt} = -\frac{\partial \mathcal{H}}{\partial \boldsymbol{q}_i}$$ *Equation 22*

$$\frac{d\boldsymbol{q}_i}{dt} = \frac{\partial \mathcal{H}}{\partial \boldsymbol{p}_i}$$ *Equation 23*

where $\boldsymbol{p}_i$ is the momentum of body $i$, $\boldsymbol{q}_i$ is the position of body $i$ and $\mathcal{H}$ is the Hamiltonian.

The Hamiltonian can be written as a sum of the kinetic and potential energies of the system (Hamilton, 1833; Calkin, 1996 ). For a $N$-body system, the Hamiltonian is:

$$\mathcal{H} = \sum_{i=0}^{N-1} \frac{\boldsymbol{p}_i^2}{2m_i} - \sum_{i=0}^{N-1} \sum_{j=i+1}^{\boldsymbol{N-1}} \frac{Gm_i m_j}{\|\boldsymbol{q}_j - \boldsymbol{q}_i\|}$$ *Equation 24*

where $\sum_{i=0}^{N-1} \frac{\boldsymbol{p}_i^2}{2m_i}$ is the kinetic energy and -$\sum_{i=0}^{N-1} \sum_{j=i+1}^{\boldsymbol{N-1}} \frac{Gm_i m_j}{\|\boldsymbol{q}_j - \boldsymbol{q}_i\|}$ is the potential energy (Rein and Tamayo, 2015).

Hamiltonian systems are used in a class of numerical integrators known as 'symplectic integrators' (Wisdom and Holman, 1991; Rein and Tamayo, 2015). These integrators often conserve quantities better than non-symplectic integrators by taking advantage of the symmetries within the Hamiltonian system (Yoshida, 1990; Wisdom and Holman, 1991; Rein and Tamayo, 2015). The efficiency and time reversibility of some symplectic integrators make them frequently used in celestial mechanics (Yoshida, 1990; Wisdom and Holman, 1991; Rein and Spiegel 2014; Rein and Tamayo, 2015).

## 1.5 Orbital Resonances

Orbital resonances are sustained gravitational influences between two or more bodies (Häusler, 1999). The two types of resonances discussed here are mean-motion resonance (Mustill and Wyatt, 2010) and secular resonance (Bordovitsyna et al., 2014), both of which can have substantial effects on orbital evolution (Franklin and Soper, 2003).

### 1.5.1 Mean-Motion Resonance

Mean-motion resonances (MMR) occur when the orbital periods of two or more bodies are related by small integer ratios (Fisher and Erickson, 2010; Mustill and Wyatt, 2010). The figure below illustrates a $1{:}\,2$ resonant scenario between planets A and B:

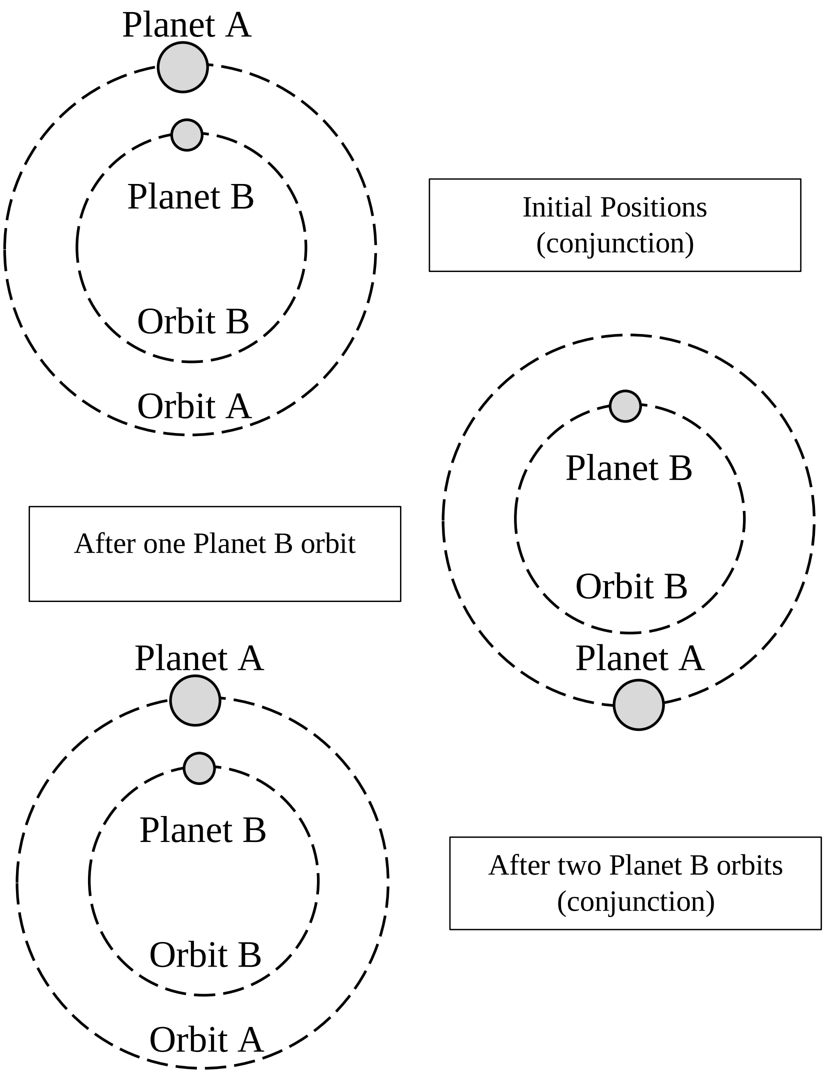


*Figure 6: Illustration of a* $1{:}\,2$ *resonance between planets A and B.*

Examples of these resonances include the 1: 2: 4 resonance between the moons of Jupiter; Ganymede, Europa and Io (Lari et al., 2020). Additionally, *near* MMR exist, such as the Saturn-Jupiter 5: 2 *near* MMR, where the orbital periods are close to being in resonance, but over time the positions of the planets drift when conjunction is expected (Michtchenko and Ferraz-Mello, 2001; Dvorak and Lhotka, 2013). Resonances between bodies causes orbital instability (Varadi, 1999), as the bodies move in and out of resonance, perturbing the orbital paths (Franklin and Soper, 2003).

## 1.5.2 Secular Resonance

Secular resonance between two bodies occurs when the apsidal precession of the argument of the periapsis, or the longitude of the ascending node, synchronise (Pälike, 2005). Below is an illustration of two bodies in a secular resonance of the periapsis:

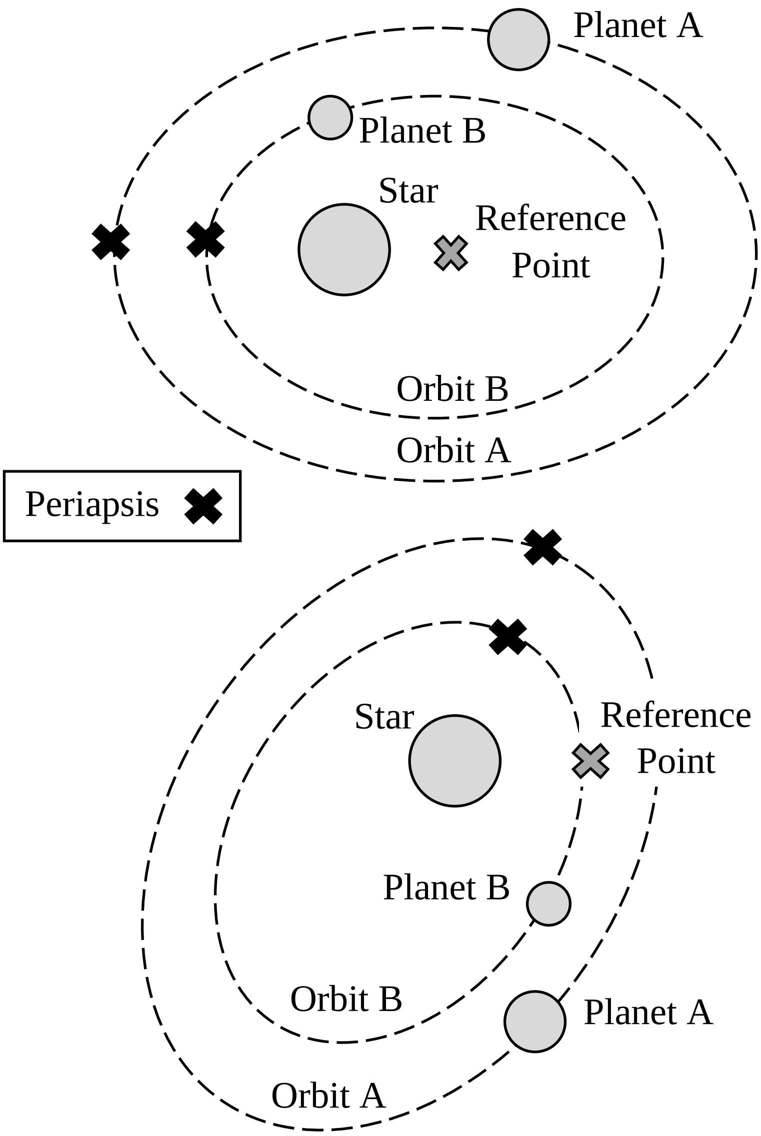


*Figure 7: Illustration of secular resonance between planets A and B*

This type of resonance occurs when the fundamental frequency of two bodies synchronise (Pälike, 2005). The table below shows the fundamental frequencies for the planets in the solar system. These frequencies are often calculated using a Modified Fourier Transform (MFT), first described by Laskar (1990) and have been used subsequently by others such as Šidlichovskỳ and Nesornỳ (1996).

| | Fundamental Frequencies for Argument of the Periapsis | | | Fundamental Frequencies for Longitude of the Ascending Node | | |
|---|---|---|---|---|---|---|
| Planet | Term | Frequency / "$yr^{-1}$ | Period / kyr | Term | Frequency / "$yr^{-1}$ | Period / kyr |
| Mercury | $g_1$ | 5.596 | 231.0 | $s_1$ | −5.618 | 230.0 |
| Venus | $g_2$ | 7.456 | 174.0 | $s_2$ | −7.080 | 183.0 |
| Earth | $g_3$ | 17.365 | 74.6 | $s_3$ | −18.851 | 68.7 |
| Mars | $g_4$ | 17.916 | 72.3 | $s_4$ | −17.748 | 73.0 |
| Jupiter | $g_5$ | 4.249 | 305.0 | $s_5$ | 0.000 | |
| Saturn | $g_6$ | 28.221 | 45.9 | $s_6$ | −26.330 | 49.2 |
| Uranus | $g_7$ | 3.089 | 419.0 | $s_7$ | −3.005 | 431.0 |
| Neptune | $g_8$ | 0.667 | 1940.0 | $s_8$ | −0.692 | 1870.0 |

*Table 1: A table showing the fundamental frequencies for ω and Ω* (Pälike, 2005).

Secular resonances can be either linear or non-linear. Linear resonances occur between the frequency of a body and one other perturbing body (such as an asteroid being perturbed by a planet) (Froeschle and Morbidelli, 1993). Non-linear resonances involve multiple linear resonances, such as the $z_k = k(g - g_6) + (s - s_6)$, and involve both frequencies from the precession of the periapsis, and of the ascending node (Carruba et al., 2005). These are more complex resonances, and involve any number of bodies (Carruba et al., 2005).

# 1.6 Milankovitch Cycles

Cyclic changes in Earth's orbital movements have been well established since the 1920's (Roe, 2006; Hays et al., 1976). Variations in Earths eccentricity, axial tilt (obliquity) and precession, collectively known as Milankovitch cycles, have been evidenced by the analysis of Benthic $\delta^{18}O$ levels in the stratigraphic record (Kingston et al., 2007; Matthews and Frohlich, 2002; Kent et al., 2018; Gale et al., 2002), and are now supported by numerical investigations (Laskar et al., 2010). The theory of the Milankovitch cycles is a cornerstone in the fields of climatology and Earth evolution and is now being extended to develop our understanding of other celestial bodies and systems (Schorghofer, 2008; Forgan, 2016).

### 1.6.1 A History

Joseph Adhémar proposed that periods of glaciation were the result of cyclic changes in the position of Earth's orbit (Adhémar, 1842). He suggested that ice sheets formed when the poles experience periods of prolonged cooling, such as during extended winters or at the apsis, and that the Antarctic ice sheet is the result of the southern hemisphere experiencing longer winters than the northern hemisphere. This work was then extended by Scottish scientist James Croll, who suggested that although Adhémar's theories were plausible, that his reasoning was incorrect (Croll, 1864). Croll argued that a reduction in the intensity of insolation at the aphelion resulted in increased snowfall, and that the albedo (the amount of light that is reflected by a surface) of snow would result in a positive feedback loop, cooling the poles (Croll, 1864; Sugden, 2013). Both Adhémar and Croll suggested that these cyclic patterns of cooling would occur every 22,000 years, in alignment with axial precession discovered by Hipparchus in 130 BC (Hipparchus, 130 BC; Sugden, 2013).

Milanković countered Croll's earlier claims and suggested that as summer in the northern hemispheres occurs at the aphelion, that the formation of the polar ice sheets occurs because of axial tilt (Roe, 2006; Macdougall 2011). He suggested that less insolation occurs in the the summer because of Earth's tilt relative to the orbital plane which prevents the complete melting of the previous winters snow, as opposed to the promoted snowfall that Croll theorised. Over a number of years, this build-up of snow forms the ice sheets we observe today (Roe, 2006; Macdougall 2011).

Using sediment from Southern Hemisphere ocean floor to measure oxygen isotope levels, Hays et al. produced a record of the Earths global ice volume and climate for the previous ~450,000 years (Hays et al., 1976; Roe, 2006). Spectral analysis on this data showed peaks at 42,000 years, 23,000 years and 100,000 years. These findings supported the predictions for axial tilt, precession and eccentricity respectively (Hays et al., 1976; Roe, 2006; Macdougall, 2011).

## 1.6.2 Eccentricity

As planets orbit around their star, their orbital path changes between more circular and more elliptical (Pälike, 2005).

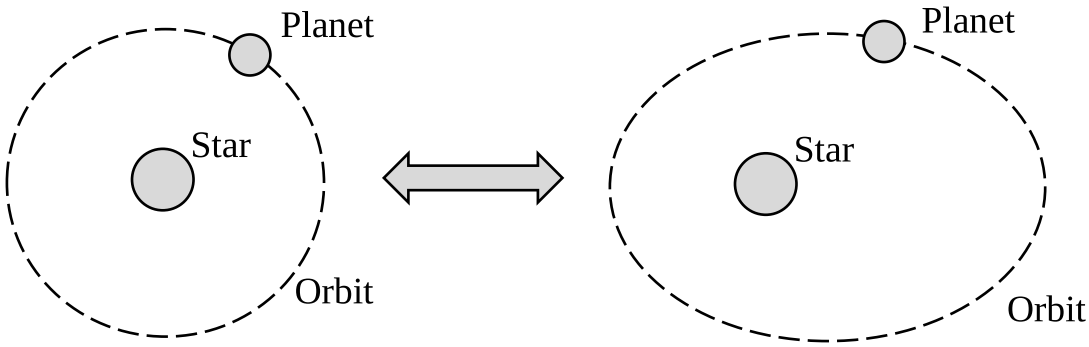


*Figure 8: Exaggerated illustration of eccentricity evolution.*

Earth's orbit currently has an eccentricity value of around 0.016 (Pälike, 2005), meaning that the orbit is almost circular. Eccentric variation occurs on a ~100,000 and ~400,000-year cycle (Berger and Loutre, 1991; Matthews and Frohlich, 2002; Kent et al., 2018), and fluctuates between 0 and 0.06 (Pälike, 2005). Combinations of the fundamental frequencies of the planets in the solar system give rise to quasiperiodic terms (see Table below):

| Term N.o. | Term | Frequency / "year$^{-1}$ | Period /kyr | Amplitude |
|---|---|---|---|---|
| 1 | $g_2 - g_5$ | 3.1996 | 406.182 | 0.0109 |
| 2 | $g_4 - g_5$ | 13.6665 | 94.830 | 0.0092 |
| 3 | $g_4 - g_2$ | 10.4615 | 123.882 | 0.0071 |
| 4 | $g_3 - g_5$ | 13.1430 | 98.607 | 0.0059 |
| 5 | $g_3 - g_2$ | 9.9677 | 130.019 | 0.0053 |

*Table 2: Quasiperiodic terms for Earth's eccentricity* (Pälike, 2005; Laskar, 1999).

The $g_2 - g_5$ term correlates with the 400,000-year cycle in Earth's eccentricity and suggests that this cycle is a result of the interactions with Venus and Jupiter (Pälike, 2005; Kent et al., 2018), with modulation depicted graphically in figure 10(a). The remaining terms make up the 100,000-year cycle (Matthews and Frohlich, 2002), and are supported by the spectral peaks at ~95,000 years, and ~125,000 years (see figure 9) (Muller and MacDonald, 1997; Pälike, 2005 ). Combinations of these quasiperiodic terms form 'beats' that modulate the amplitude of the ~400,00-year cycle, subtraction of terms 2 and 3 (figure 10(b)), and 4 and 5, (figure 10(c)) are examples of this (Pälike, 2005).

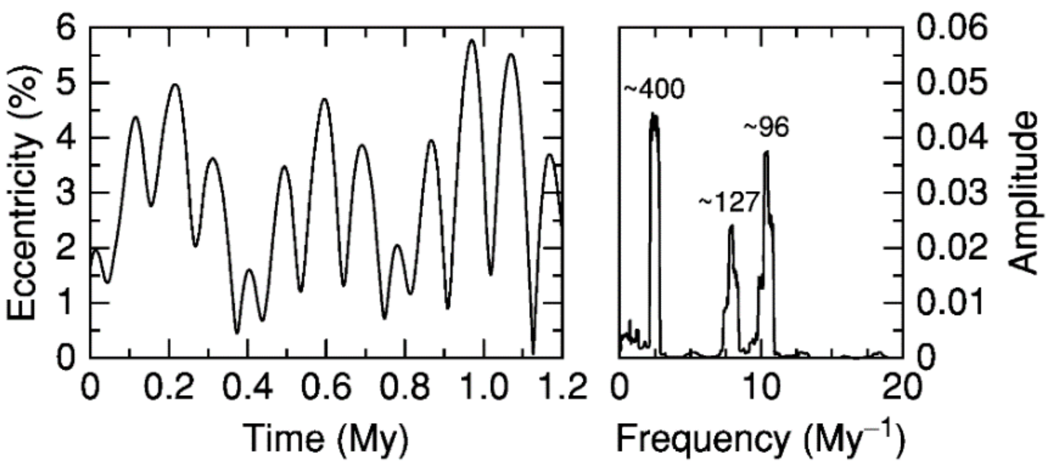


*Figure 9: Left: Plot of Earth's eccentricity over a 1.2-million-year period. Right: spectral plot of eccentricity data showing peaks at ~400 kyr, ~127 kyr and ~96 kyr* (Pälike, 2005).

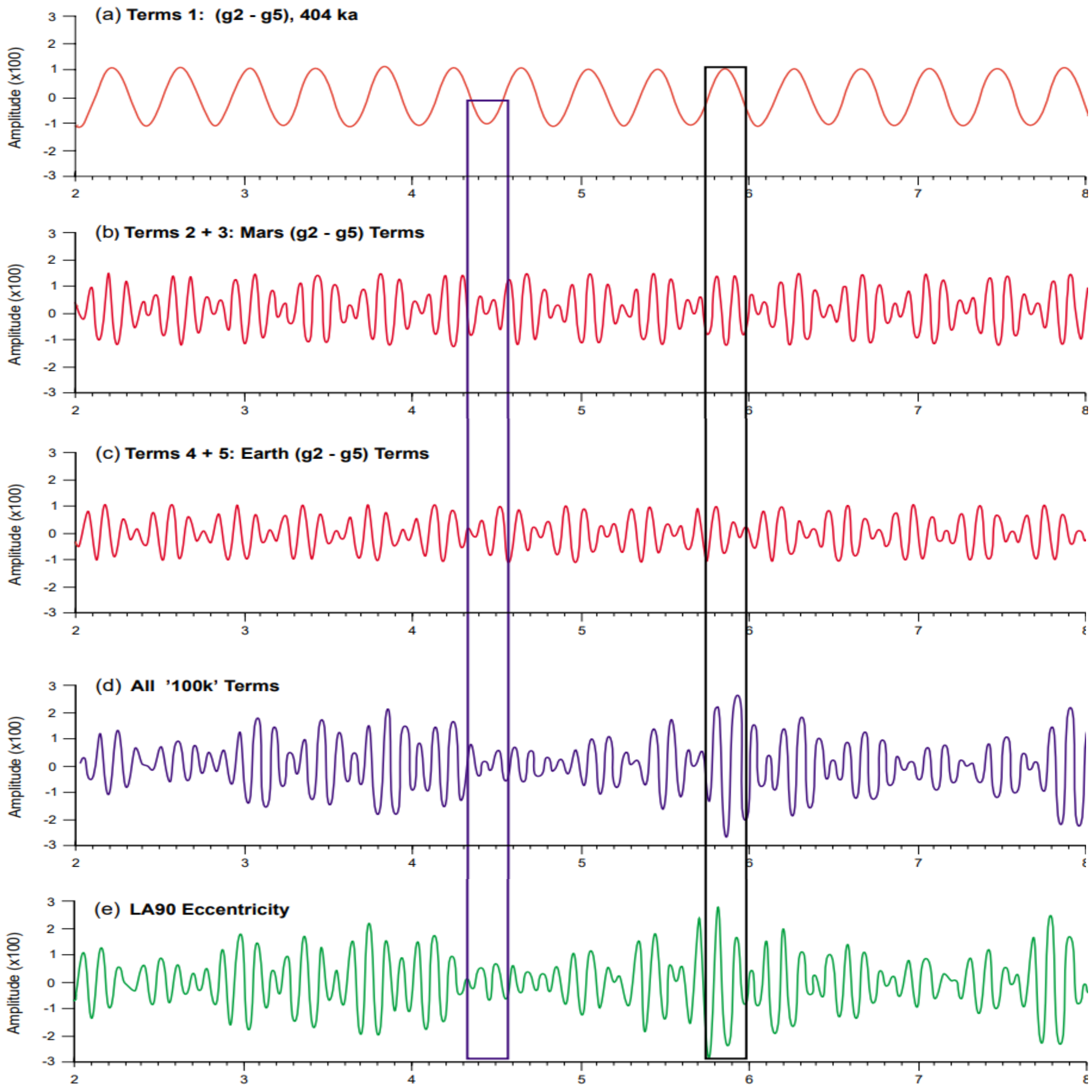


*Figure 10: (a) Plot of term 1 in Table 2, (b) Plot of term 2 - term 3, (c) Plot of term 4 - term 5, (d) Plot of all terms relating to 100 kyr cycle, (e) Plot of Earth eccentricity as modelled by La90 (Laskar, 1990; Matthews and Frohlich, 2002).*

## 1.6.3 Axial Tilt

The angle that a planet's rotational axis makes with the normal of the orbital plane is known as obliquity, or axial tilt.

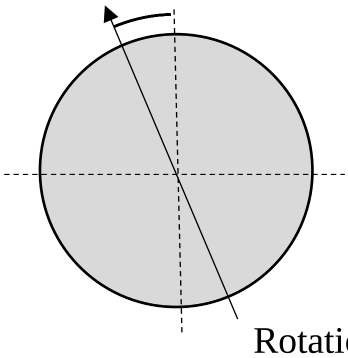


*Figure 11: Illustration of Earth's axial tilt (obliquity).*

Earth's axial tilt varies on a ~41,000-year cycle between 22.25° and 24.5°. Earth's current axial tilt is approximately 23.45° and is currently decreasing (Pälike, 2005). The frequencies of axial tilt vary in relation to both the fundamental frequencies of the argument of the periapsis and longitude of the ascending node, as well as with the precessional constant $p$ (Pälike, 2005). The precessional constant varies over time and can be altered by tidal dissipation (Pälike, 2005) and Earth oblateness (Mitrovica and Forte; 1995). The table below shows the six highest amplitude axial tilt frequencies:

| Term N.o. | Term | Frequency / "$\text{year}^{-1}$ | Period /kyr | Amplitude |
|---|---|---|---|---|
| 1 | $p + s_3$ | 31.613 | 40.996 | 0.0112 |
| 2 | $p + s_4$ | 32.680 | 39.657 | 0.0044 |
| 3 | $p + s_3 + g_4 - g_3$ | 32.183 | 40.270 | 0.00301 |
| 4 | $p + s_6$ | 24.128 | 53.714 | 0.0029 |
| 5 | $p + s_3 - g_4 + g_3$ | 31.098 | 41.674 | 0.0026 |
| 6 | $p + s_1$ | 44.861 | 28.889 | 0.0015 |

*Table 3: Quasiperiodic terms for Earth's axial tilt* (Pälike, 2005; Laskar, 1999 ).

Terms 1, 2, 3, and 5 make up the 41,000-year cycle, with terms 4 and 6 acting as beats (Pälike, 2005).

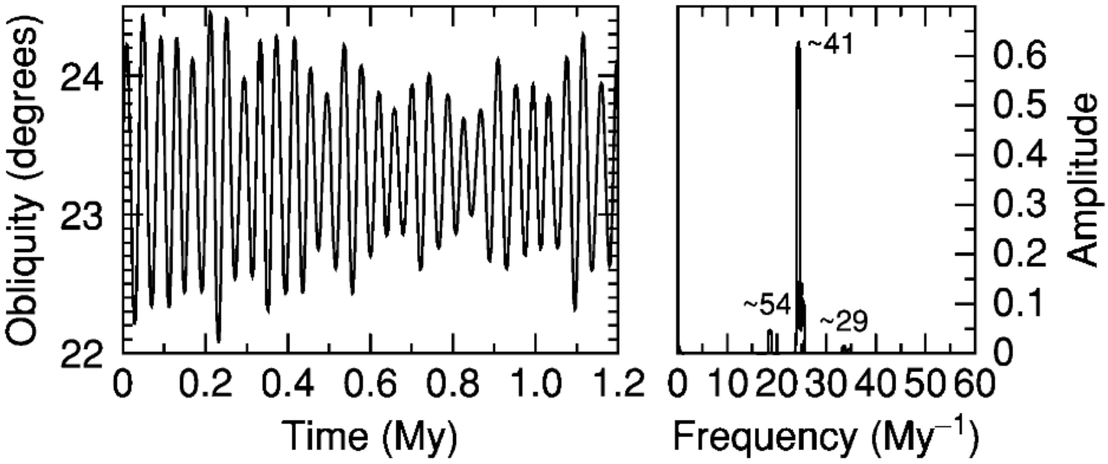


*Figure 12: Left: Plot of Earth's axial tilt over a 1.2-million-year period. Right: spectral plot of axial tilt data showing peaks at ~41 kyr, and beats at ~54 kyr and ~29 kyr* (Pälike, 2005).

### 1.6.4 Climatic Precession

Climatic precession is made up of two types of pression, axial precession (precession of the equinoxes (Hipparchus, 130 BC)) and apsidal precession (Kostadinov and Gilb, 2014). Axial precession describes the variation in the direction the rotational axis points. This precession slowly traces a cone, normal to the orbital plane.

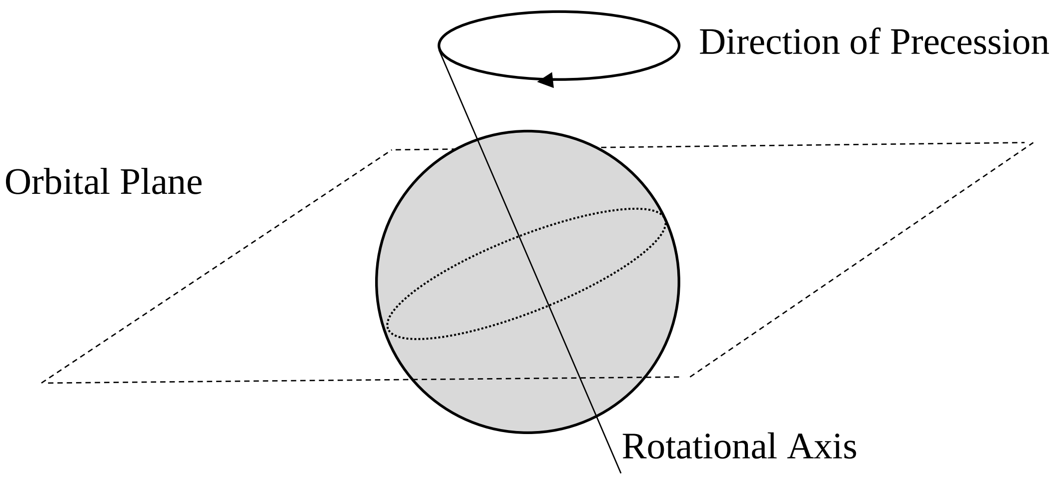


*Figure 13: An illustration of Earth's axial precession.*

Axial precession occurs on a ~26,000-year cycle as a result of sun and moon torques exerted on Earth (Pälike, 2005). Apsidal precession is the precession of the argument of the periapsis (discussed in section 1.5.2), with a cycle period of ~112,000-years (Heller and Pudritz, 2015). Together axial and apsidal precession form two cycles of period ~19,000-years and ~23,000-years (Kostadinov and Gilb, 2014). As with axial tilt, the quasiperiodic terms involve the constant of precession (Pälike, 2005):

| Term N.o. | Term | Frequency / "$year^{-1}$ | Period /kyr | Amplitude |
|---|---|---|---|---|
| 1 | $p + g_5$ | 54.7064 | 23.680 | 0.0188 |
| 2 | $p + g_2$ | 57.8949 | 22.385 | 0.0170 |
| 3 | $p + g_4$ | 68.3691 | 18.956 | 0.0148 |
| 4 | $p + g_3$ | 67.8626 | 19.097 | 0.0101 |
| 5 | $p + g_1$ | 56.0707 | 23.114 | 0.0042 |

*Table 4: Quasiperiodic terms for Earth's climatic precession* (Pälike, 2005; Laskar, 1999)

Terms 1,2 and 5 correspond to the ~23,000-year period, with 3,4 corresponding to the ~19,000-year period (Pälike, 2005).

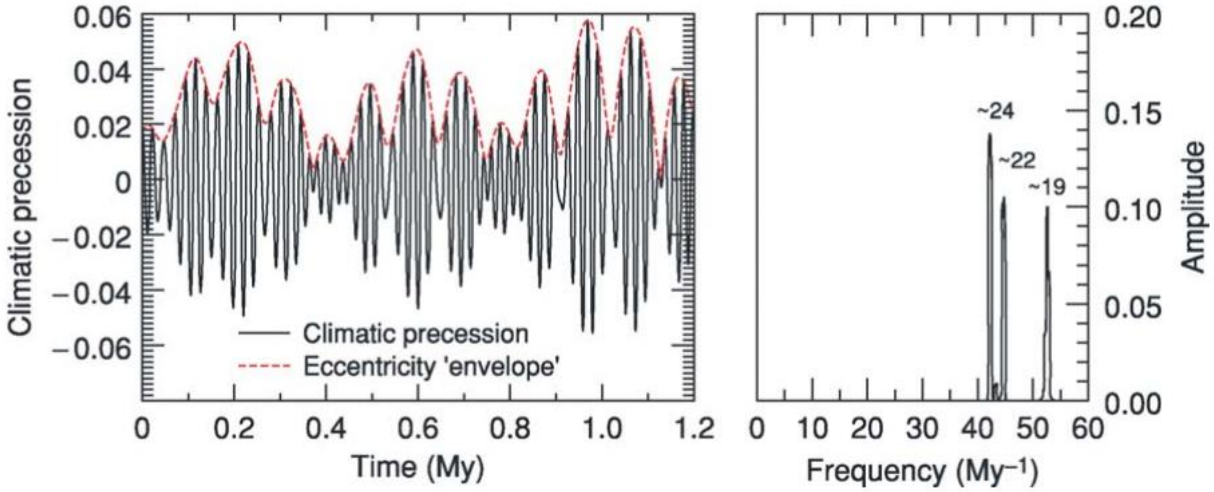


*Figure 14: : Left: Plot of Earth's axial tilt over a 1.2-million-year period. Right: spectral plot of climatic precession showing a peak at ~19 kyr, and two peaks at ~22 kyr and ~24 kyr making the ~23 kyr cycle signal* (Pälike, 2005).

## 1.6.5 Inclination

Although inclination is not one of the Milankovitch cycles (Roe, 2006), cyclic patterns in Earth's inclination are known (Muller and MacDonald, 1997). Variation in inclination may be measured from the invariable plane, i.e. the plane passing through the barycentre of the system and perpendicular to the angular momentum vector (Laplace, 1878; Souami and Souchay, 2012) or from the ecliptic or zodiacal plane i.e. the plane that contains Earth's orbit (Muller and MacDonald, 1997).

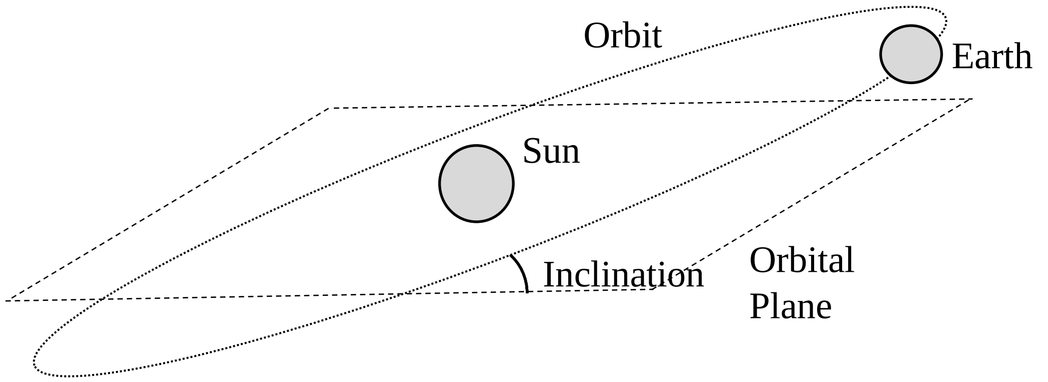


*Figure 15: An illustration of Earth's inclination.*

Inclination varies between ∼0° and ∼4° (Laskar et al., 2004) on a 100,000-year cycle when measured with respect to the invariable plane, or a 70,000-year cycle with respect to the ecliptic plane (Muller and MacDonald, 1997). Additionally, cycles are present at 190,000 years and 230,000 years (Berger et al., 2005). Similarly to the Milankovitch cycles, the inclination cycles are governed by combinations of the fundamental frequencies of the planets in the solar system. The terms that influence are those that come from the fundamental frequencies of the longitude of the ascending node (Pälike, 2005). Below are the terms that modulate the inclination cycles (Berger et al., 2005).

| Term N.o. | Term | Frequency / "year$^{-1}$ | Period /kyr | Amplitude |
|---|---|---|---|---|
| 1 | $s_5$ | 0.0000 | − | 0.0277 |
| 2 | $s_3$ | −18.829 | 68.829 | 0.0200 |
| 3 | $s_1$ | −5.611 | 230.977 | 0.0120 |
| 4 | $s_4$ | −17.819 | 72.732 | 0.0761 |
| 5 | $s_2$ | −6.771 | 191.404 | 0.0051 |
| 6 | $s_3 - s_5$ | −18.829 | 68.829 | 0.0005 |
| 7 | $s_1 - s_5$ | −5.611 | 230.977 | 0.0003 |
| 8 | $s_4 - s_5$ | −17.819 | 72.732 | 0.0002 |
| 9 | $s_2 - s_5$ | −6.771 | 191.404 | 0.0001 |

*Figure 16: Quasiperiodic terms for Earth's inclination* (Berger et al., 2005; Brentagon, 1974)

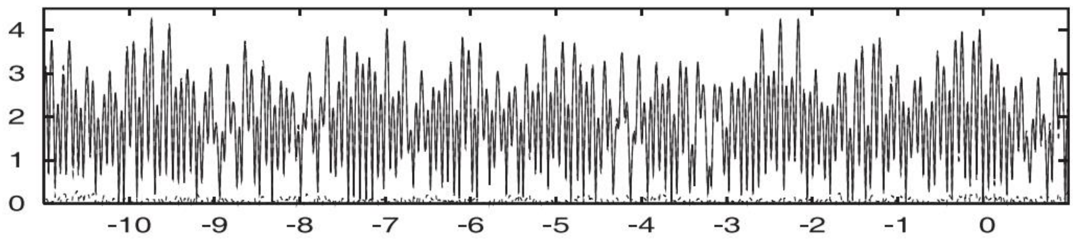


*Figure 17: Earth's inclination ( ° ) from $-11$ $Myr$ to $+1$ $Myr$ as produced from La2004* (Laskar et al., 2004)

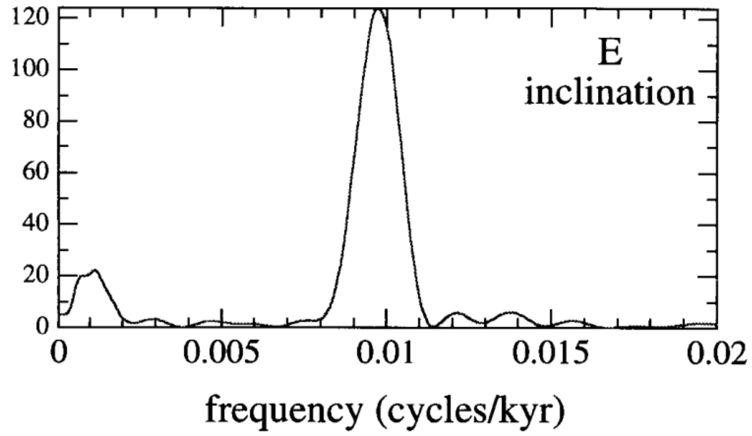


*Figure 18: Spectral plot for Earth inclination frequency, with peak representing period* 100 kyr *(*0.01 *$cycles/kyr$ frequency)* (Muller and MacDonald, 1997)

## 16.6 The Impact

The scientific community has used the ideas proposed by Milankovitch to explain phenomena across many fields. From sea level rise (Gale et al., 2002) to species evolution (Bennett, 1990), the Milankovitch cycles have become integral building blocks of many studies. However, despite the acknowledgement of the validity of the Milankovitch cycles, portions of the scientific community have expressed concern at how the Milankovitch cycles are used. For example, Puetz et al. (Puetz et al., 2016) argue that the use of 'orbital tuning' in geological data, the recalibration of sedimentary data chronologies to match the expected patterns from the Milankovitch cycles, may introduce biases which the data does not support.

The 100,000-year problem describes a significant inconsistency between the theory of the Milankovitch cycles and the empirical data (Raymo and Nisancioglu, 2003; Rial et al., 2013). The 100,000-year problem describes the shift from a dominant frequency of 41,000-year climate cycles, associated with axial tilt, up until 800,000 years ago where the dominant frequency shifted to 100,000 years, in phase with eccentricity. The figure overleaf illustrates the shift from a ~41,000-year cycle, to a ~100,000-year cycle ((Raymo and Nisancioglu, 2003).

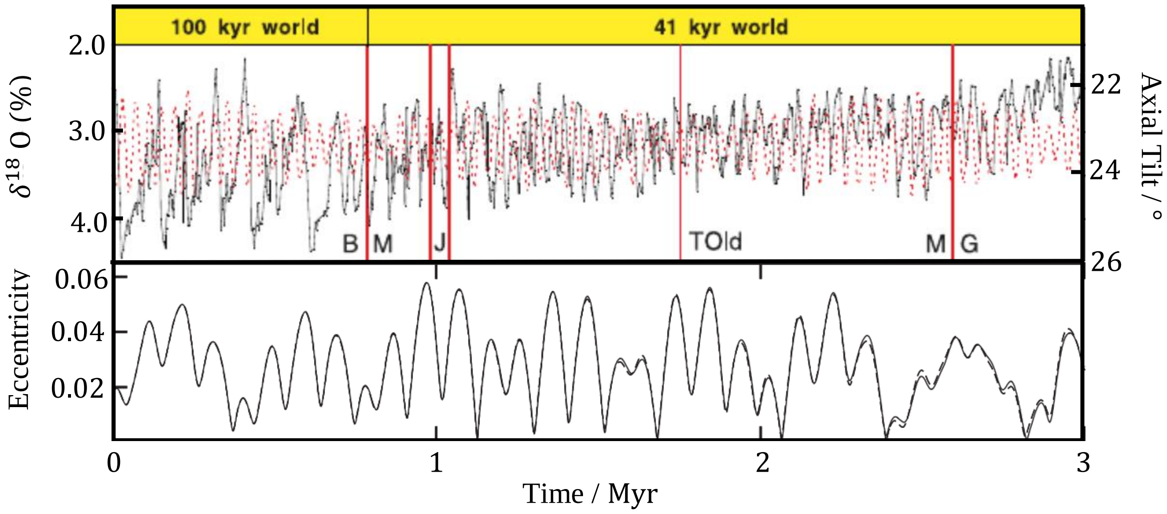


*Figure 19: Plots of Earth's axial tilt and Benthic δ^18 O levels with indications of paleomagnetic field reversals and the* 41 kyr *cycle/*100 kyr *cycle boundary at* ~800 kyr *(Raymo and Nisancioglu, 2003), and numerical solution of eccentricity as derived from La2004 (Laskar, 2004) and equivalent to output from La2010 over the last 3 million years (Laskar, 2010).*

Some have argued that the role of eccentricity in climate change may be the result of non-linear feedback (Hays et al. 1976; Davis and Brewer, 2008; Imbrie et al., 1992). Similarly to the interaction between axial tilt and Earth's 400,000 year cycle (Rial et al., 2013) this may cause eccentricity to amplify or inhibit the impact of axial tilt and precession (Davis and Brewer, 2008). Others argue that cycles in Earths orbital inclination, also on a 100,000 year cycle, may be responsible for the observed shift (Muller and MacDonald, 1995; Muller and MacDonald 1997). Variation in the inclination of Earth's orbit may move Earth into regions containing higher or lower amounts of debris. However, fundamentally no one cause has been agreed upon within the scientific community for the 100,000-year cycle in climate change, and its relationship to eccentricity.

Many mass extinctions are associated with a rise in global temperatures (Bond and Grasby, 2016), and the Milankovitch cycles are considered the pacemakers of climate change (Hays et al., 1976), therefore it follows that the Milankovitch cycles are a driver of Natural Selection (Bennett, 1990). Studies have identified links between the Milankovitch cycles and evolutionary processes throughout the Quaternary (Bennett, 1990), and forcing of mammal turnover over a 2.5 Myr period (van Dam, 2006). Events such as rises in volcanism (Macleoad, 2003), sea-level fall (Macleaod, 2003; Peters, 2008), gamma ray bursts (Melott et al., 2004) and asteroid impacts (Chiarenza et al., 2020), have all been identified as having a significant impact on extinction events, and many of these events have relationships to global climate change (Kaiho and Oshima, 2017; Chiarenza et al., 2020; Peters, 2008; Macleod, 2003). Understanding the changes in the Earth's orbital patterns may help us understand the events and factors that play a role in species loss which is of increasing importance as we progress further into the Anthropocene.

## 1.7 Galactic Cycles

Extinction events on Earth are also associated with the passage of the solar system through the Milky Way (Gillman and Erenler, 2008). Increases in asteroids from the Oort cloud impacting with Earth and vertical oscillations of the solar system have both been linked to extinction events (Gillman et al. 2018; Rampino 1998). The passing of the solar system through the galactic spiral arms is also associated with a higher than the average number of extinction events (Gillman and Erenler, 2008; Gillman et al.; 2018). Density wave theory describes that the spiral arms of the galaxy contains more celestial bodies and material (Lin and Shu, 1964). The passage of the solar system through a higher density region may trigger an increase in extinction events because of increased asteroid impacts and gamma ray bursts (Gillman et al., 2018). Gillman et al. also suggest that a potential driver of extinctions within the spiral arms may be an enhanced Milankovitch cycle effect (Gillman et al., 2018). This may be brought on by the perturbative effects of the increased surrounding mass, and the passing of stellar flybys.

## 1.8 Stellar Flybys

The study of flybys elucidates the impact and effects of so called ‘close encounters’ on celestial bodies and systems (Bailey and Fabrycky, 2019; De Rosa and Kalas, 2019; Malmberg et al., 2010). These close encounters may include the passing of planets in planetary flybys (Carusi et al., 1990), where the bodies encountering one another may be bound to the same primary, leading to planet scattering events (Bailey and Fabrycky, 2019), or the flyby may be stellar in nature, where another star unbounded to the primary perturbs the orbits in the primary’s system (De Rosa and Kalas, 2019) which can results in planet capture events (Malmberg et al., 2010). The term ‘close encounter’ refers to a wide range of distances, and therefore the term ‘close’ is poorly defined. Examples of ‘close encounter’ events include distances ranging from $1000$ AU or below (Bailey and Fabrycky, 2019; Malmberg et al., 201; Picogna and Marzari, 2014) up to distances of $2$ pc or $413{,}000$ AU (Bailer-Jones, 2015). Consequently, the term ‘close encounter’ has come to mean encounters with the celestial body or systems, at distances where an exchange of energy has occurred, which may have impacts on the evolution or events within the system.

The effects that stellar flybys have on the solar system, or components of the solar system, has been investigated in a number of studies, including the impact on the objects within the Oort cloud (Bailey and Fabrycky, 2019; Collins and Sari, 2010; Garcia-Sanchez et al., 2001) , and the effect on a 4-body system containing just the gas giants (Malmberg et al., 2010). Additionally, realistic and probable past encounters with the solar system have been identified, such as Scholz’s star 70,000 years ago (Mamajek et al., 2015) being the closest known stellar flyby at $\approx 50{,}000$ AU, as well possible future encounters (Bailer-Jones et al., 2018), such as the Gliese 710 flyby, expected to pass within $14{,}000$ AU of the solar system (Bailer-Jones et al. 2018; Berski and Dybczynski, 2016). Once again, the impacts of these events on the Oort cloud is acknowledged (Bailer-Jones, 2015; Bailer-Jones et al., 2018; Berski and Dybczynski, 2016), however, their impact on larger bodies in the solar system remains unclear.

Although it may be the case that even the closest of encounters, such as Gliese 710 flyby, have little impact on the orbits of the major bodies in the solar system (Berski and Dybczynski, 2016), the assumption is that these events are singular and their impact isolated. Yet analysis of the Hipparcos data suggested that encounters below 1 pc occurred approximately every 100,000 years (Garcia-Sanchez, 2001), with more recent analysis suggesting they may occur as regularly as $\approx 50{,}000$ years (Bailer-Jones, 2018). The effects of flybys potentially take millions of years to be realised (Malmberg et al., 2010). Perturbations of a bodies orbit from a close encounter may cause destabilisation, which may eventually lead to more significant events millions of years after the encounter (Malmberg, 2010). With additional flybys providing regular gravitational pulses, potentially insignificant variations of a planets orbit caused by a single flyby may be exacerbated. Moreover, even lack of effect from steady gravitational perturbations may reveal factors that play a role in the stabilisation of the solar system.

To investigate whether stellar flybys have a significant effect on the evolution of Earth's orbit, a selection of cases are investigated over a 15 Myr period. Discussions on 100 kyr problem suggest that eccentricity or inclination may have a substantial effect on Earth's glacial cycles (Muller and Macdonald, 1997; Raymo and Nisancioglu, 2003; Lisiecki, 2010; Rial et al., 2013). Therefore, the cases investigated focus on how Earth's eccentricity and inclination are effected by close encounters with stars.

# CHAPTER 2

# METHODS

## 2.1 REBOUND

The simulations in this project use the REBOUND (Rein and Liu, 2012) $N$-body integrator package, utilising the Python wrapper. The package is designed to model the motions of particles as they are influenced by gravity. REBOUND has been used frequently in projects investigating the perturbative effects of flybys, including the impact of the upcoming Gliese 710 encounter on the Oort cloud (Tesink, 2019) and close encounters between HD 106906 and other bodies in the Scorpius-Centaurus Association (De Rosa and Kalas, 2019).

## 2.2 Parameters

A set of parameters for the perturbers mass, velocity and encounter distance were generated using data from the *Gaia* DR2 catalogue. Bailer-Jones et al. use the *Gaia* DR2 data to look for candidate encounters with the solar system below 1 pc (2018). Table 5 shows the mass, median velocity at the perihelion, and median perihelion distance, for the stars identified. From this dataset, a median mass of $0.82\ M_{\odot}$, an average encounter velocity of $48.5\ \mathrm{km\ s^{-1}}$, and a median encounter distance of $152000$ AU were obtained and used as cases 101-107. Previous work using the Hipparcos data concluded that stellar encounters within 1 pc of the sun occur $11.7$ times per Myr (Garcia-Sanchez et al. 2001), equating to approximately once per $100$ kyr. However, more recent data from the *Gaia* DR2 catalogue, suggests that encounters may in fact occur as regularly of every $50$ kyr, specifically $19.7$ times per Myr (Bailer-Jones et al., 2018).

A frequency of encounter rate was therefore set at $\approx 50{,}000$ years. Seven cases in total were investigated; one case passing a single perturber, coplanar to the system at encounter point A (figure 20) and six cases passing multiple perturbers, in which the encounter inclinations and encounter points were varied (figure 21) to account for natural variation. Table 6 assigns case IDs to these simulations.

| *Gaia* DR2 source ID | $M/M_{\odot}$ | $v_{ph}$ / km s$^{-1}$ | $d_{ph}$/ pc |
|---|---|---|---|
| 4270814637616488064 | 0.68 | 14.5 | 0.068 |
| 955098506408767360 | 1.26 | 38.5 | 0.151 |
| 5571232118090082816 | 0.82 | 82.3 | 0.232 |
| 2946037094755244800 | NA | 42.1 | 0.338 |
| 4071528700531704704 | 1.00 | 44.2 | 0.374 |
| 510911618569239040 | 1.07 | 26.5 | 0.429 |
| 154460050601558656 | NA ✶ | 233.5 ✶ | 0.44 |
| 6608946489396474752 | 0.82 | 45.3 | 0.491 |
| 3376241909848155520 | 1.04 | 79.9 | 0.508 |
| 1791617849154434688 | 0.8 | 56.4 | 0.579 |
| 4265426029901799552 | 0.49 | 46.6 | 0.58 |
| 5261593808165974784 | 0.55 | 71.1 | 0.636 |
| 5896469620419457536 | 0.62 | 16.8 | 0.657 |
| 4252068750338781824 | 0.89 | 27.6 | 0.668 |
| 1949388868571283200 | NA ✶ | 347.4 ✶ | 0.673 |
| 1802650932953918976 | 0.98 | 53 | 0.74 |
| 3105694081553243008 | 0.75 | 38.3 | 0.76 |
| 5231593594752514304 | 0.67 | 715.9 ✶ | 0.815 |
| 4472507190884080000 | 0.96 | 52 | 0.819 |
| 3996137902634436480 | 0.95 | 38.5 | 0.82 |
| 3260079227925564160 | 0.47 | 33.4 | 0.824 |
| 5700273723303646464 | 0.95 | 38.1 | 0.836 |
| 5551538941421122304 | 0.65 | 30.4 | 0.866 |
| 2924378502398307840 | 0.75 | 87.1 | 0.88 |
| 6724929671747826816 | 0.72 | 54.8 | 0.884 |
| 3972130276695660288 | 0.58 | 31.9 | 0.888 |
| 5163343815632946432 | 0.76 | 37.1 | 0.896 |
| 2926732831673735168 | 1.15 | 66.5 | 0.917 |
| 2929487348818749824 | 1.34 | 70 | 0.926 |
| 939821616976287104 | NA ✶ | 568.4 ✶ | 0.989 |
| 3458393840965496960 | 1.17 | 86.4 | 0.996 |

*Table 5: Parameters acquired from Bailer-Jones et al. for stellar encounters below* 1 pc*. Values marked with a star were discounted either due to lack of data, or due to extreme values that skewed the average used* (Bailer-Jones et al, 2018).

| Case ID | Encounter Type | Encounter Point | Encounter Point A Inclination / ° | Encounter Point B Inclination / ° |
|---|---|---|---|---|
| 101 | Single | Static | 0 | N/A |
| 102 | Multiple | Static | 0 | N/A |
| 103 | Multiple | Static | N/A | 0 |
| 104 | Multiple | Alternating | 0 | 0 |
| 105 | Multiple | Static | 60 | N/A |
| 106 | Multiple | Alternating | 39.6 | 2.52 |
| 107 | Multiple | Alternating | 45.7 | 53.8 |

*Table 6: Parameters for cases 101-107. Encounter type refers to the number of bodies passing the system, either single (one body) or multiple (a body every 50,000 years). Encounter point references whether the bodies pass at either encounter point A or encounter point B (see figure 21), denoted as static, or whether the bodies pass on alternating sides such that if a body passes at encounter point A, the next body passes at encounter point B and visa-versa (see figure 21), denoted as alternating.*

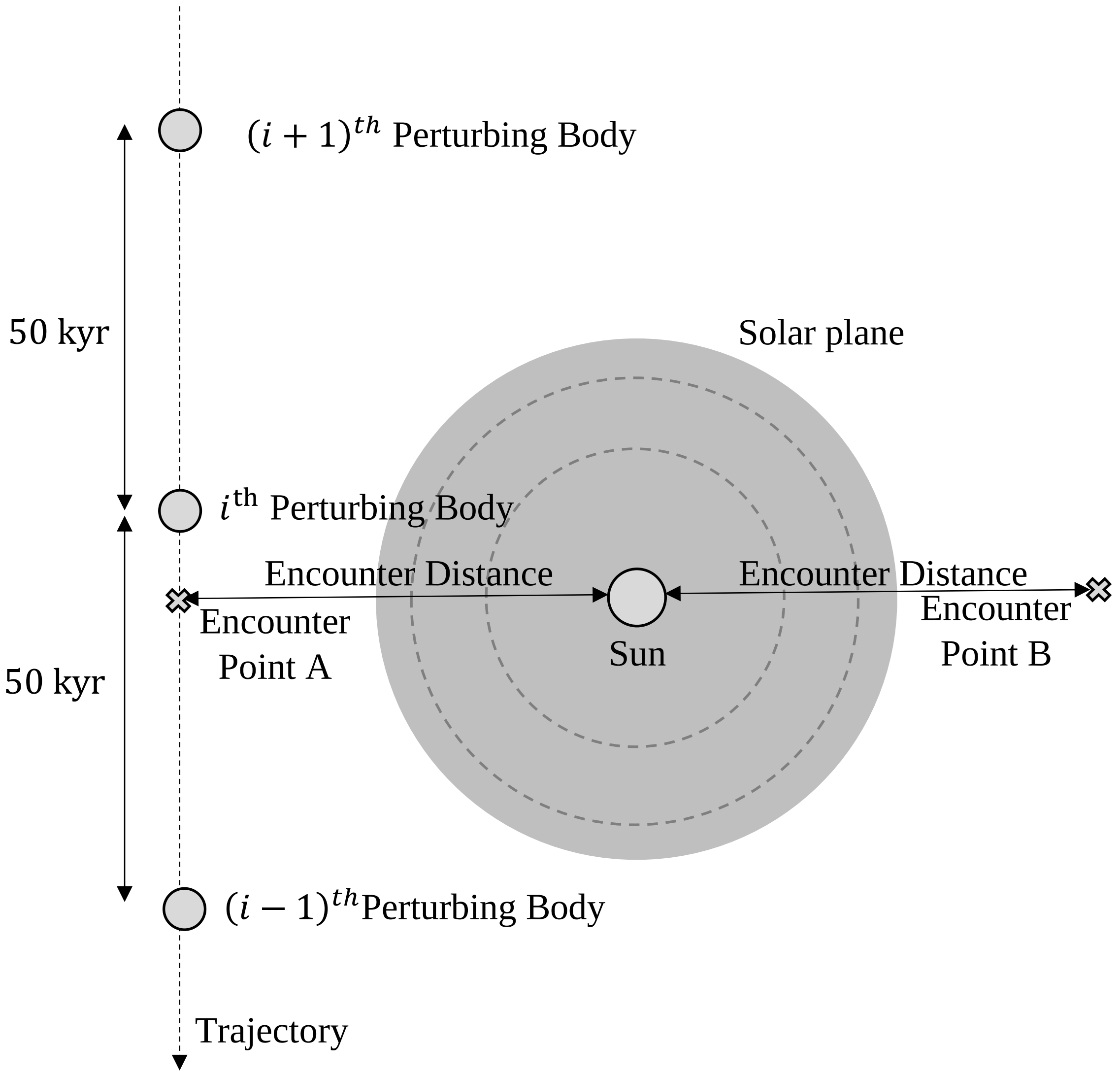


*Figure 20: Diagram of a multiple encounter type simulation, with static encounter point (at encounter point A)). Inclination not observable in this reference frame.*

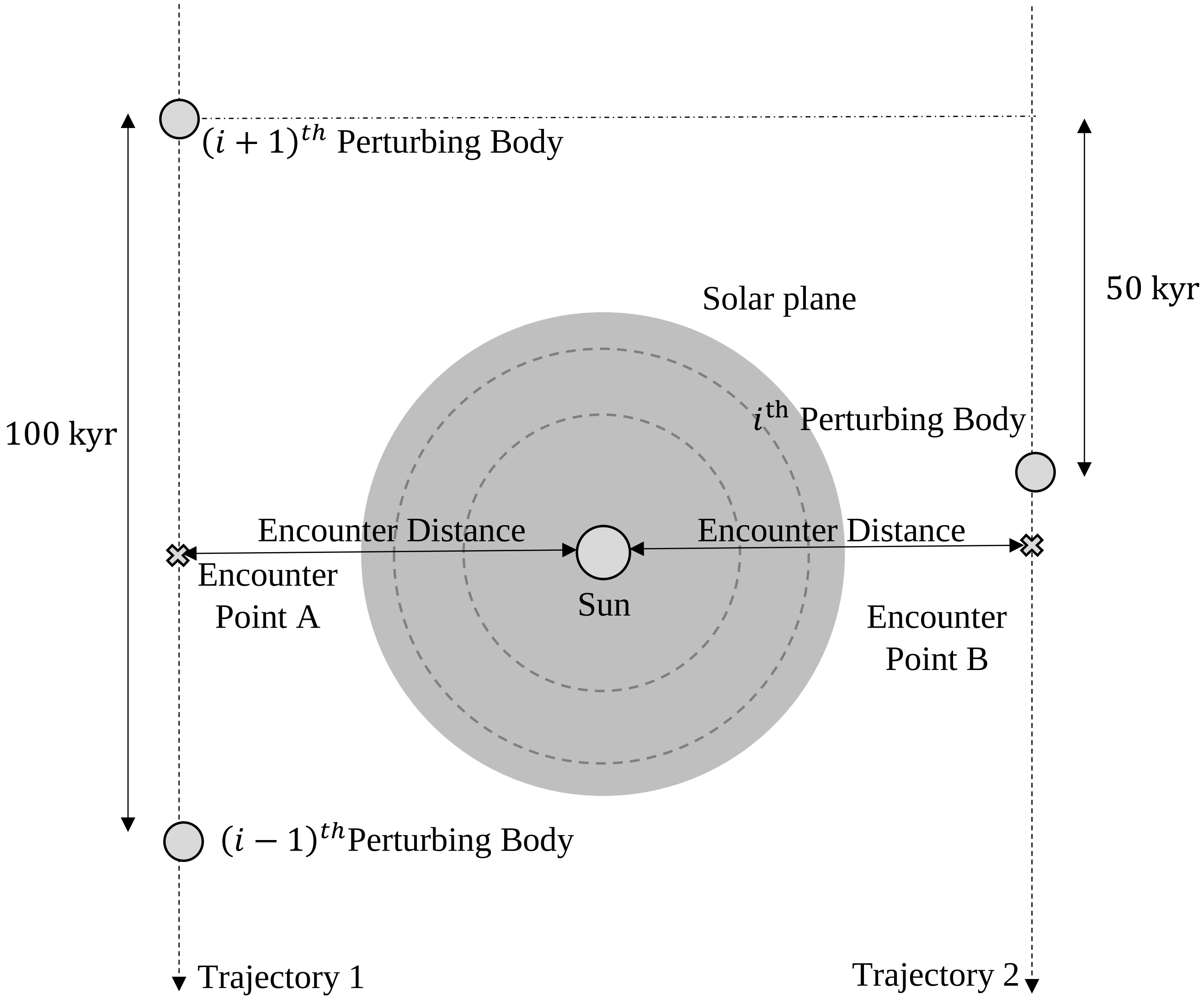


*Figure 21: Diagram of a multiple encounter type simulation, with alternating encounter point (alternating between encounter point A and encounter point B). Inclination not observable in this reference frame.*

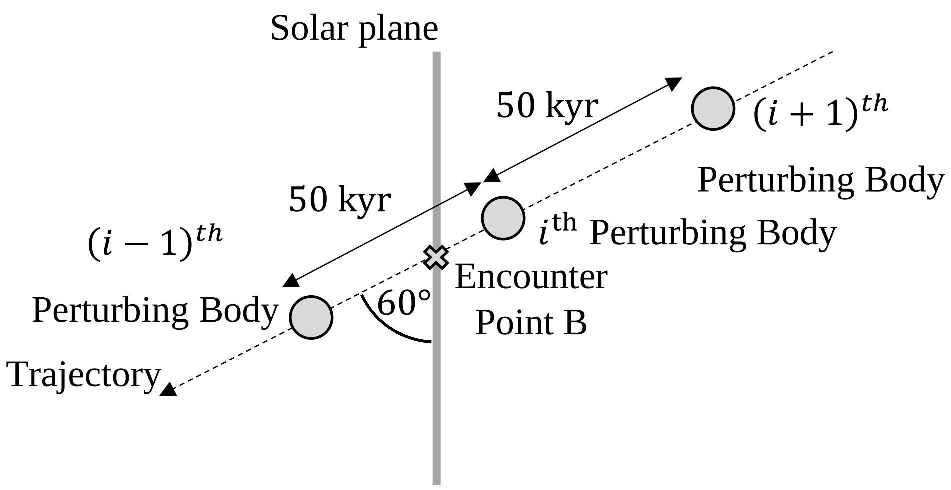


*Figure 22: Diagram of a multiple encounter type simulation, with a static encounter point (encounter point B), inclined 60°.*

Three further simulations, cases 108-110 were run to determine the chaos within the system in relation to the mass of the perturber. In each case, perturbers passed the solar system at intervals of $\sim 50{,}000$ years and coplanar to the system, in the opposing direction to case 102. All that was changed between the models were the masses. The masses selected were marginally different from one another to determine how small changes in the initial parameters effected the development of the system. The table below shows these cases.

| Case ID | $M / M_{\odot}$ |
|---|---|
| 108 | $1$ |
| 109 | $1.0001$ |
| 110 | $1.01$ |

*Table 7: Case parameters for mass with associated case ID.*

To test the effect of larger perturbing masses and closer encounters, further simulations were run using a combination of increasing masses, decreasing encounter distance and varying perturber inclination. Three parameter values were selected for each case, and all 27 parameter combinations were run. The values selected for mass were $0.82\ M_{\odot}$, $1\ M_{\odot}$ and $1.34\ M_{\odot}$, which respectively represents the median mass, the mass of a sun-like star and the largest mass star identified by Bailer-Jones et al. as a possible flyby (Bailer-Jones et al., 2018). Encounter distances were selected within the range of values set out by Bailer-Jones et al., but analogous to researched stellar flybys. The Gliese 710 (*Gaia* DR2 4270814637616488064) flyby is expected to pass by the solar system at a distance of $\approx 14{,}000$ AU, and is the closest potential encounter identified. A mid-range value of $\approx 50{,}000$ AU was also selected, which is comparable to the closest known flyby encounter (Mamajek et al., 2015). Three inclinations to the solar plane were investigated, $0°$ being coplanar to the solar plane, $60°$ coplanar to the galactic plane and $90°$ perpendicular to the solar plane. Table 3 shows the 27 combinations, and assigns each a case ID.

| Case ID | $M / M_{\odot}$ | $d /$ AU | $i/°$ |
|---|---|---|---|
| 201 | 0.82 | 152000 | 0° |
| 202 | 0.82 | 50000 | 0° |
| 203 | 0.82 | 14000 | 0° |
| 204 | 1 | 152000 | 0° |
| 205 | 1 | 50000 | 0° |
| 206 | 1 | 14000 | 0° |
| 207 | 1.34 | 152000 | 0° |
| 208 | 1.34 | 50000 | 0° |
| 209 | 1.34 | 14000 | 0° |
| 210 | 0.82 | 152000 | 60° |
| 211 | 0.82 | 50000 | 60° |
| 212 | 0.82 | 14000 | 60° |
| 213 | 1 | 152000 | 60° |
| 214 | 1 | 50000 | 60° |
| 215 | 1 | 14000 | 60° |
| 216 | 1.34 | 152000 | 60° |
| 217 | 1.34 | 50000 | 60° |
| 218 | 1.34 | 14000 | 60° |
| 219 | 0.82 | 152000 | 90° |
| 220 | 0.82 | 50000 | 90° |
| 221 | 0.82 | 14000 | 90° |
| 222 | 1 | 152000 | 90° |
| 223 | 1 | 50000 | 90° |
| 224 | 1 | 14000 | 90° |
| 225 | 1.34 | 152000 | 90° |
| 226 | 1.34 | 50000 | 90° |
| 227 | 1.34 | 14000 | 90° |

*Table 8: Case parameters for mass, encounter distance and inclination, with associated case ID.*

Following the results from cases 201-227, a simulation without Jupiter for each of the cases was run, with case numbers 301-327, where perturbers in case 301 had the same parameters as the perturbers in case 201 etc. The purpose of these models was to determine the role of Jupiter in the effects observed in cases 201-227. Jupiter features heavily in the quasiperiodic terms of the secular resonances that influence Earth's eccentricity cycles (Matthews and Frohlich, 2002; Pälike, 2005; Horner et al., 2017). Therefore, removal of Jupiter from the system should determine how passing perturbers interact with Jupiter's orbit, and how this subsequently impacts Earth's orbit.

## 2.3 Numerical Models

Bodies in REBOUND can be added using either the body's initial position and velocity, or the body's semi-major axis and eccentricity. The true anomaly $f$, argument of the periapsis $\omega$, longitude of the ascending node $\Omega$, and inclination $i$ can also be adjusted as required. However, these values are bounded within REBOUND and as such parameters will adjust to within the bounded range if values outside of this range are provided, whilst keeping the trajectory the same. Additionally, the mass of the particles is required, given by default in solar masses, with test particles being conventionally set to $1\mathrm{e}^{-3}$.

Preliminary work showed that all planets in the system were required to replicate past work (Pluto was also included) (Laskar, 2004; Laskar, 2010). For solar system objects, REBOUND has the functionality to load body positions and velocity from the NASA HORIZONS database (Giorgini, and JPL Solar Systems Dynamic Group, 2020). This database does not include masses of solar system bodies, however a list of masses and barycentres for major solar system bodies is available within REBOUND (Giorgini, 2015). Therefore, the planets were added to a REBOUND simulation, before saving the simulation as an archive bin to improve simulation efficiency, by removing the time required to import this data, and ensure all simulations began with the same solar system environment.

The path of a perturber is modelled as having a hyperbolic orbit to the solar system, similar to the approach taken in by Picogna and Marzari (2014) and Malmberg et al. (2010), amongst others. Perturbers were added to the system for 50,000 years, before they were removed and another perturber added. To find the initial position of each perturber, the perturber was added to a simple two body system (sun – perturber system) as a test particle with the required velocity, inclination, encounter distance and encounter point, before being backwardly integrated 25,000 years (half the encounter frequency). Integrating back this amount of time ensured that the perturbers were at their closest approach midway through their 50,000 years in the simulations, and that appropriate representation of the effect the perturber had as it both approached and exited the solar system occurred. Once this position had been obtained, perturbers could be added to a full solar system model, and the perturber mass increased to required levels. The perturber was then allowed to pass the system until 50,000 years passed, at which point the perturber was removed. To remove artefacts generated by adding the next perturber within the same timestep, the simulation was run for 1 year before being added. 1 year was selected as this was the minimum amount of time between two iterations, therefore keeping to a minimum the amount of time that a perturber was not in the simulation.

## 2.4 Integrator

REBOUND offers a plethora of integrators, providing flexibility and ease to switch between integrators. Some of the papers reviewed that use REBOUND for flyby investigations use IAS15, an adaptive timestep integrator of order 15, as the integrator of choice (Bailey and Fabrycky, 2019). However, in this case the flybys encounter the system at much closer distances than those in this study. Reviewing the REBOUND documentation discussing the HERMES integrator, a hybrid of the IAS15 and WHFAST integrators, revealed that IAS15 although needed in close encounter situations, is generally less preferable to the WHFAST integrator (Silburt et al., 2016). WHFAST is an implementation of a Wisdom-Holman symplectic integrator (Rein and Tamayo, 2015), and therefore its efficiency is improved by utilising the Hamiltonian $\mathcal{H}$ of the system, reduce the number of calculations required per timestep (Rein and Tamayo, 2015). Symplectic integrators are used frequently in the study of celestial systems, notably by Laskar when also looking at the evolution of Earth's eccentricity (Laskar, 2004; Laskar 2010). Versions of the Wisdom-Holman integrator have been used in numerous $N$-body models to investigate the evolution of dynamic systems (Laughlin and Adams, 1999). Testing of both IAS15 and WHFAST demonstrated the reduced computational time. As the perturbations to the orbits of the planets from a distant perturber were likely to be small, and with planets unlikely to be ejected even in the most extreme cases, the benefits of IAS15 were muted, and the efficiency of WHFAST the most desirable feature, as well as the symplectic nature being comparable to other works (Laskar et al., 2004; Laskar et al., 2010). Therefore, WHFAST was chosen as the integrator for the project, with a timestep of $1 \times 10^{-3}\ \mathrm{yr}/2\pi$ used in all simulations.

As WHFAST is a symplectic integrator, it uses the Hamiltonian $\mathcal{H}$ within its calculations (Rein and Tamayo, 2015). The Hamiltonian is split into the sum of the kinetic energy and potential energy of the system, as shown in equation 25. However, this equation is solely in terms of cartesian co-ordinates, whereas WHFAST uses Jacobi co-ordinates for the kinetic energy component (Rein and Tamayo, 2015). Jacobi co-ordinates differ from cartesian co-ordinates in their measuring reference point (Rein and Tamayo, 2015). In Jacobi co-ordinates, a bodies position is measured from the centre of mass of the system (Rein and Tamayo, 2015). Replacing the kinetic term in Cartesian co-ordinates, for the Jacobi co-ordinate equivalent, the following Hamiltonian is formed:

$$\mathcal{H} = \sum_{i=0}^{N-1} \frac{\boldsymbol{p}_i'^2}{2m'_i} - \sum_{i=0}^{N-1} \sum_{j=i+1}^{\boldsymbol{N-1}} \frac{Gm_i m_j}{\|\boldsymbol{q}_j - \boldsymbol{q}_i\|} \quad \textit{Equation 25}$$

where $\sum_{i=0}^{N-1} \frac{\boldsymbol{p'}_i^2}{2m'_i}$ is the kinetic energy in Jacobi co-ordinates, and $-\sum_{i=0}^{N-1} \sum_{j=i+1}^{\boldsymbol{N-1}} \frac{Gm_i m_j}{\|\boldsymbol{q}_j - \boldsymbol{q}_i\|}$ is the potential energy in Cartesian co-ordinates (Rein and Tamayo, 2015).

Rearranging the Hamiltonian yields three terms; $\mathcal{H}_{\text{Kepler}}$ the Keplerian motion for body $i$, $\mathcal{H}_{\text{Interaction}}$ the perturbation term, and $\mathcal{H}_0$ the motion of the centre of mass along a straight line (Rein and Tamayo, 2015). Rein and Tamayo (2015) note that this term is usually ignored but has been kept within this integrator to enable integration with respect to any frame of reference. The Hamiltonian in these terms becomes:

$$\mathcal{H} = \mathcal{H}_0 + \mathcal{H}_{\text{Kepler}} + \mathcal{H}_{\text{Interaction}} \quad \textit{Equation 26}$$

where

$$\mathcal{H}_0 = \frac{p_0'^2}{2m_0'} \quad \textit{Equation 27}$$

$$\mathcal{H}_{\text{Kepler}} = \sum_{i=1}^{N-1} \frac{\boldsymbol{p}_i'^2}{2m'_i} - \sum_{i=1}^{N-1} \frac{Gm_i' M_i}{|q_i'|} \quad \textit{Equation 28}$$

$$\mathcal{H}_{\text{Interaction}} = \sum_{i=1}^{N-1} \frac{Gm_i' M_i}{|q_i'|} - \sum_{i=0}^{N-1} \sum_{j=i+1}^{\boldsymbol{N-1}} \frac{Gm_i m_j}{\|\boldsymbol{q}_j - \boldsymbol{q}_i\|} \quad \textit{Equation 29}$$

The Hamiltonians $\mathcal{H}_0$ and $\mathcal{H}_{\text{Interaction}}$ have analytical solutions, and $\mathcal{H}_{\text{Kepler}}$ is a set of Kepler orbits which can be solve iteratively (Rein and Tamayo, 2015). Together they can be used to form a 'Drift-Kick-Drift' operator, where the position of the body *drifts* into the position it would travel according to a Kepler orbit, before being *kicked* by the perturbing force, before *drifting* again along a Kepler orbit (Rein and Tamayo, 2015). The Wisdom-Holman map of the Drift-Kick-Drift operator scheme is such that:

Drift: $$\hat{\mathcal{H}}_{\text{Kepler}}\left(\frac{dt}{2}\right)\circ\hat{\mathcal{H}}_0\left(\frac{dt}{2}\right)$$ *Equation 30*

Kick: $$\hat{\mathcal{H}}_{\text{Interaction}}(dt)$$ *Equation 31*

Drift: $$\hat{\mathcal{H}}_{\text{Kepler}}\left(\frac{dt}{2}\right)\circ\hat{\mathcal{H}}_0\left(\frac{dt}{2}\right)$$ *Equation 32*

where $\hat{\mathcal{H}}_a(dt)$ is the evolution of the particles in Hamiltonian $a$ for timestep $dt$, and $\hat{\mathcal{H}}_b(dt)\circ\hat{\mathcal{H}}_a(dt)$ is evolution of the particles in Hamiltonian $a$, before evolution of the particles in Hamiltonian $b$ for timestep $dt$ (Rein and Tamayo, 2015).

Splitting the Hamiltonian results in the addition of high frequency terms being added to the Hamiltonian (Rein and Tamayo, 2015). Although these average out and therefore do not affect the long-term evolution of the system, a 11$^{\text{th}}$ order symplectic corrector is available to reduce the number of these high frequency terms (Rein and Tamayo, 2015). This is implemented throughout the models.

## 2.5 Fast Fourier Transform

The Fast Fourier Transform (FFT) from the SciPy Python package (Virtanen, 2020) was used to analyse the frequencies and periods shown in the outputted data. The FFT is an optimised version of the Discrete Fourier Transform (DFT), giving the same result, but with shorter computation times (Parker, 2017); the DFT requiring $O(N^2)$ operations to complete, whereas the FFT requires only $O(N\log(N))$ (Parker, 2017). The DFT and FFT are transforms that convert a signal in the time domain, to a spectrum in the frequency domain, with peaks at points with higher signal energy (Parker, 2017) using the formula:

$$X_k = \sum_{n=0}^{N-1} x_n e^{-\frac{i(2\pi kn)}{N}} \text{ for } k = \{0,1,\ldots,N-1\}$$

*Equation 33*

where $X_k$ is the frequency domain representation of the signal, $x_n$is the time domain representation of the signal, $N$ is the number of data points,

The DFT and FFT transform the data by splitting the data into a sum of sine and cosine waves, all with differing frequencies (Parker, 2017). The FFT uses periodicity in the signal to simplify terms in the calculation (Parker, 2017,). The butterfly diagram overleaf shows a flow diagram of the calculations required for a small signal where $N = 4$, and calculations expressed formulaically (Parker, 2017)  Because of this the FFT is often more preferable to the DFT, especially with signals with a large number of data points (Parker, 2017), particularly useful when dealing with signal frequencies on geological timeframes.

Given the nature of the system, it is possible that the power of particular frequencies or periodicities may vary over the timeframe investigated, as shown in work by Lisiecki (2010). To map these changes, an FFT windowing technique was adopted (Parker, 2017; Lisiecki, 2010). This involves taking a period of time within the signal (the window), performing a FFT, and noting the power of peaks associated with a particular frequency or period (Parker, 2017; Lisiecki, 2010). There are a variety of window shapes with each having advantages and disadvantages (Parker, 2017). Throughout this investigation, a boxcar window was applied (a rectangular window) similar to Lisiecki (2010). The window used requires a frequency or period range (Parker, 2017). This is the range that peaks are accepted in (Parker, 2017). The table below shows the boxcar ranges for the periodicities investigated.

| Orbital Element | Orbital Cycle Period | Lower Bound of Boxcar | Upper Bound of Boxcar |
|---|---|---|---|
| Eccentricity | ~95 kyr | 90 kyr | 110 kyr |
| Eccentricity | ~125 kyr | 110 kyr | 140 kyr |
| Eccentricity | ~400 kyr | 400 kyr | 450 kyr |
| Inclination | ~70 kyr | 60 kyr | 100 kyr |
| Inclination | ~190 kyr | 170 kyr | 210 kyr |
| Inclination | ~230 kyr | 210 kyr | 250 kyr |

*Table 9: Table showing the upper and lower bounds of the FFT boxcars used for eccentricity and inclination.*

$$\rightarrow \text{define } A = [x_0 + x_2], B = [x_1 + x_3]$$

$$X_0 = [x_0 + x_2] + [x_1 + x_3] = A + B$$

$$\rightarrow \text{define } C = \left[x_0 + x_2 \cdot e^{-j2\pi 2/4}\right], D = \left[x_1 + x_3 \cdot e^{-j2\pi 2/4}\right]$$

$$X_1 = \left[x_0 + x_2 \cdot e^{-j2\pi 2/4}\right] + \left[x_1 + x_3 \cdot e^{-j2\pi 2/4}\right] \cdot e^{-j2\pi/4} = C + D \cdot e^{-j2\pi/4}$$

$$X_2 = [x_0 + x_2] + [x_1 + x_3] \cdot e^{-j4\pi/4} = A + B \cdot e^{-j4\pi/4}$$

$$X_3 = \left[x_0 + x_2 \cdot e^{-j2\pi 2/4}\right] + \left[x_1 + x_3 \cdot e^{-j2\pi 2/4}\right] \cdot e^{-j6\pi/4} = C + D \cdot e^{-j6\pi/4}$$

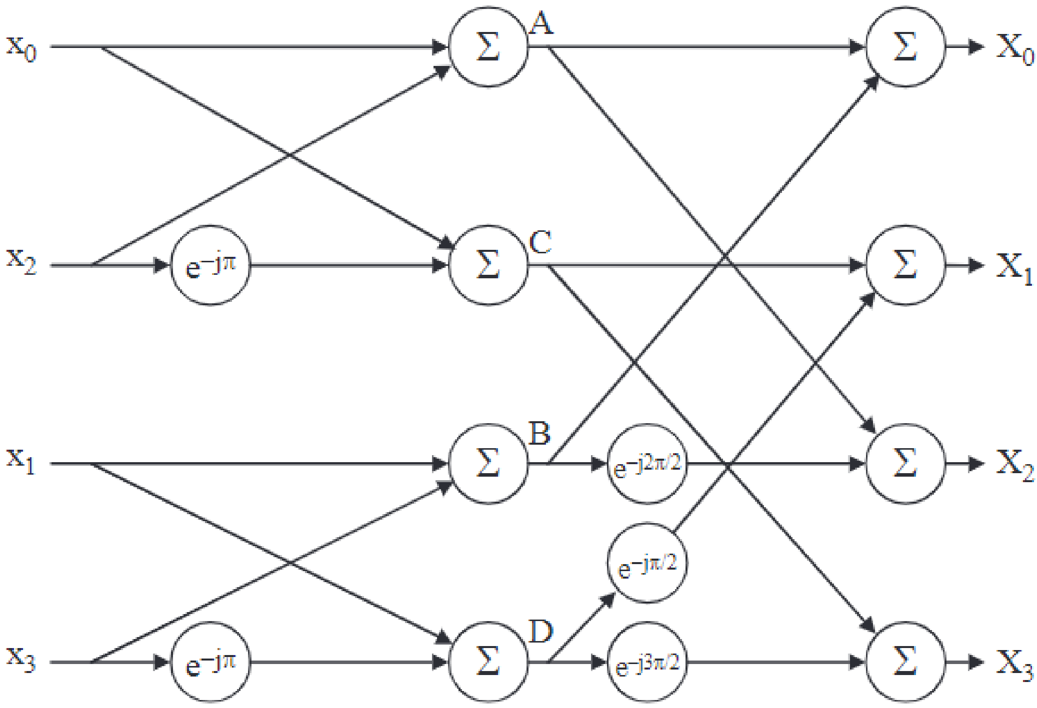


*Figure 23: A butterfly diagram of the calculations required to perform the FFT on an $N = 4$ signal with corresponding calculations and definitions written formulaically* (Parker, 2017)

# CHAPTER 3

# RESULTS AND DISCUSSIONS

## 3.1 Eccentricity

### 3.1.1 Baseline Models

The system was evolved over a 15 Myr period with no perturbers added to the system, to provide a reference of how the system would have naturally evolved. This is referred to as the 'full-system baseline model'. Comparing the models with perturbers to this baseline model allowed for the impact perturbing bodies had on the system to be measured. The figure below shows the evolution of Earth's eccentricity over the 15 Myr time period and shows eccentricity values ranging between 0 and 0.06, comparable with the literature (Pälike, 2005).

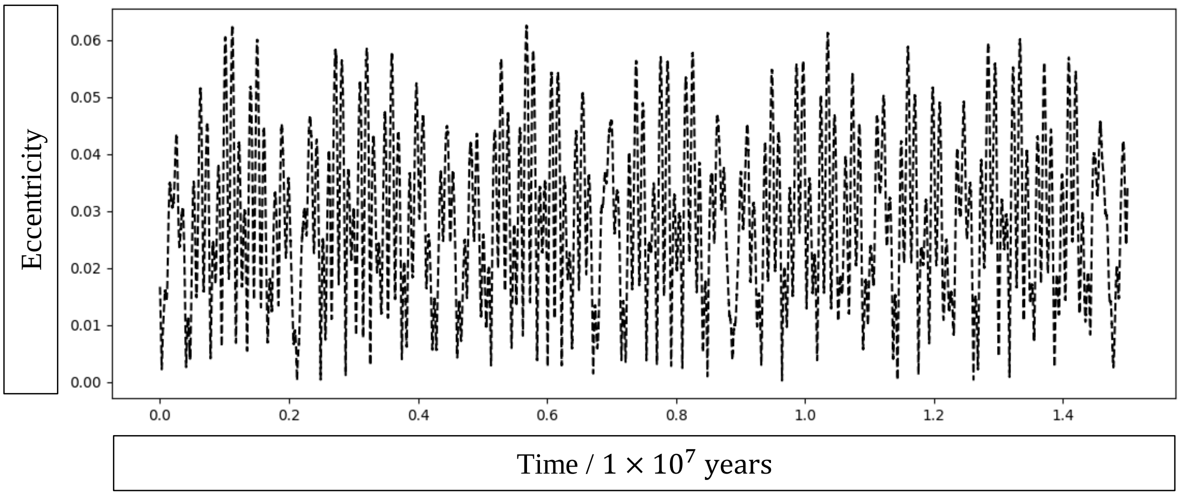


*Figure 24: A graph of Earth's eccentricity over a 15 Myr period starting from 2020 under the gravitational influence of a full system.*

Conducting an FFT on the eccentricity evolution results from the full-system baseline model produced a power spectrum of the eccentricity signal. This provides the periodic frequencies present in the signal. Figure 25 shows the periodogram of the FFT of the baseline model normalised such that the strongest peak had a value of 1.

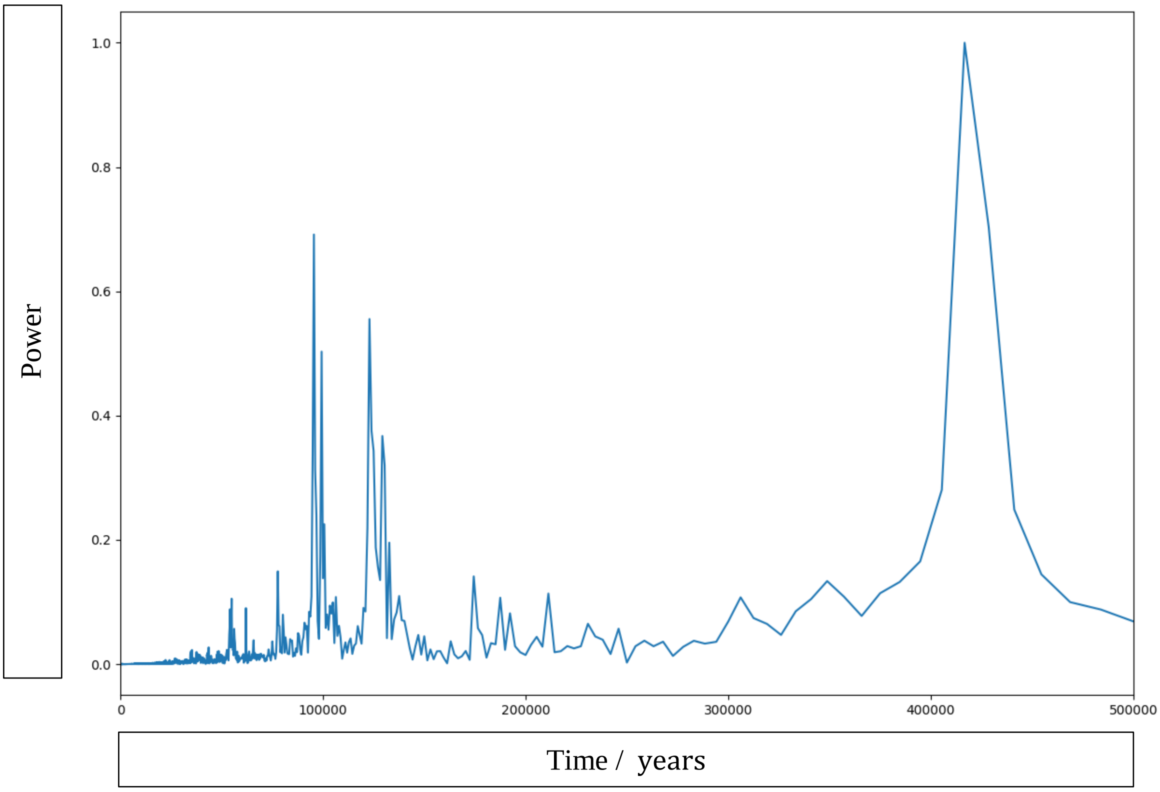


*Figure 25: Periodogram of Earth's eccentricity in full-system baseline model*

The five strongest spectral peaks on the periodogram match up with the periods of the quasiperiodic terms detailed in section 1.6.2, in both position and relative peak strength, as expected (Matthews and Frohlich, 2002). When Jupiter is removed from the system the evolution of Earth's eccentricity changes substantially, with eccentricity ranging only from 0 to 0.03 (see figure 26). This model is referred to as the 'Jupiter-less baseline model'.

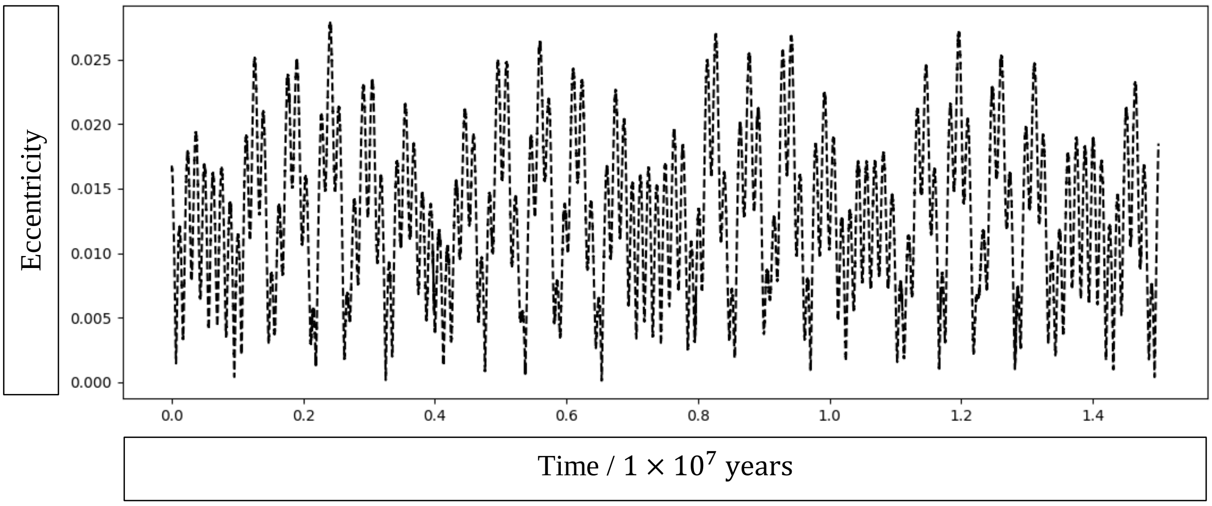


*Figure 26: A graph of Earth's eccentricity over a* 15 *Myr period starting from 2020 under the gravitational influence of a system without Jupiter*

Somewhat intuititively the changes in the evolution of Earth's eccentricity means that the frequencies in the signal have also changed. Below is the FFT periodogram for the Jupiter-less baseline model.

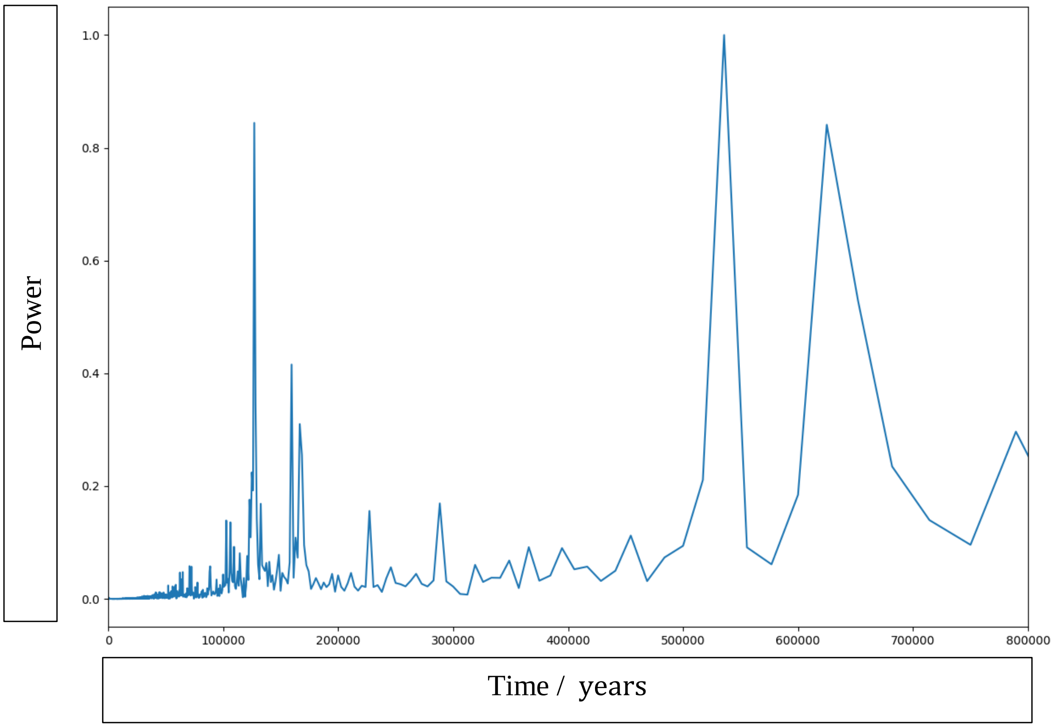


*Figure 27: Periodogram of Earth's eccentricity Jupiter-less baseline model*

Removing Jupiter from the system removed the spectral peaks at ~400 kyr, ~95 kyr and ~99 kyr displayed in the full-system baseline model and discussed in the literature (Matthews and Frohlich, 2002). As all these terms involve the Jupiter $g_5$ term this result is not unexpected. However, new peaks at ~525 kyr and ~625 kyr which do not match any of the 19 quasiperiodic terms discussed by Matthews and Frohlich appear (Matthews and Frohlich, 2002). As this system does not exist in reality, this result is of little value, but may be a consequence of some more complex secular resonances which have had their amplitude increased as a result of Jupiter's removal. The value of this model is to evaluate how Jupiter interacts with perturbing bodies and illustrate Jupiter's importance in the evolution of Earth.

## 3.1.2 Initial Testing: Cases 101-110

In cases 101-107 perturbing bodies were passed at a variety of encounter points and inclinations (see 2.2 for details). In case 101 a single perturbing body was passed by the solar system at a distance of 152000 AU with inclination 0° (coplanar with the solar system). Plotting the eccentricity of Earth in this model produces a graph indistinguishable from the full-system baseline model. Subtracting the baseline model from results for case 101 produces a plot of the differences between the models (figure 28). These differences can be attributed to the perturbers influence as this is only difference between the models.

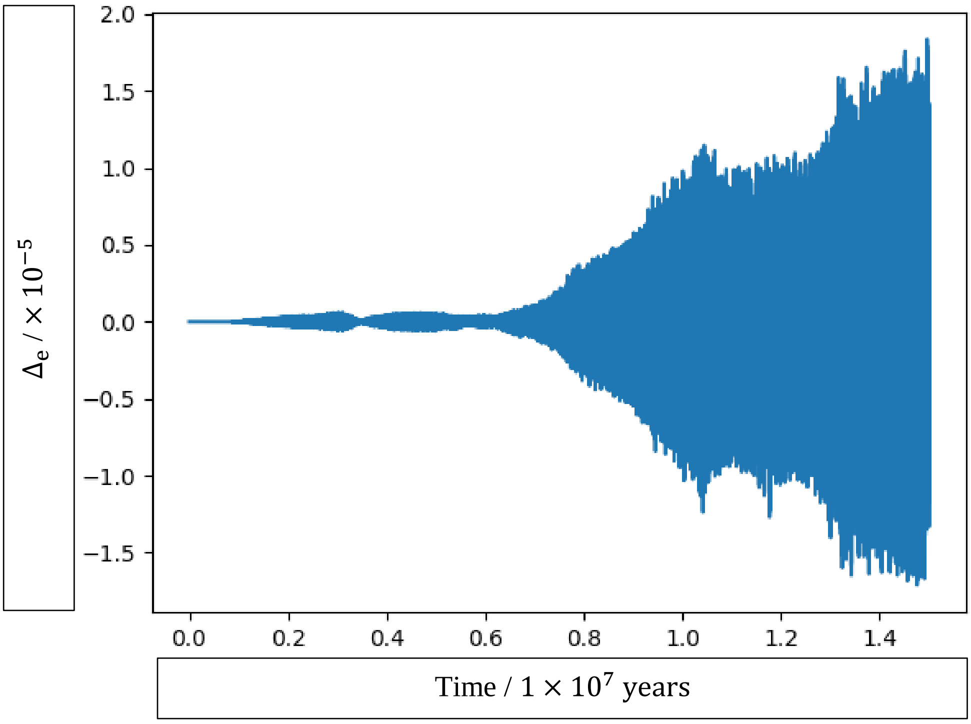


*Figure 28: A graph of the difference in eccentricity ($\Delta_e$) between the baseline model and the case 101 model.*

The graph shows that:

$$|\Delta_e|_{\max} \approx 2 \times 10^{-5}$$

Given that the cyclic changes in eccentricity in a perturber-less model are three orders of magnitude greater than this, the result suggests that the passing of a single perturber has negligible effect on the evolution of Earth's eccentricity over a 15 Myr period. To confirm that changes in eccentricity in this order of magnitude have an indistinguishable impact on the cyclic changes in eccentricity (Matthews and Frohlich, 2002; Pälike, 2005), an FFT of a rolling boxcar at three intervals has been implemented to show the evolution of the eccentricity cycles. The graphs in figures 29 and 30 show that the power of each of the eccentricity cycle periods is unaffected by the passing of a single perturber, as the graph of the full-system baseline model is covered by that of the case 101 graph. This supports the hypothesis Berski and Dybczynski propose that single close encounters with the solar system have little impact on the planetary bodies (Berski and Dybczynski, 2016).

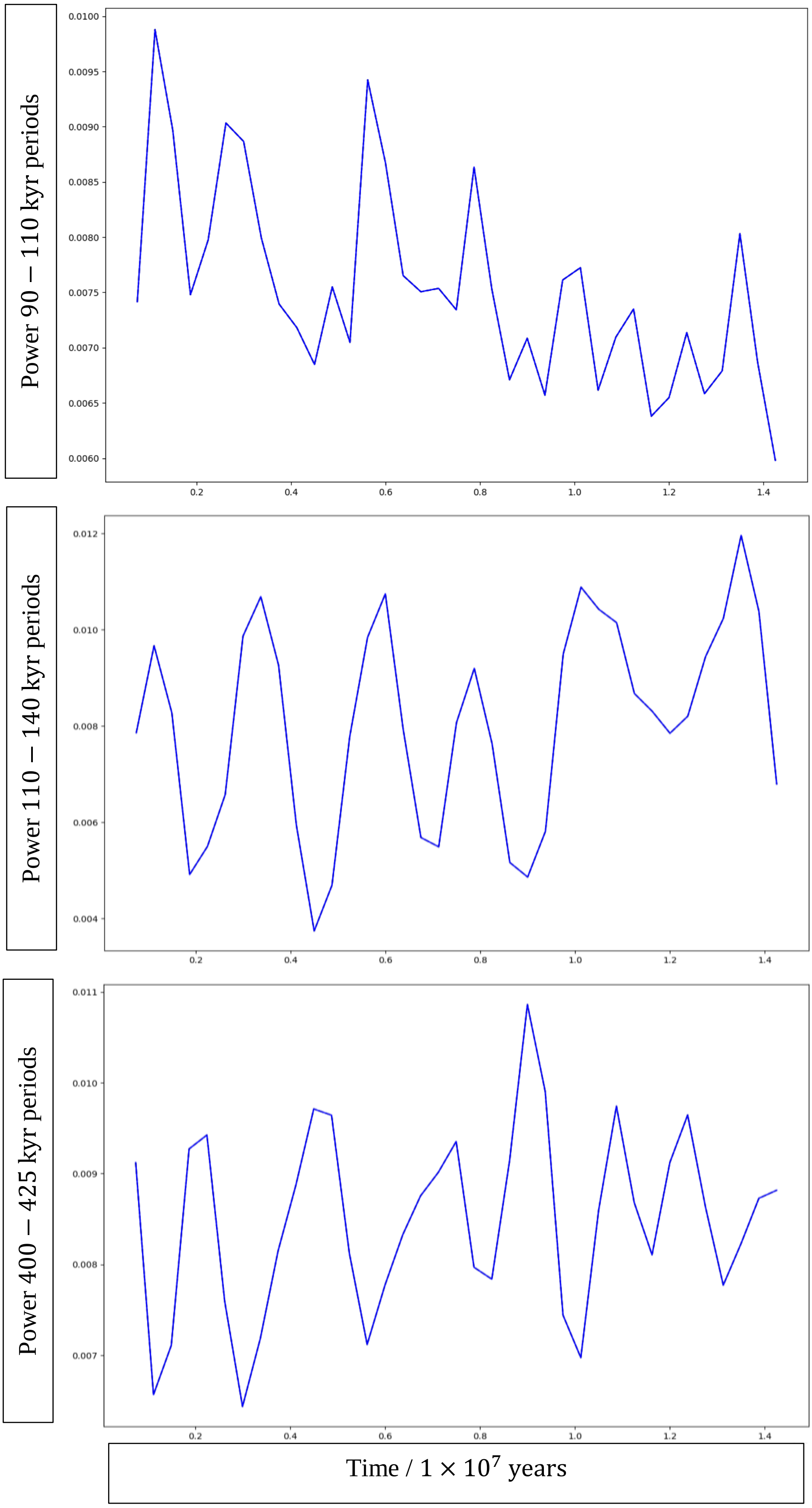


*Figure 29: FFTs of a 1.5 Myr rolling boxcar for periods 90-110 kyr , 110-140 kyr and 400-425 kyr showing the evolution of the power of eccentricity periods in these ranges over a 15 Myr time for case 101 (blue line) and baseline model (dashed black line – completely covered by the case 101 line).*

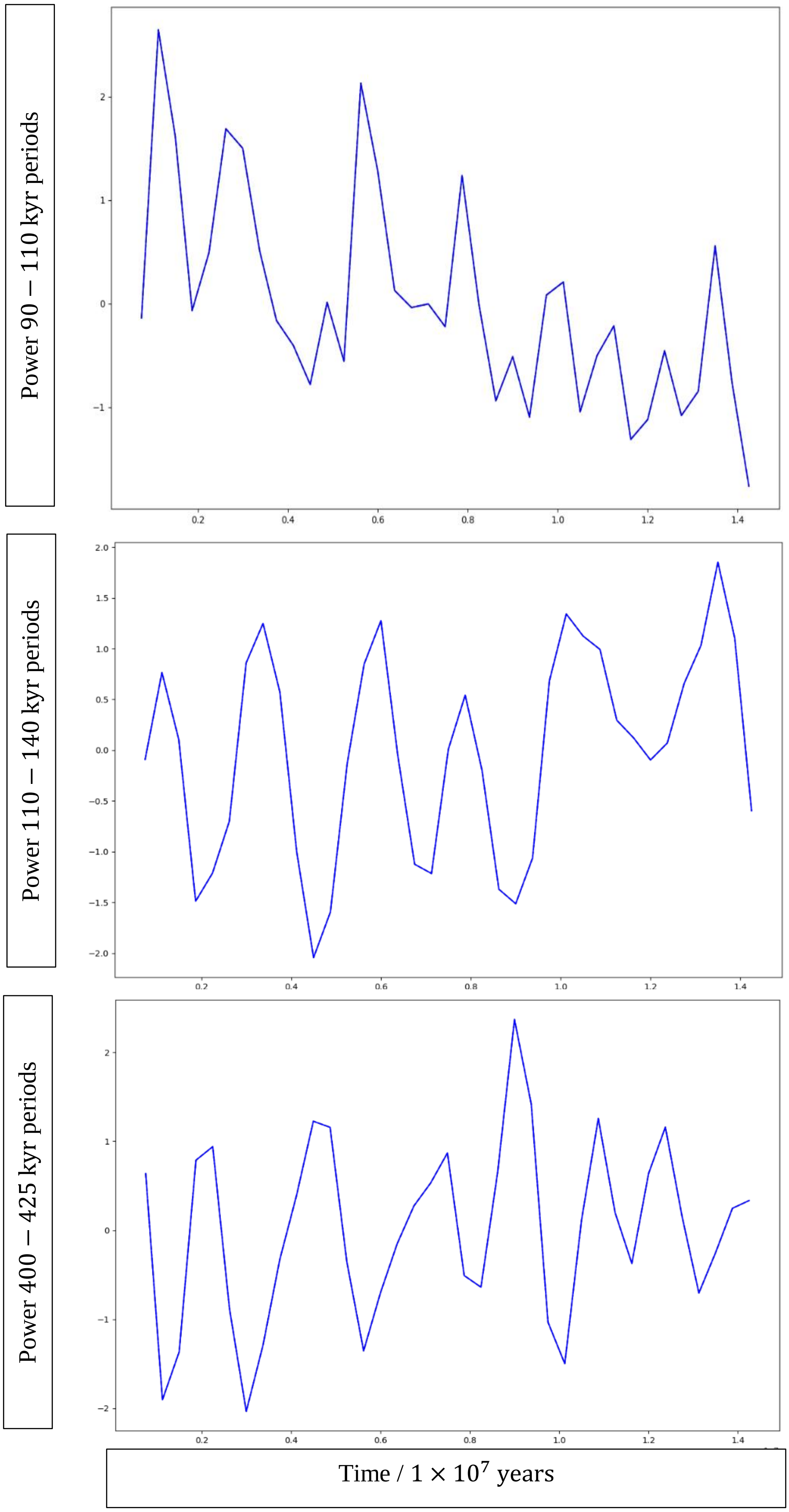


*Figure 30: FFTs of a 1.5 $Myr$ rolling boxcar for periods 90 – 110 $kyr$, 110 – 140 $kyr$ and 400 – 425 $kyr$ showing the evolution of the power of eccentricity periods (normalised to have a mean value of 0 and a standard deviation of 1) in these ranges over a 15 $Myr$ timescale for case 101 (blue line) and baseline model (dashed black line – completely covered by the case 101 line).*

Although, a single perturber has been shown to have little impact on Earth's eccentricity evolution, the passing of many bodies may yield differing results. The graphs below show the results of cases 102-107.

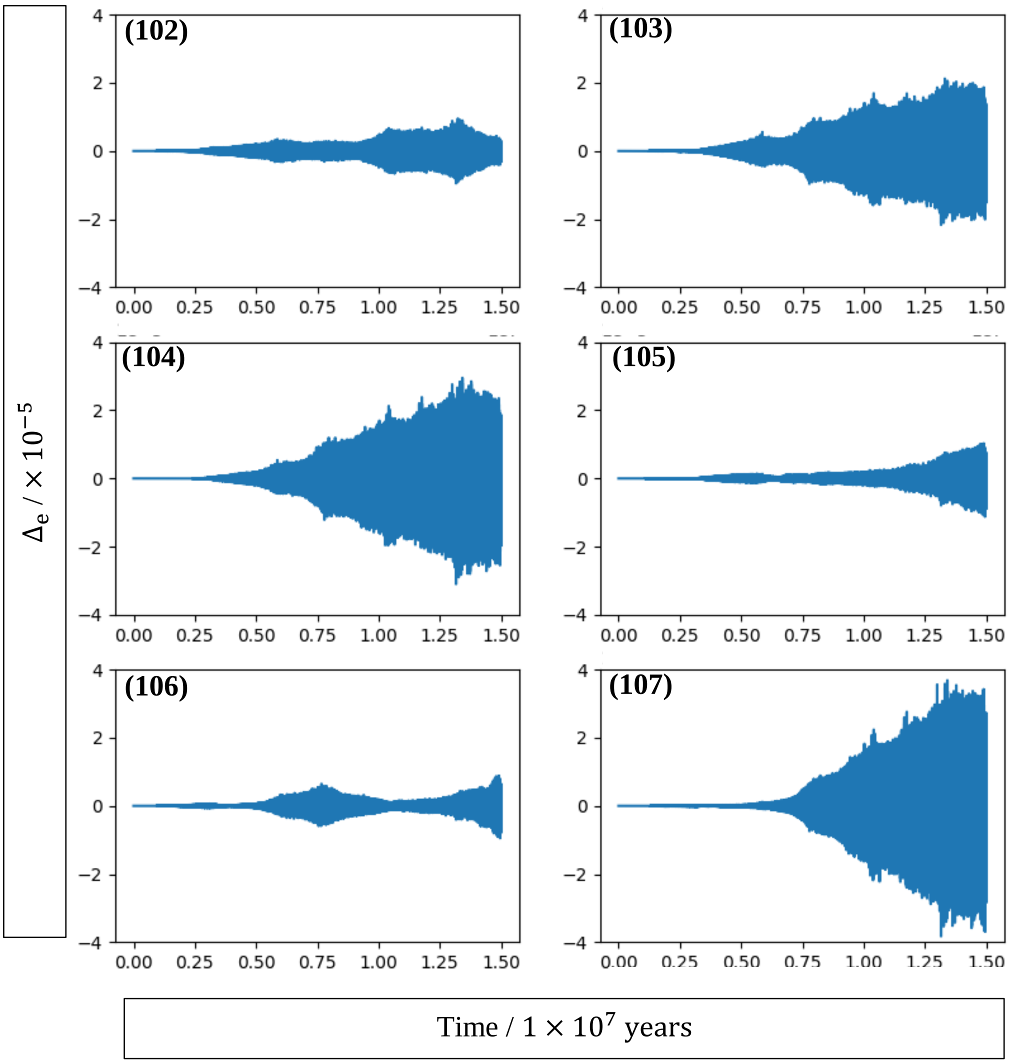


*Figure 31: A graph of the difference in eccentricity ($\Delta_e$) between the baseline model and cases 102-107.*

The results in figure 31 show that even with many perturbers passing every 50000 years, that the eccentricity of Earth varies only marginally from what was shown in the full-system baseline model. The cases do show though that the direction the perturber passed the system does have some influence the magnitude of $\Delta_e$. However, at an order of $10^{-5}$ concluding that particular regimes affect the system more than others is difficult, as the difference between the plots is small. The results suggest that for distances of 152000 AU, multiple flybys affect the system no more significantly than a single flyby.

To determine the impact of chaos on the system, three simulations, cases 108-110, were run. Each case passed perturbers at the same encounter distance, 152000 AU, coplanar to the system at 50 kyr intervals, but the masses of the perturbers were changed marginally between each case, 1 $M_{\odot}$, 1.0001 $M_{\odot}$ and 1.01 $M_{\odot}$ respectively. The results are shown in the figure below:

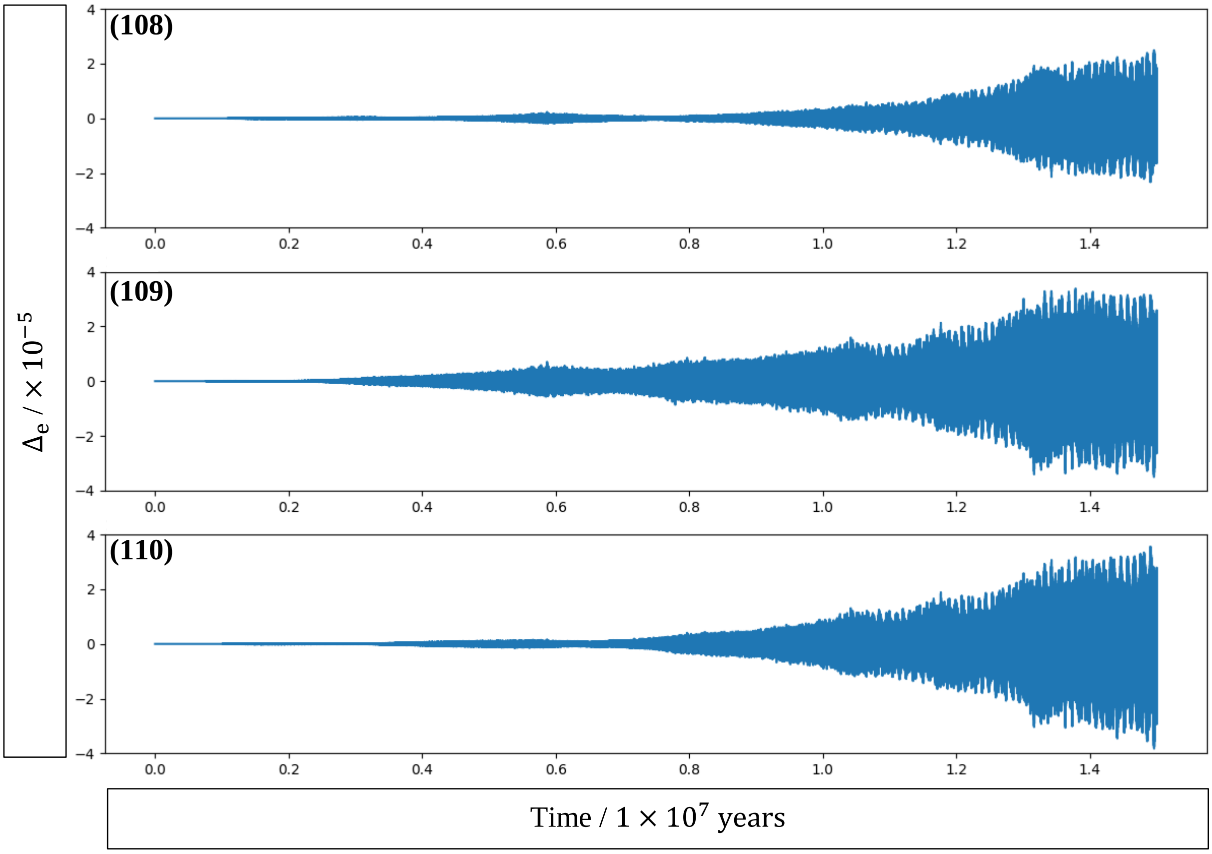


*Figure 32: A graph of the difference in eccentricity (Δe ) between the baseline model and cases 108-110*

All three cases see changes to Earth's eccentricity in the magnitude $10^{-5}$, demonstrating none of the masses investigated have a significant impact over the 15 myr timeframe. However, it can been seen that minor changes to the mass of the perturbing bodies can change the impact within the same magnitude. Case 110 demonstrates changes to Earth's eccentricity that are almost twice as large as those seen in case 108.

To investigate the nature of the growth of differences between cases 108-110 and the baseline model, the absolute difference in eccentricity, $|\Delta_e|$, was plotted on a log-linear scale. The upper envelope of the signals below correspond with the upper envelope of the signals formed by taking the absolute values of all points shown in figure 32. The results are shown in the figure overleaf.

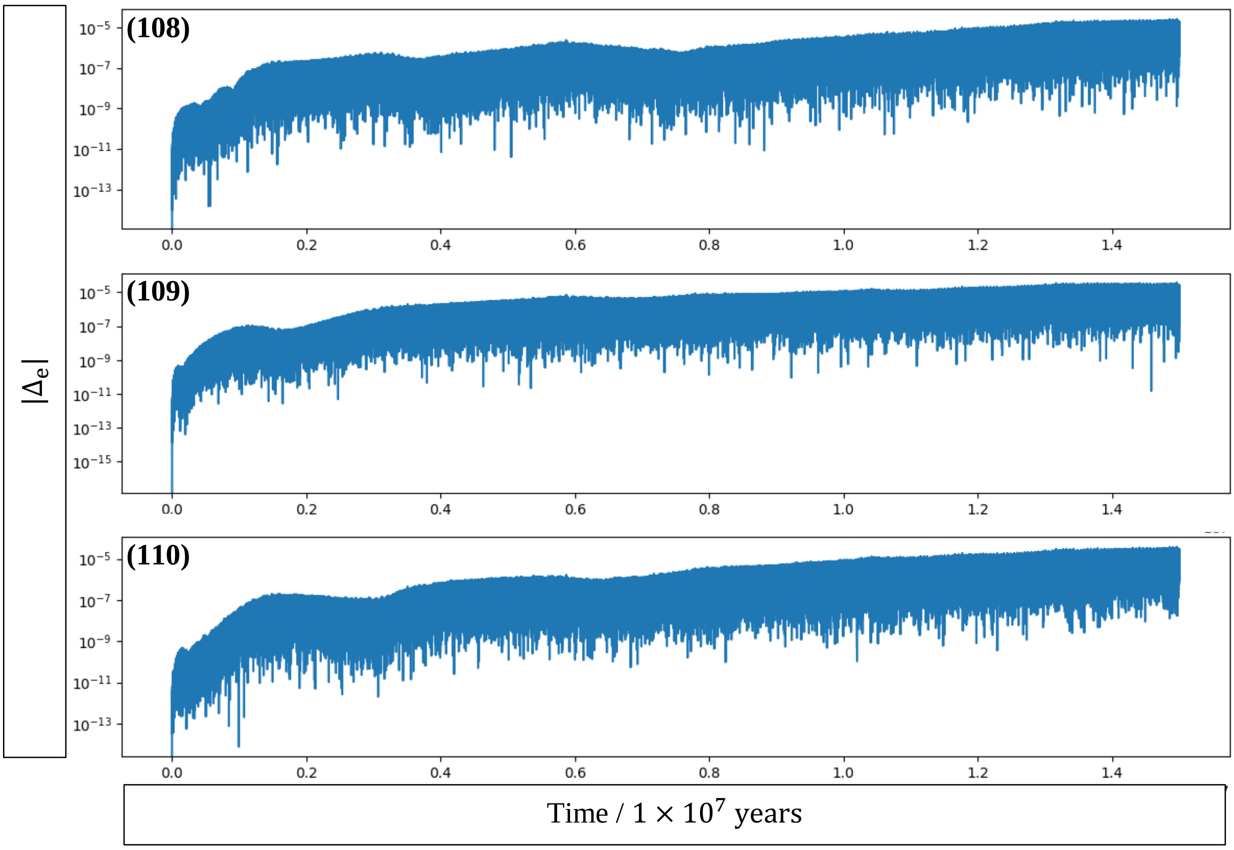


*Figure 33: A graph of the absolute difference in eccentricity ($|\Delta e|$ ) between the baseline model and cases 108-110 on a log-linear scale*

The graphs suggest that in all cases the differences in eccentricity initially grow erratically, changing between periods of exponential and sub-exponential growth, and even experiencing periods of decay. However, in all three cases the growth eventually moves to a more consistent exponential growth pattern. In case 108, the system experiences erratic sub-exponential growth for the first ~1.5 Myr. The following ~1.5 Myr sees exponential growth, at which point the change in eccentricity begins to decline for approximately ~0.5 Myr. Exponential growth resumes after this until around ~6 Myr into the simulation. Another period of decline is shown between ~6 Myr – ~7.5 Myr, before returning to an exponential growth for the remainder of the 15 Myr investigation.

Case 109 experiences similar changes to case 108, however, these occur earlier within the simulation. The initial sub-exponential growth lasts only ~1 Myr rather than the ~1.5 Myr experienced in case 108. This is followed by a period of decline for around ~0.5 Myr. Sub-exponential growth returns until around ~6 Myr, before experiencing a decline similar to that experienced by case 108. This decline lasts for ~1 Myr before exponential growth returns for the rest of the model.

In case 110, the first ~0.25 Myr shows growth in the differences of Earth's eccentricity, followed by a short period of decline. This is followed by ~0.75 Myr of exponential growth, which tapers of to a sub-exponential growth for ~0.25 Myr. The changes between the baseline model and case 110 begins to decline for a longer period than experienced by cases 108 and 109, lasting around ~1.25 Myr. Sub-exponential growth then resumes for approximately ~3 Myr. At around ~6 Myr, and similar to cases 108 and 109, the model experiences a decline in the changes to eccentricity for ~0.5 Myr. Exponential growth then resumes for the remainder of the model.

To further analyse the results, the results were plotted on a log-log plot, the results of which are shown below:

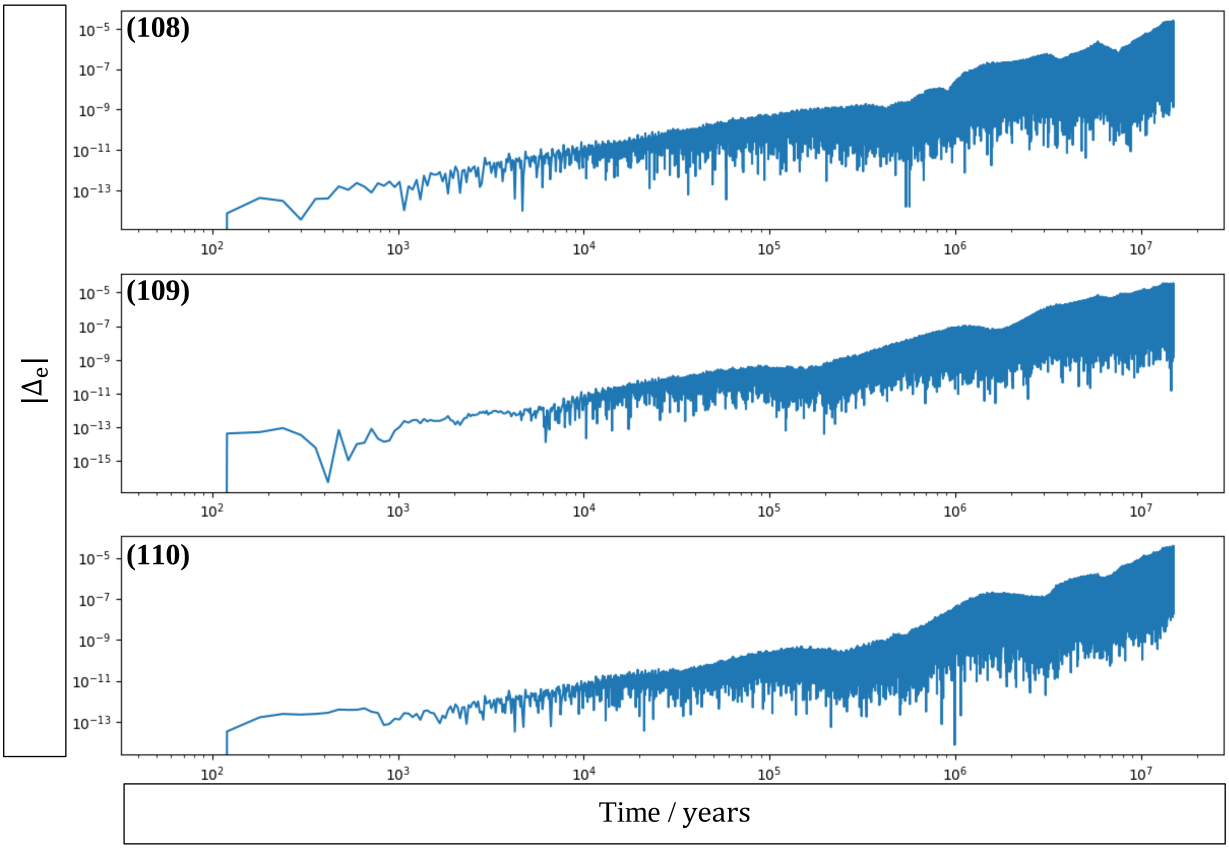


*Figure 34: A graph of the absolute difference in eccentricity (|Δe| ) between the baseline model and cases 108-110 on a log-log scale*

When shown on a log-log plot, the results from cases 108-110 show an increase in error throughout the model due to round-off error during each calculation step. It can be seen that the smallest values measured in the models are in the magnitude of $10^{-15}$. However, as the simulation progresses the minimum values of $|\Delta_e|$ registered begin to rise, despite the values of $\Delta_e$ passing through 0, demonstrating a build-up of error.

### 3.1.3 Coplanar flybys: Cases 201-209 & 301-309

Cases 201-227 were conducted to test the impact of decreasing encounter distance and increasing perturber mass compared to those outlined in cases 102-107. These were repeated again but with Jupiter removed to determine the role of Jupiter within these simulations. Further to this, cases 201-227 were repeated once more, this time with a slower encounter rate to also investigate how the speed at which the perturbers passed the system, influenced the effects observed.

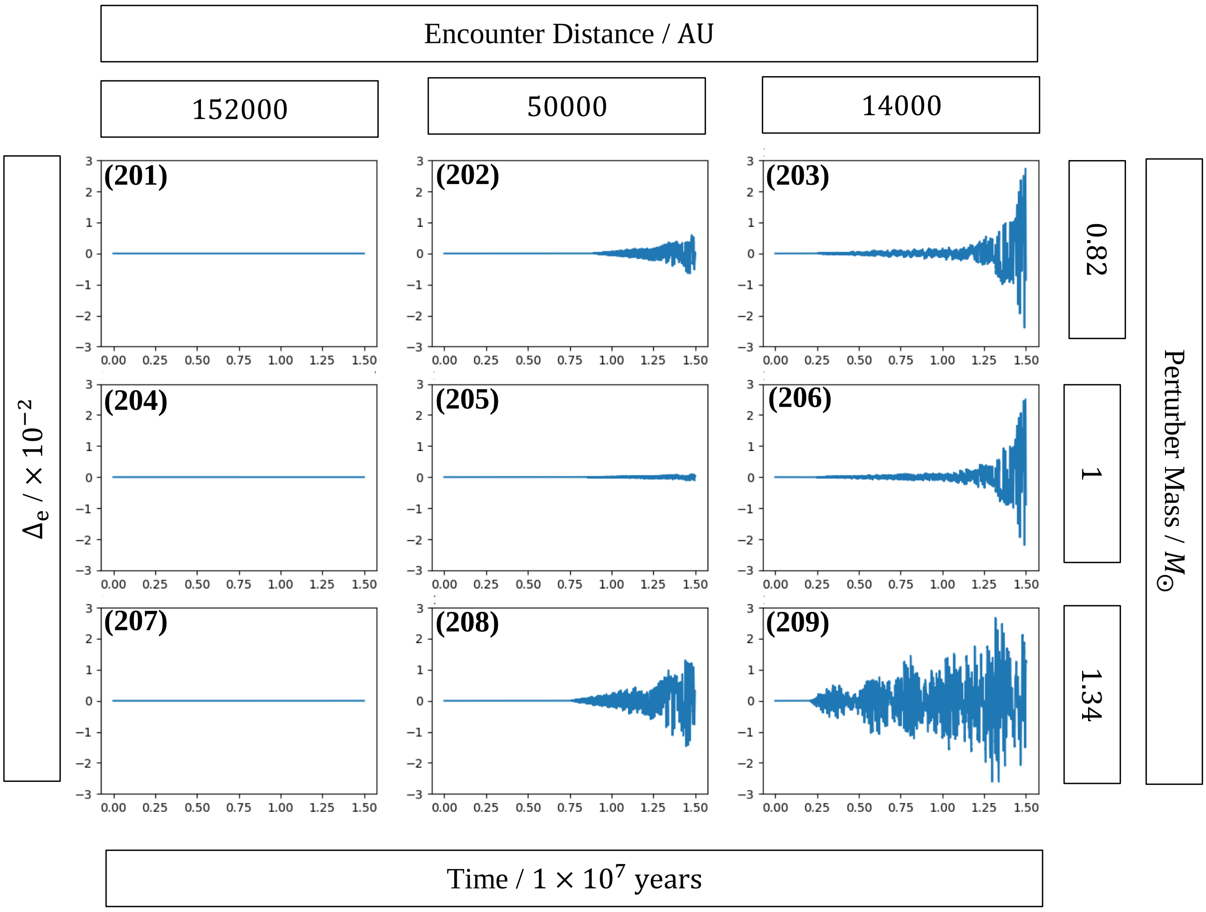


*Figure 35: Graphs of cases 201-209 showing the change in Earth's eccentricity $\Delta_e$ compared to the full-system baseline model.*

For all cases 201-209 with an encounter distance 152000 AU, there was little change in eccentricity compared with the baseline. However, at an encounter distance of 50000 AU more substantial changes in the eccentricity were presented. For masses 0.82 $M_\odot$ and 1.34 $M_\odot$ the magnitude of $\Delta_e$ is the same order as in the changes in the baseline, showing a significant effect. Surprisingly, the 1 $M_\odot$ encounter showed a lesser change than the smaller 0.82 $M_\odot$ encounter, suggesting an element of randomness in the results. Encounters at the closest distance showed a greater effect, with the largest mass encounter of these being the largest of these. Changes of the same magnitude as those in the baseline suggest some significant impact of the perturber. This may be either an increase/decrease in the maxima's/minima's of the eccentricity signal, or a change to the periods of the eccentricity cycles. Conducting FFTs on a rolling boxcar of 1.5 Myr for periods $90 - 110$ kyr, $110 - 140$ kyr and $400 - 425$ kyr, a graphical representation of the strength of the periods within these ranges was obtained, similar to the work conducted by Lisiecki (2010), and provides a more useful way of evaluating the impact the effect on the cycle variations..

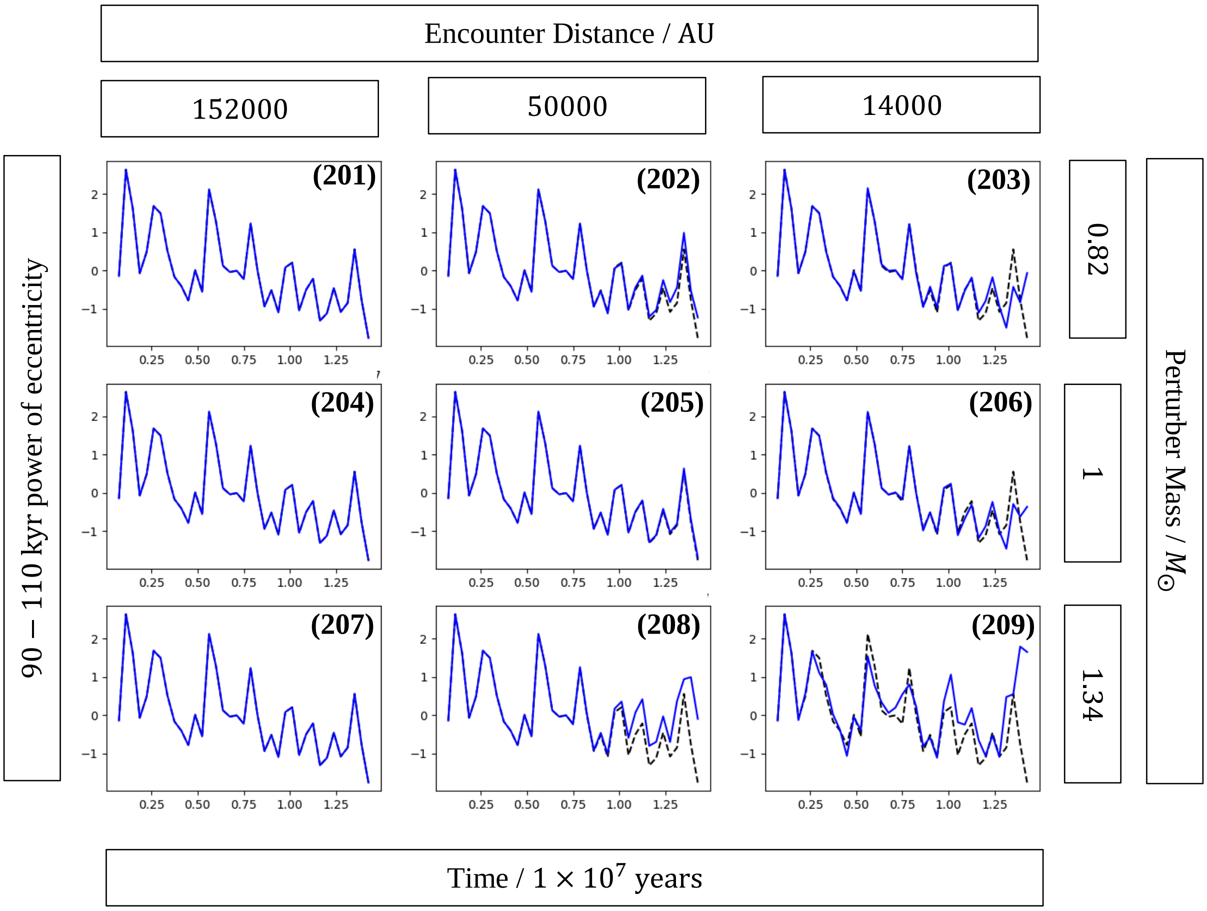


*Figure 36: Graphs of the FFT performed on a rolling boxcar of* 1.5 *Myr on Earth's eccentricity periods for* $90 - 110$ *kyr normalised to have a mean value of* 0 *and a standard deviation of* 1. *The dashed line is the result from the baseline data, and the blue is the result from the respective case 201-209*

The results from the FFTs show that in the 50000 AU encounters for masses 0.82 $M_{\odot}$ and 1.34 $M_{\odot}$ the power of the $90 - 110$ kyr periods was increased in the last ~4 Myr. In comparison, in the 14000 AU encounters for masses 0.82 $M_{\odot}$ and 1 $M_{\odot}$ the power of the $90 - 110$ kyr periods was initially increased in between the last ~4 Myr – ~2 Myr, before being decreased for ~2 Myr, finally being increased again in the last ~1 Myr. Finally, in the 14000 AU encounter for mass 1.34 $M_{\odot}$ from ~1.25 Myr the power of the $90 - 110$ kyr periods varies compared to the full-system baseline FFT, more frequently being increased in power than decreased.

The quasiperiodic terms within this range, term 2 and term 4, both involve the $g_5$ Jupiter term (Matthews and Frohlich, 2002). This suggests that that the effects observed in the power spectrum may be related to Jupiter. Additionally, as the flybys in these models were coplanar to the solar system, they would almost be in the plane of Jupiter, also pointing to Jupiter as playing a role in these results. Eccentricity modulates the precession of a planet's perihelion and effects the fundamental frequencies of that precession (Huybers and Aharonson, 2010). In follows that large enough perturbations to a planet's eccentricity will result in alterations to the planet's fundamental frequency of precession, and that secular resonances involving this frequency would change. Therefore, looking at the perturbations to Jupiter's eccentricity may yield values of $\Delta_e$ that correlate with noticeable changes to Earth's eccentricity cycles.

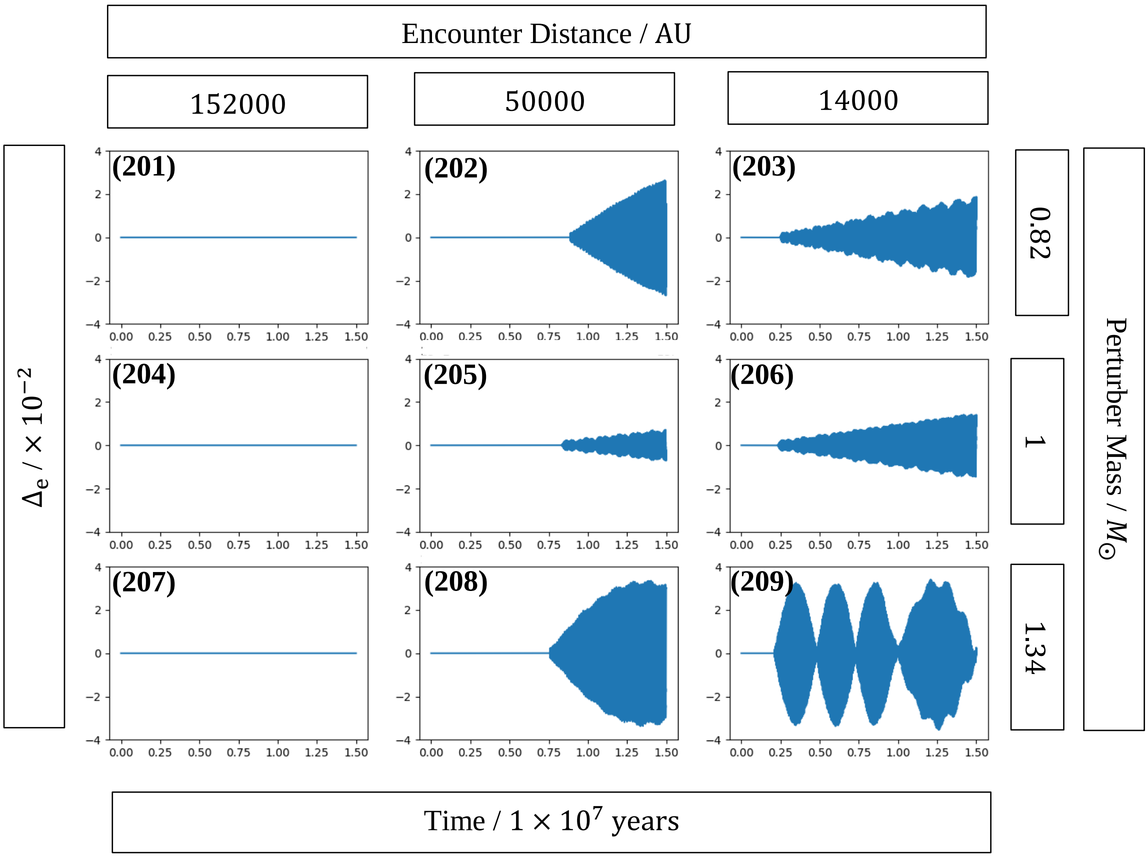


*Figure 37: Graphs of cases 201-209 showing the change in Jupiter's eccentricity $\Delta_e$ compared to the full-system baseline model.*

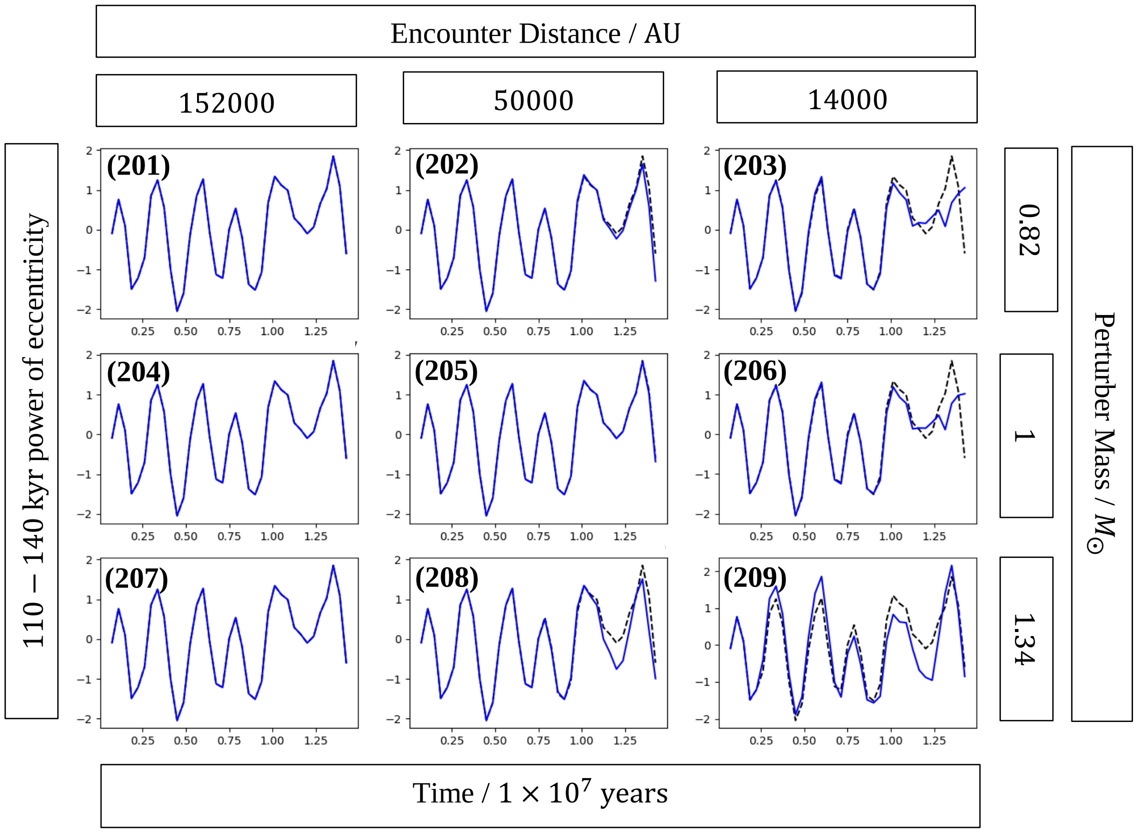


*Figure 38: Graphs of the FFT performed on a rolling boxcar of* 1.5 *Myr on Earth's eccentricity for periods* $110 - 140$ *kyr normalised to have a mean value of* 0 *and a standard deviation of* 1. *The dashed line is the result from the baseline data, and the blue is the result from the respective case 201-209*

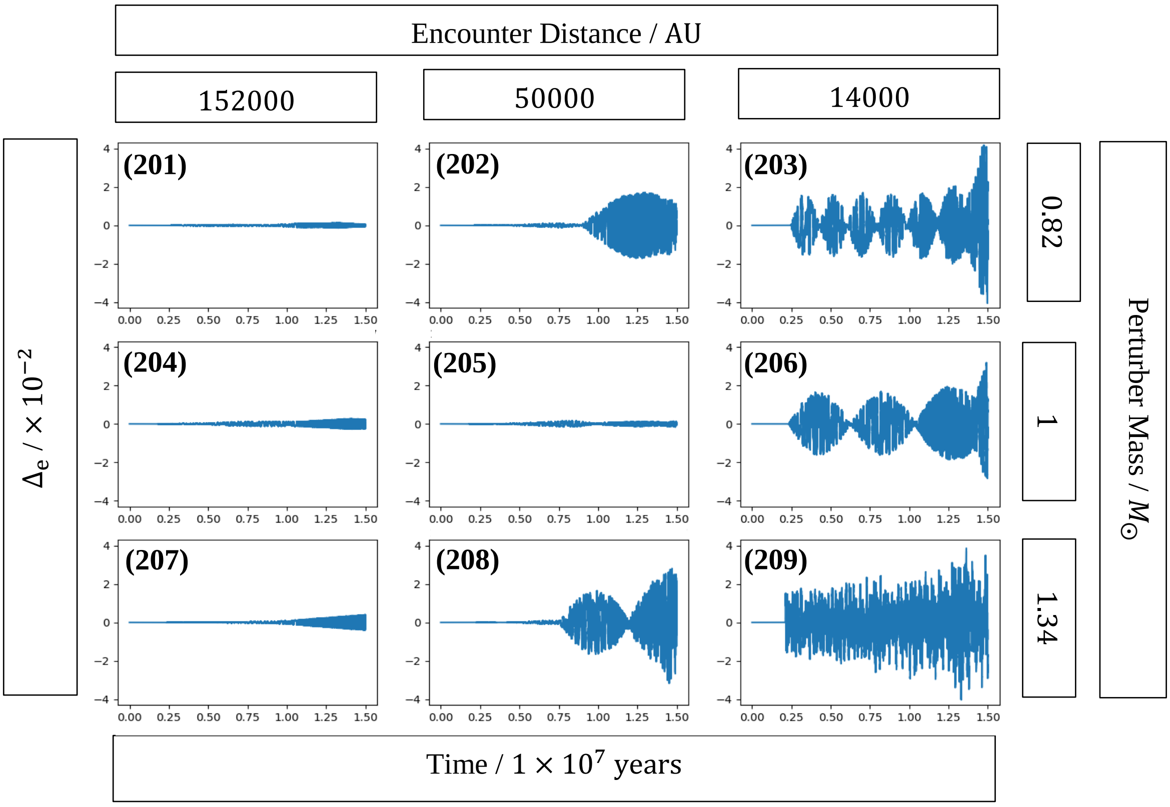


*Figure 39: Graphs of cases 201-209 showing the change in Venus's eccentricity* $\Delta_e$ *compared to the full-system baseline model.*

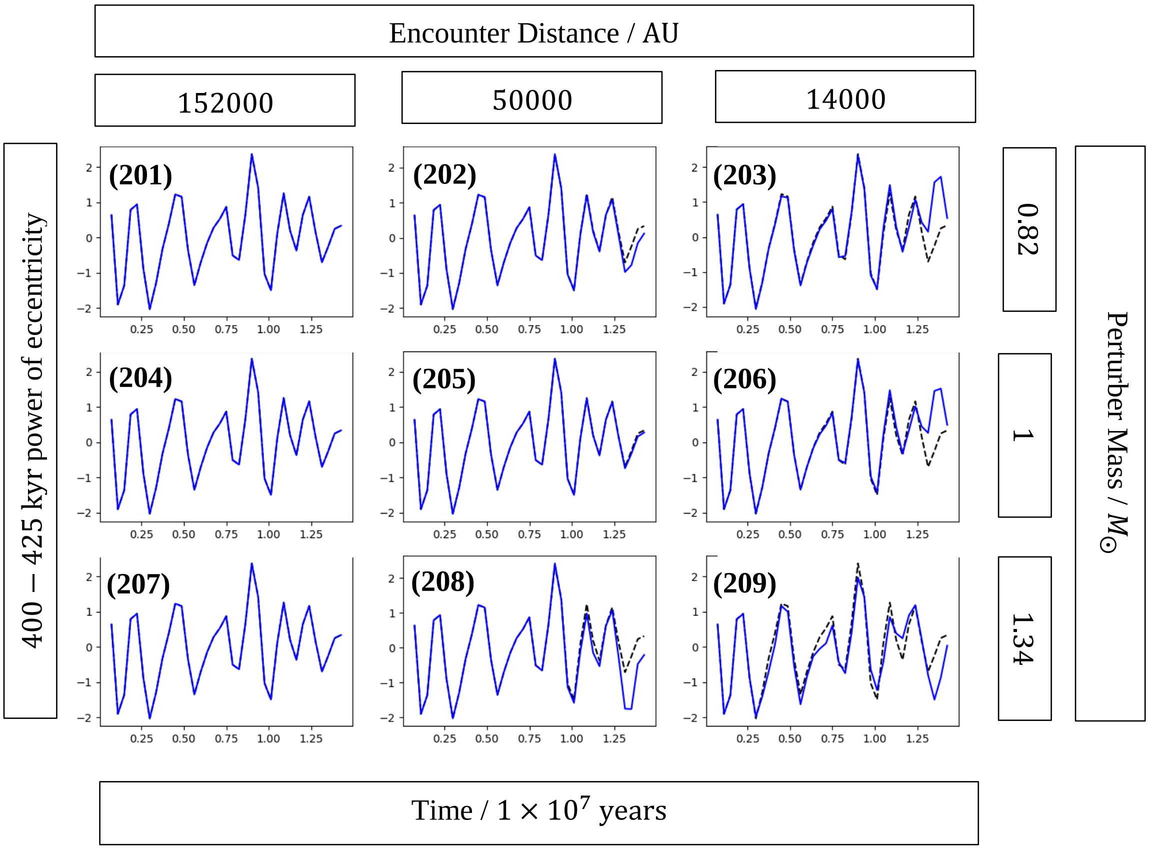


*Figure 40: Graphs of the FFT performed on a rolling boxcar of* $1.5$ *Myr on Earth's eccentricity for periods* $400 - 425$ *kyr normalised to have a mean value of* $0$ *and a standard deviation of* $1$*. The dashed line is the result from the baseline data, and the blue is the result from the respective case 201-209*

Figure 37 shows the how Jupiter's eccentricity varied against to the baseline model. Comparing this with the FFTs in figure 36, it can be seen that noticeable variations to the power of the $90 - 110$ kyr cycles in Earth's eccentricity begin to occur when Jupiter's eccentricity is perturbed by $\sim 1.55 \times 10^{-2}$; either positively or negatively. This pattern is displayed throughout the cases and gives reason to the lack of effect observed in the $50000$ AU encounter at $1_\odot$, case 205. Although the perturbation to Jupiter's orbit is in the order of $10^{-2}$, they do not reach the $\sim 1.5 \times 10^{-2}$ threshold, and so no sizeable impact is observed in the power spectrum. This association is also observed with the power spectrums of the $110 - 140$ kyr eccentricity cycles (figure 38) despite Jupiter not being involved in the terms which modulate these cycles. However, these terms both involve Venus, and when looking at the plots of the changes to Venus's eccentricity, a similar pattern emerges. Looking at figure 39, the changes to the power of Earth's $110 - 140$ kyr eccentricity cycles occur when Venus's eccentricity is perturbed $\sim 1.65 \times 10^{-2}$. The moment that Venus's eccentricity is perturbed by this amount approximately coincides with Jupiter being perturbed by the $\sim 1.55 \times 10^{-2}$ threshold in several cases. This suggests that there may be some interaction between the planets and that potentially Jupiter has an indirect effect by modulating the orbit of Venus.

The $\sim$400 kyr cycle is primarily as a result of the interaction between Venus and Jupiter in the first of the quasiperiodic terms (Matthews and Frohlich, 2002), and is modulated by beats formed from other resonances (Matthews and Frohlich, 2002; Pälike, 2005). Yet the plots for the $400 - 425$ kyr cycle (figure 40) do not match neatly with either the changes in Venus or Jupiter. Most notably, in the previous discussion, a rationale to why no noticeable effect was observed in case 205. However, an effect on the power of the $400 - 425$ kyr cycle is seen in the last 1.25 Myr.This suggests that the causes of the changes to the to $400 - 425$ kyr cycle are the result of more complex interactions. This is supported by the fact that the modulating beats involve at least four planets (Matthews and Frohlich, 2002; Pälike, 2005).

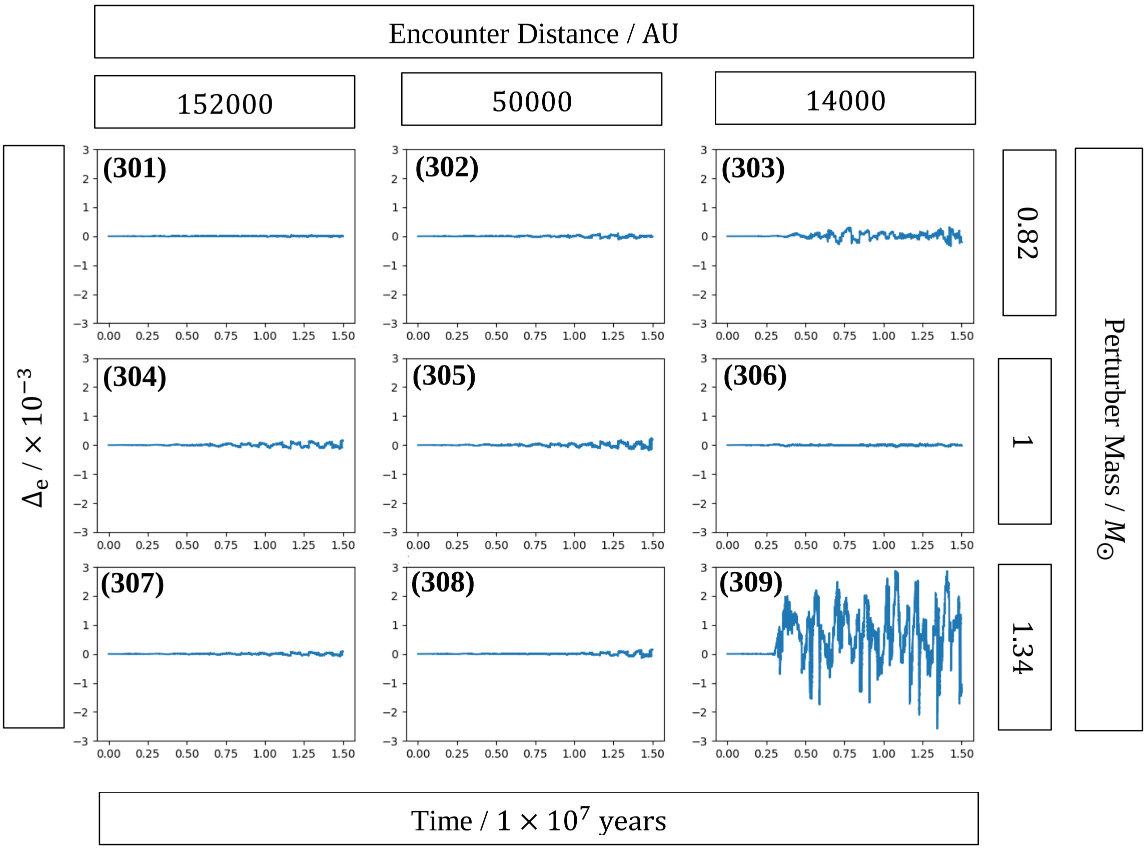


*Figure 41: Graphs of cases 301-309 showing the change in Earth's eccentricity $\Delta_e$ compared to the Jupiter-less baseline model*

.

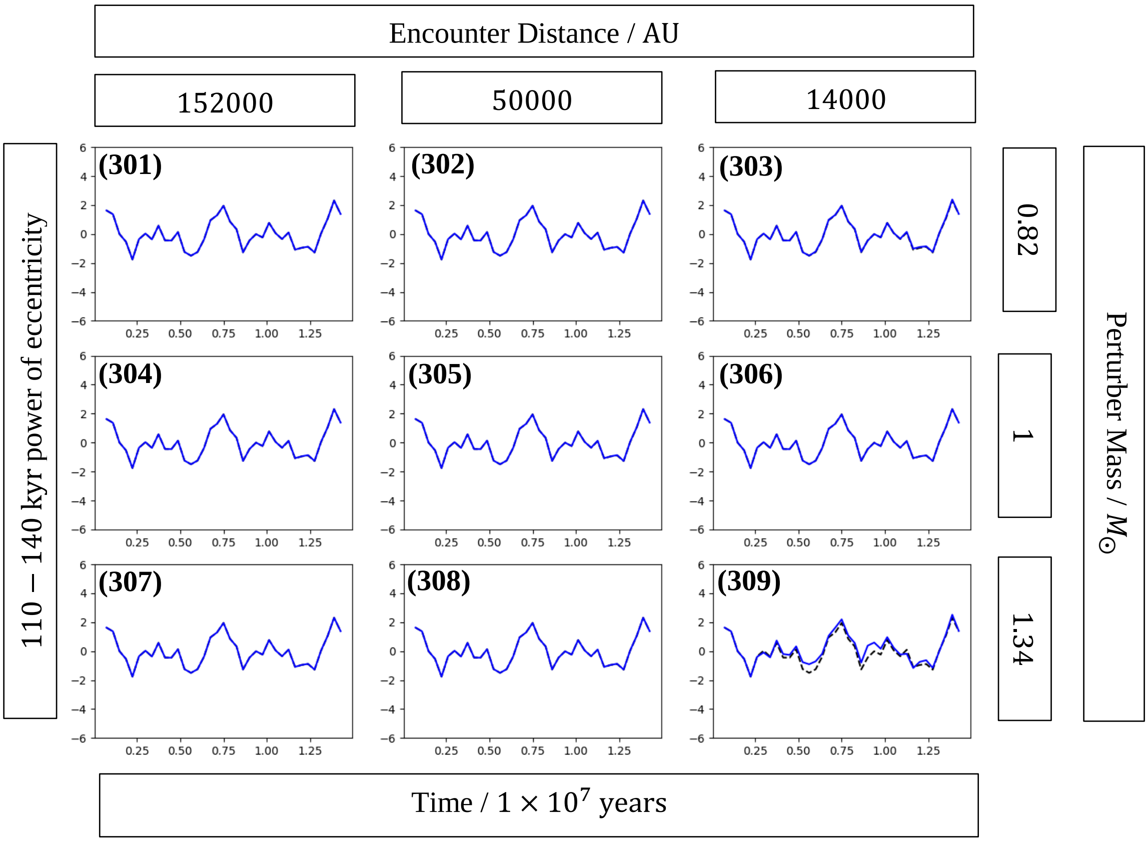


*Figure 42: Graphs of the FFT performed on a rolling boxcar of* 1.5 *Myr on Earth's eccentricity for periods* 110 – 140 *kyr normalised to have a mean value of* 0 *and a standard deviation of* 1. *The dashed line is the result from the baseline data, and the blue is the result from the respective case 301-309*

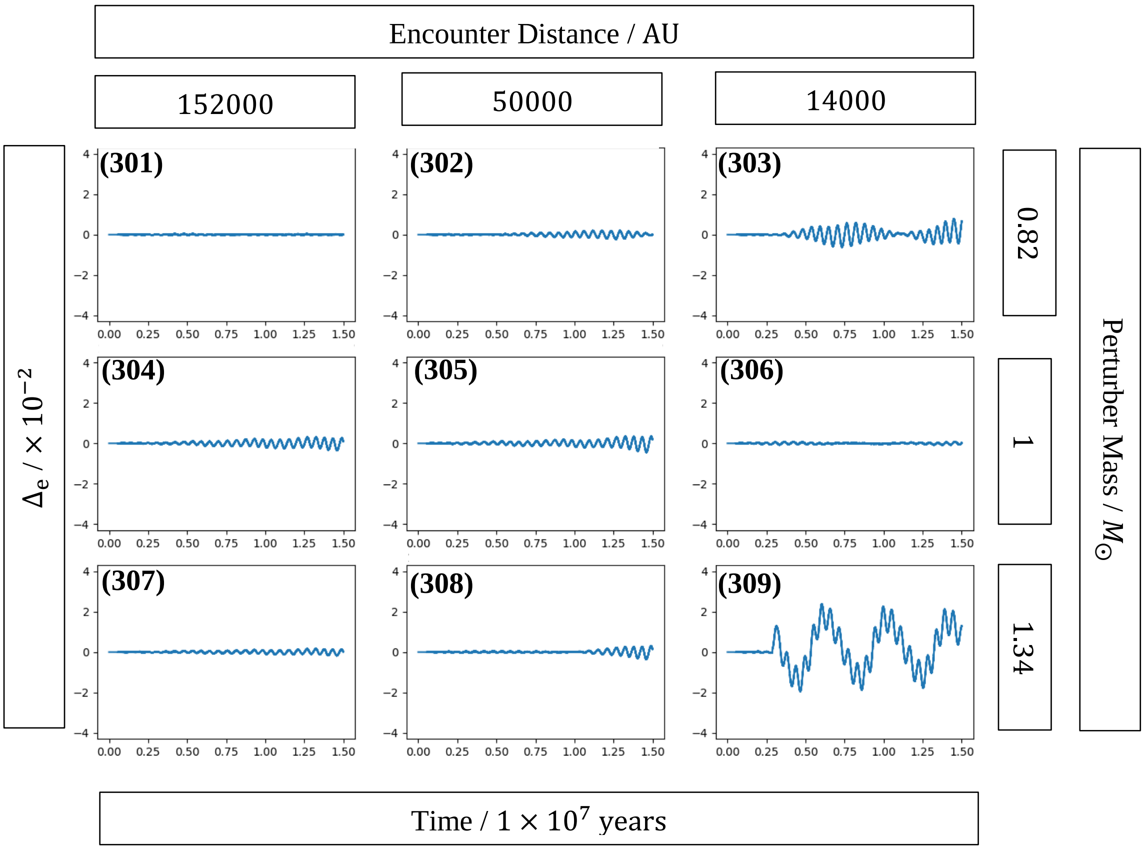


*Figure 43: Graphs of cases 301-309 showing the change in Venus's eccentricity $\Delta_e$ compared to the full-system baseline model.*

The results suggest that Jupiter and Venus both play a role in the most substantial perturbations of Earth's eccentricity observed in figure 35. To evaluate these claims, the models were run again but without the presence of Jupiter and compared with the Jupiter-less baseline model. Figure 41 shows the results of cases 301-309. Without Jupiter in the system, the changes to Earth's eccentricity is an order of magnitude lower that observed in the full-system equivalents. Although Earth's eccentricity in the Jupiter-less baseline model does vary less than in the full-system model, the difference is not substantial enough to account solely for the significant reduction in the perturbations observed in cases 301-309. This suggests that Jupiter does indeed influence the magnitude of the perturbations observed in cases 201-209.

In the Jupiter-less model, the peaks at $\sim 95$ kyr and $\sim 400$ kyr are removed or shifted. This leaves the $\sim 125$ kyr cycle as the only comparable cycle between the models. Figure 42 show the evolution of the $\sim 125$ kyr cycle. The evidence in cases 201-209 suggested that Venus may be the cause of the changes to the power of the $\sim 125$ kyr cycle, but that a possible interaction with Jupiter may also be a factor. In cases 301-309, only the case with the smallest encounter distance and greatest perturber mass showed any noticeable difference to the power of the cycle in the 15 Myr timeframe. This suggests that Jupiter does exacerbate the perturbations of the $\sim 125$ kyr cycle, despite not being featured in the quasiperiodic terms that lead to the cycle (Matthews and Frohlich, 2002; Pälike, 2005). Similarly to in cases 201-209, the changes to the $\sim 125$ kyr cycle appear once Venus reaches a perturbation of $\sim 1.65 \times 10^{-2}$, with case 309 being the only case to reach this (see figure 43). Therefore, it seems that Jupiter's role in the perturbations of these cycles from the passing perturbers may be an indirect link; one where the perturbations of Jupiter's eccentricity result in greater variation to the eccentricity of Venus, subsequently changing the power of the cycles that Venus influences.

### 3.1.4 Non-coplanar flybys: Cases 210-227 & 310-327

Cases 201-209 showed that in some scenarios where the encounter distance of the flybys was reduced or the perturber mass was increased that noticeable changes to Earth's eccentricity are plausible as a result of perturbations to Jupiter's and Venus's orbits. Yet, it may be expected that these changes will be the greatest when the perturber passes in a similar plane to Jupiter, and that more inclined orbits may show a reduced effect (Jiménez-Torres et al., 2011). Cases 210-227 investigate the same array of encounter distances and masses as in cases 201-209, but with two different encounter inclinations; $60°$ for cases 210-218, and $90°$ for cases 219-227.

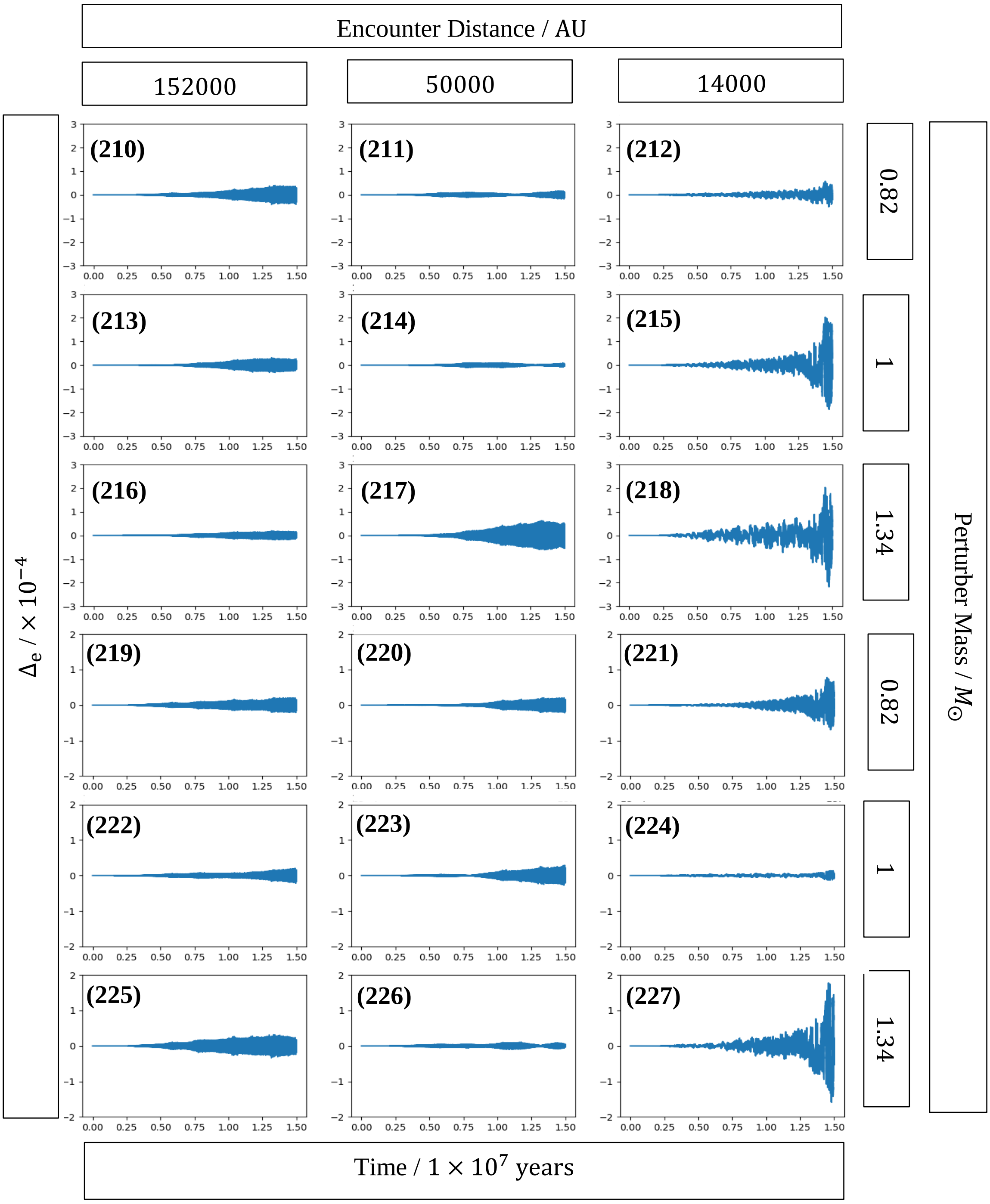


*Figure 44: Graphs of cases 210-218 (at an inclination of 60°) and cases 219-227 (at an inclination of 90°) showing the change in Earth's eccentricity $\Delta_e$ compared to the full-system baseline model.*

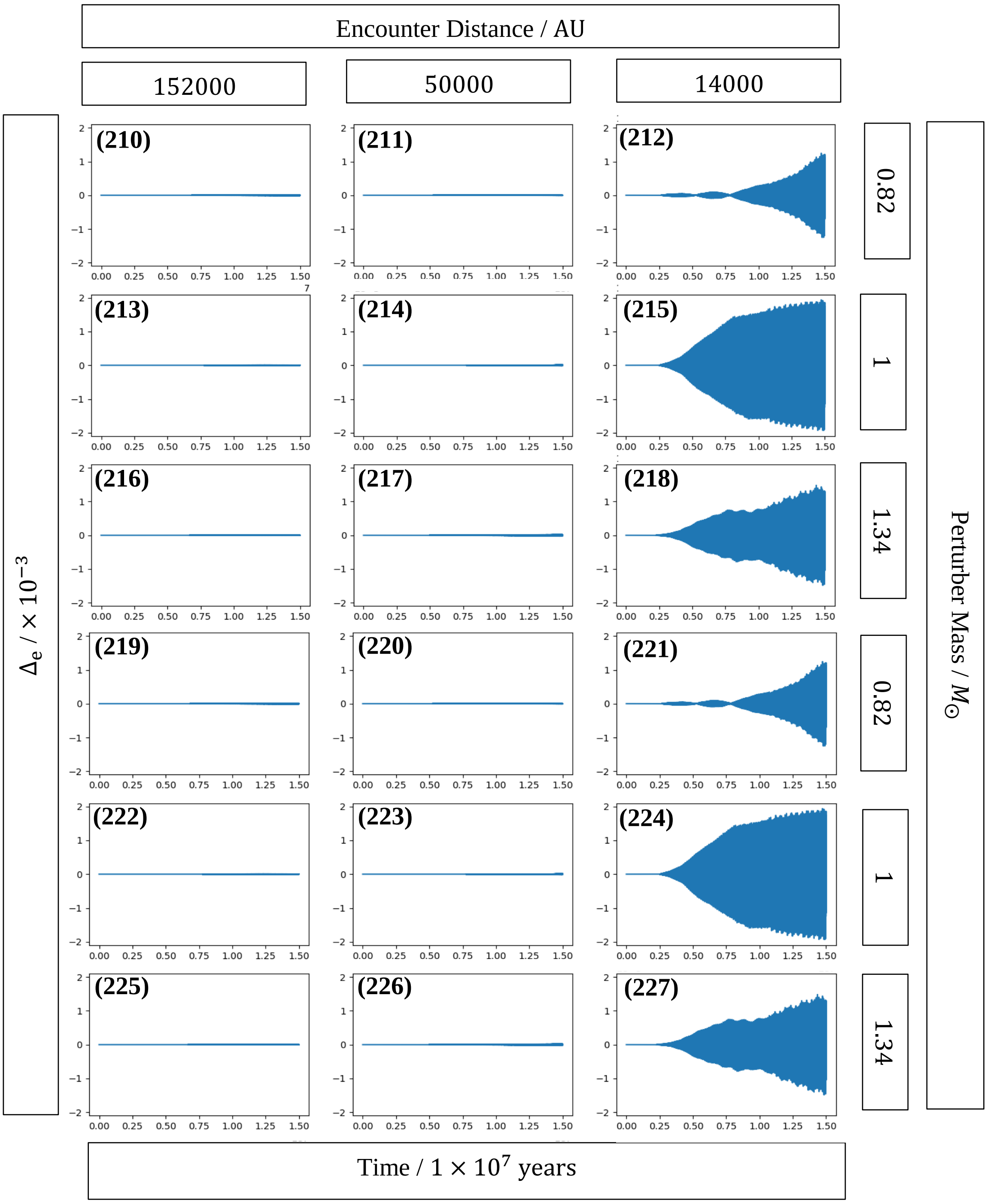


*Figure 45: Graphs of cases 210-218 (at an inclination of 60°) and cases 219-227 (at an inclination of 90°) showing the change in Jupiter's eccentricity $\Delta_e$ compared to the full-system baseline model.*

The results from cases 210-227 show changes to Earth's orbit two orders of magnitude below those observed in cases 201-209. This suggests that Jupiter has not been perturbed by the required amount to cause noticeable changes to Earth's eccentricity cycles. Figure 45 shows that Jupiter is only perturbed in the magnitude $10^{-3}$, significantly below the $\sim 1.55 \times 10^{-2}$ threshold found in cases 201-209. Comparing these results against the Jupiter-less models demonstrates how Jupiter interacts with Earth during a series of inclined fly-bys.

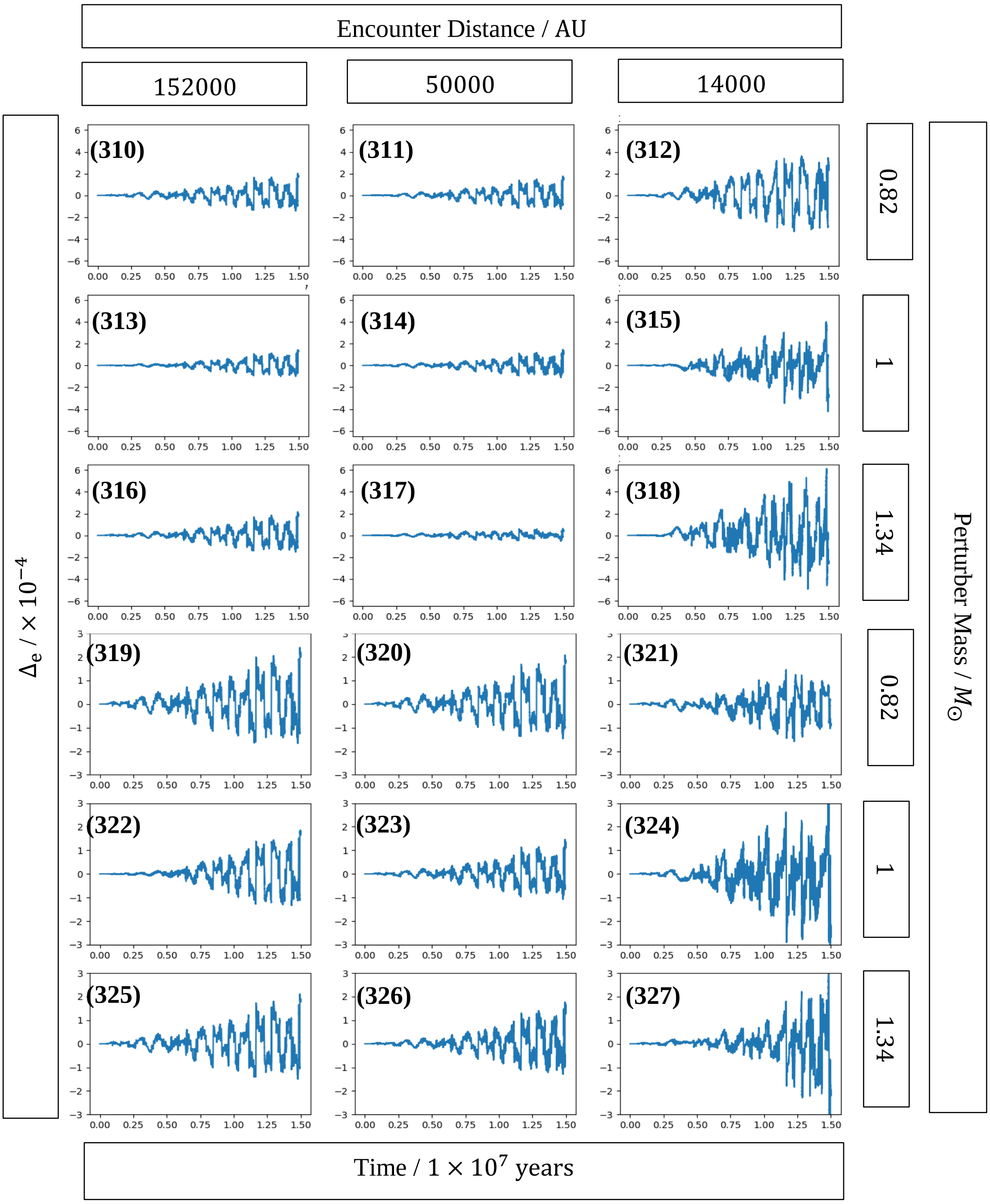


*Figure 46: Graphs of cases 310-318 (at an inclination of 60°) and cases 319-327 (at an inclination of 90°) showing the change in Earth's eccentricity $\Delta_e$ compared to the Jupiter-less baseline model.*

Figure 46 shows that although the changes to $\Delta_e$ in the Jupiter-less model are in the same order of magnitude as in the full-system model, the changes to Earth's eccentricity are actually greater with Jupiter removed. This suggests that Jupiter provides some stability when the perturbers' path is inclined. However, as the differences between the Jupiter-less and full-system models are small, it may be argued that there is insufficient evidence to suggest Jupiter provides this stability, especially given the chaotic nature of the system.

## 3.1.5 Summary

The results from cases 201-227 suggest that when passing stars are near-coplanar to the system, significant changes to Earth eccentricity can be achieved. However, as the encounter inclination increases, the impact on Earth's orbit decreases substantially. The figure below summarises cases 201-227:

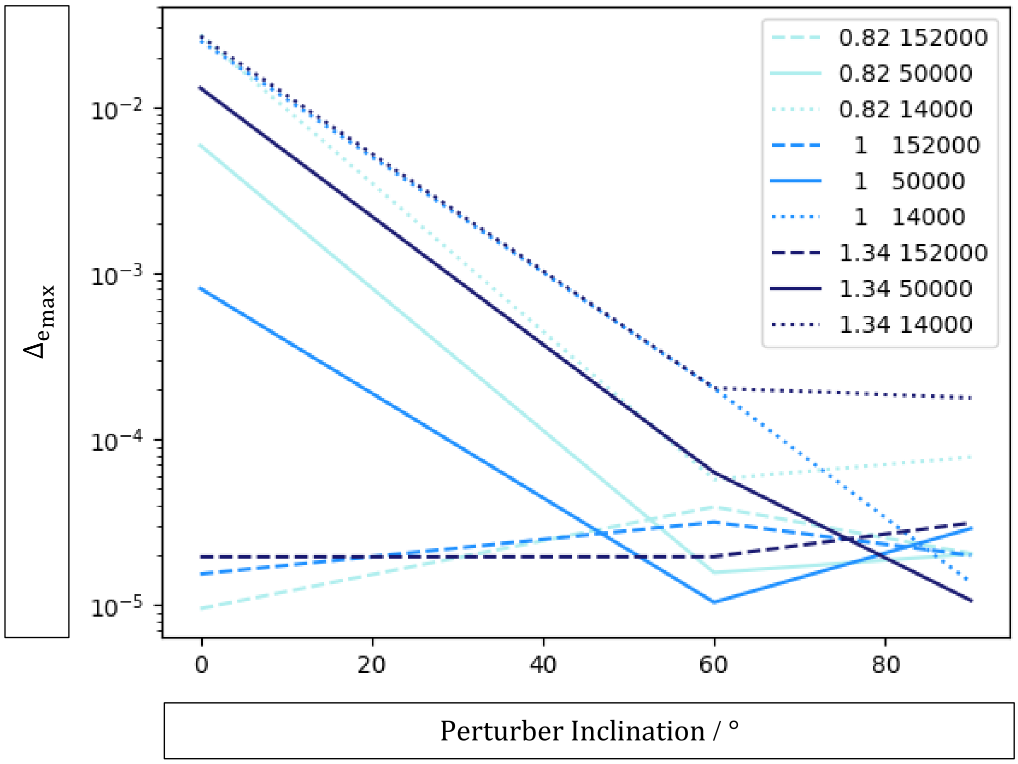


*Figure 47: Graph of the maximum $\Delta_e$ recorded plotted against encounter inclination for 9 combinations of perturber mass ($0.82\ M_\odot$, $1\ M_\odot$ and $1.34\ M_\odot$) and perturber encounter distance ($152000\ AU$, $50000\ AU$ and $14000\ AU$).*

Further analysis from cases 301-327 suggest that the impact caused from near-coplanar encounters is a result of Jupiter's orbit being perturbed enough ($\Delta_e > \sim 1.55 \times 10^{-2}$) to exacerbate changes to Earth's orbit. Yet when these stars are inclined Jupiter may offer some stability to the cycles. The models showed that perturbations to Jupiter's orbit could promote alterations to Venus's eccentricity enough ($\Delta_e > 1.65 \times 10^{-2}$) to produce changes in the eccentricity cycles governed primarily by Venus, and that do not feature Jupiter in the quasiperiodic terms of the cycle (Pälike, 2005). In the cases where Earth's eccentricity cycles were noticeably changed, the encounter distances were small ($< 50{,}000$ AU) and the largest effects were associated with the largest perturber masses. Although there is some evidence of randomness shown in the results, for example where the $1\ M_\odot$ perturbers caused a smaller effect than the $0.82\ M_\odot$ perturbers, this is most likely to be due to the chaotic nature of the system.

The changes to Earth's eccentricity are the result of increases or decreases to the power of the $\sim 95$ kyr, $\sim 125$ kyr and $\sim 400$ kyr cycles, rather than increases to the maximum eccentricity value observed for Earth. The $\sim 95$ kyr and $\sim 125$ kyr cycles together make a $\sim 100$ kyr cycle (Matthews and Frohlich, 2002; Muller and MacDonald, 1997; Pälike, 2005). This cycle is shown to anticorrelate with the $\sim 100$ kyr cycle in glaciations (Lisiecki, 2010). Eccentricity modulates precession (Huybers and Aharonson, 2010), and it is suggested that this interaction subsequently causes the anticorrelation with glaciations (Lisiecki, 2010). Lisiecki (2010) suggests that strong eccentricity forcing interrupts $100$ kyr cycles in glaciations on Earth. Therefore, increases or decreases in the power of the of the $\sim 95$ kyr and $\sim 125$ kyr from passing perturbers would disrupt the natural cycles of glaciation on Earth. Many mass extinction events are associated with rises in global temperature (Bond and Grasby, 2017). Stellar flybys that promote or inhibit changes in global temperatures from the standard Milankovitch cycle, subsequently may promote or inhibit extinction events. However, the cases where a noticeable change to these cycles is observed requires consecutive coplanar flybys at relatively close distances, and therefore may be unlikely. Yet the results show proof of principle that some cases of multiple stellar flybys can influence Earth's eccentricity evolution substantially over a $15$ Myr timeframe.

# 3.2 Inclination

## 3.2.1 Baseline Models

Inclination, although not dubbed a Milankovitch cycle (Pälike, 2005), does undergo cycles similar to those accredited to Milankovitch, and has been suggested as a solution to the 100,000 year problem (Muller and Macdonald, 1997). A baseline model was produced as a reference point for comparison in a similar fashion to the eccentricity investigation. Figure 48 shows the full-system baseline model over the 15 Myr investigation timeframe.

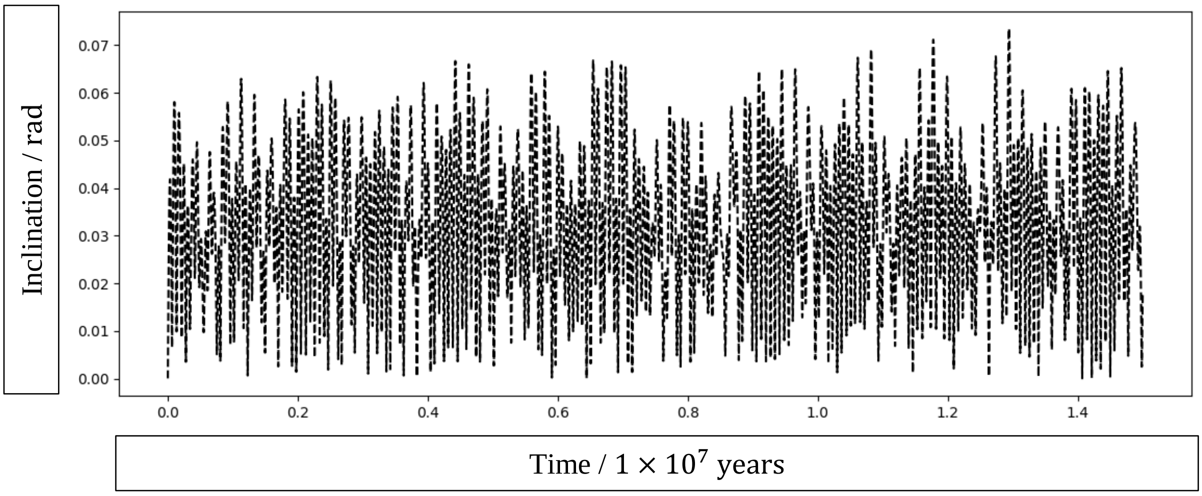


*Figure 48: A graph of Earth's inclination over a* 15 *Myr period starting from 2020 under the gravitational influence of a full system.*

An FFT was conducted on the data to confirm that periodicities in the signal matched with the periodicities expected in the literature.

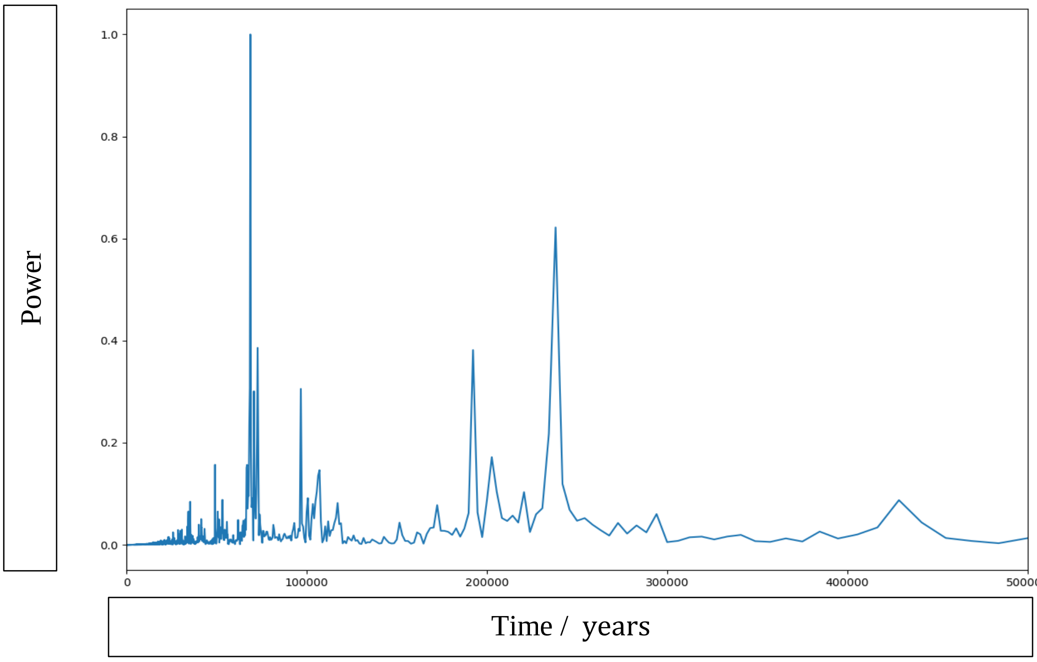


*Figure 49: Periodogram of inclination in full-system baseline model normalised such that the greatest peak has a value of* 1.

Figure 49 shows the expected peaks at ~70 kyr, ~190 kyr and ~230 kyr in accordance with the literature (Muller and MacDonald, 1997; Berger et al., 2005). As with eccentricity, a Jupiter-less baseline model was produced for comparison when analysing the Jupiter-less system results. Figure 50 shows the evolution of Earth's inclination with Jupiter absent from the system.

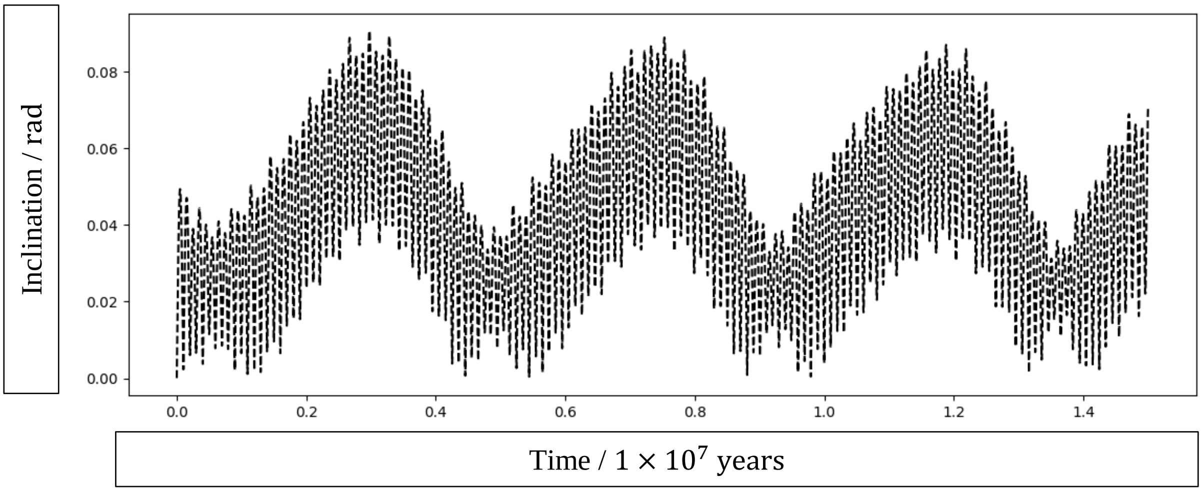


*Figure 50: A graph of Earth's inclination over a 15 Myr period starting from 2020 under the gravitational influence of a system without Jupiter.*

The graph shows that the inclination of Earth's orbit reaches a larger maximum in the Jupiter-less model at ~0.09 rad. Figure 51 shows the FFT of the results in order to analyse the periodicities of the system.

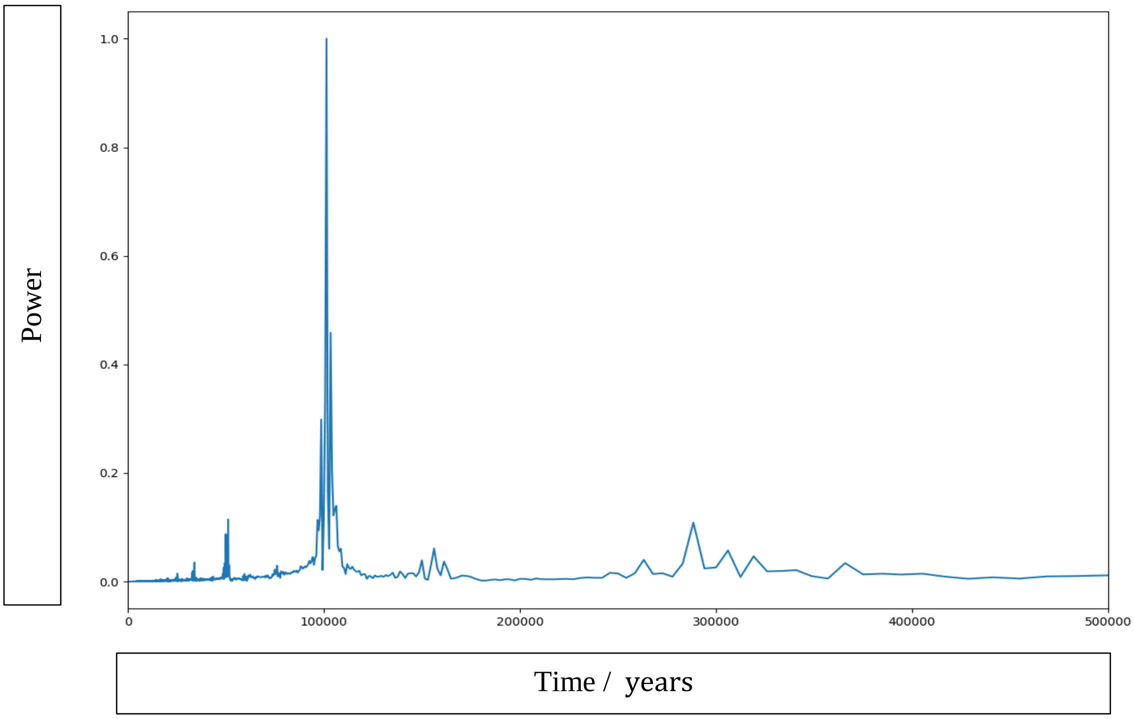


*Figure 51: Periodogram of inclination in the Jupiter-less baseline model normalised such that the greatest peak had a value of 1.*

The results from the FFT show that all the main periodicities present in the full-system model are either removed or shifted, leaving no comparable elements. As Jupiter's orbit is almost in the invariable plane (Laplace, 1878; Souami and Souchay, 2012) and as it features heavily is the resonances that evolve Earth's inclination (Berger et al., 2005), it is understandable why Jupiter's removal has caused a substantial change to the periodicities present in the inclination signal. The new peak at ~100 kyr may also be the result changes to the ecliptic plane and as such the peak at ~100 kyr only usually identifiable in the invariable plane (Muller and MacDonald, 1997) becoming more prominent. Due to the substantial differences in the periodicities of the two systems, direct comparison between peaks is not possible.

### 3.2.2 Initial Testing: Cases 101-107

In case 101 (figure 52) where a single perturber was passed by the solar system, it can be seen that a negligible effect was observed over the 15 Myr period, with changes between the baseline and case 101 only reaching $|\Delta_i|_{\max} \approx 1.45 \times 10^{-6}$. This result is similar to that shown in the eccentricity investigation.

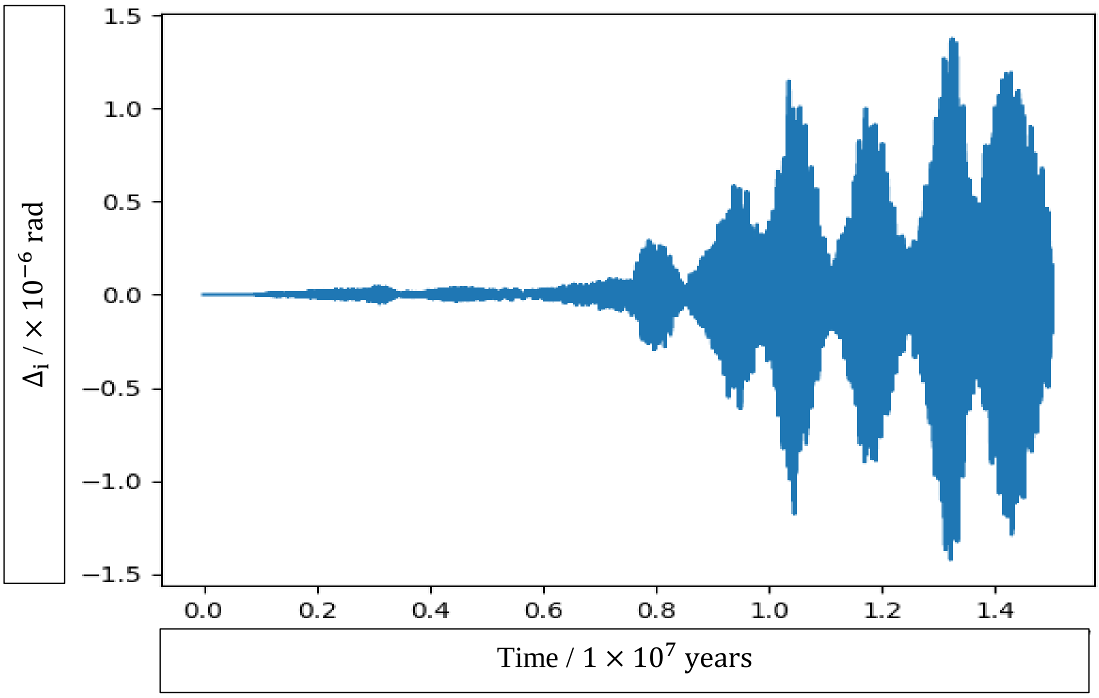


*Figure 52: A graph of the difference in inclination ($\Delta_i$) between the full-system baseline model and the case 101 model.*

To confirm that changes in this order of magnitude has little effect on the periodicities in the system, three FFT boxcars were run for the peaks at ~70 kyr, ~190 kyr and ~230 kyr. Figure 53 shows that no noticeable difference is present between the baseline powers and the powers observed in case 101.

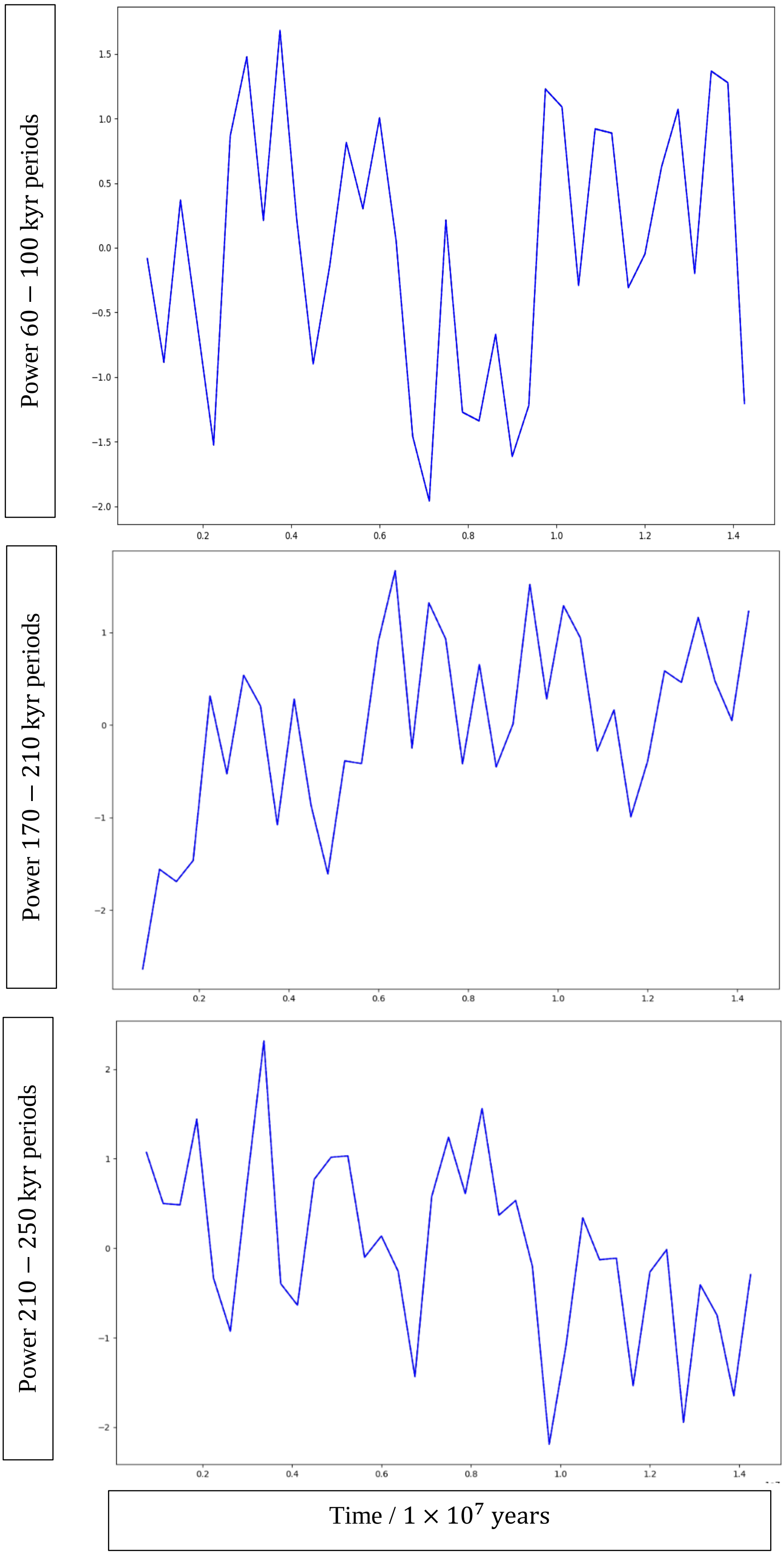


*Figure 53: FFTs of an* $1.5\ Myr$ *rolling boxcar for periods* $60 - 100\ kyr$, $170 - 210\ kyr$ *and* $210 - 250\ kyr$ *showing the evolution of the power of inclination periods in these ranges over a* $15\ Myr$ *timescale for case 101 (blue line) and baseline model (dashed black line – completely covered by the case 101 line).*

Cases 102-107 also show no changes to Earth's inclination outside of the $10^{-6}$ order of magnitude and therefore have no observable impact on the evolution of Earth's inclination.

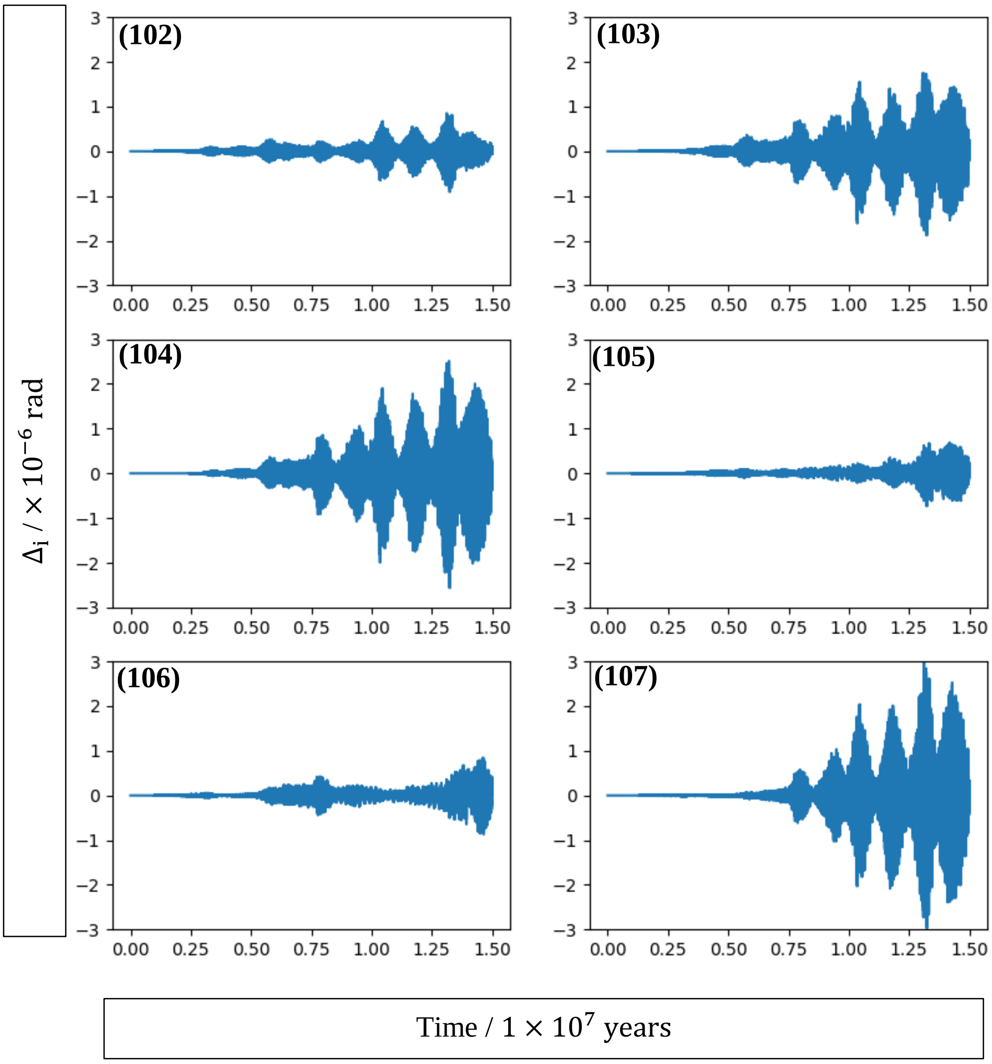


*Figure 54: A graph of the difference in Earth's inclination ($\Delta_i$) between the baseline model and cases 102-107.*

## 3.2.3 Coplanar flybys: Cases 201-209 & 301-309

A similar effect to what was observed in the eccentricities of the cases 201-209 is present in the inclinations of the cases. Figure 55 shows that the most substantial changes to Earth's inclination occurred at smaller encounter distances, with the largest mass having the greatest impact. Again, it can be seen that the 1 $M_{\odot}$ mass perturbers produced a smaller change in the inclination than the 0.82 $M_{\odot}$ perturbers, as was shown in the eccentricity investigation. This further demonstrates the potential randomness that features within the results. FFTs boxcars were run on the ~70 kyr, ~190 kyr and 230 kyr cycles to determine what impact these changes had on the power of the inclination cycles. Additionally, a plot of the changes to Earth's inclination in a Jupiter-less model was also produced to investigate Jupiter's role in the perturbations observed.

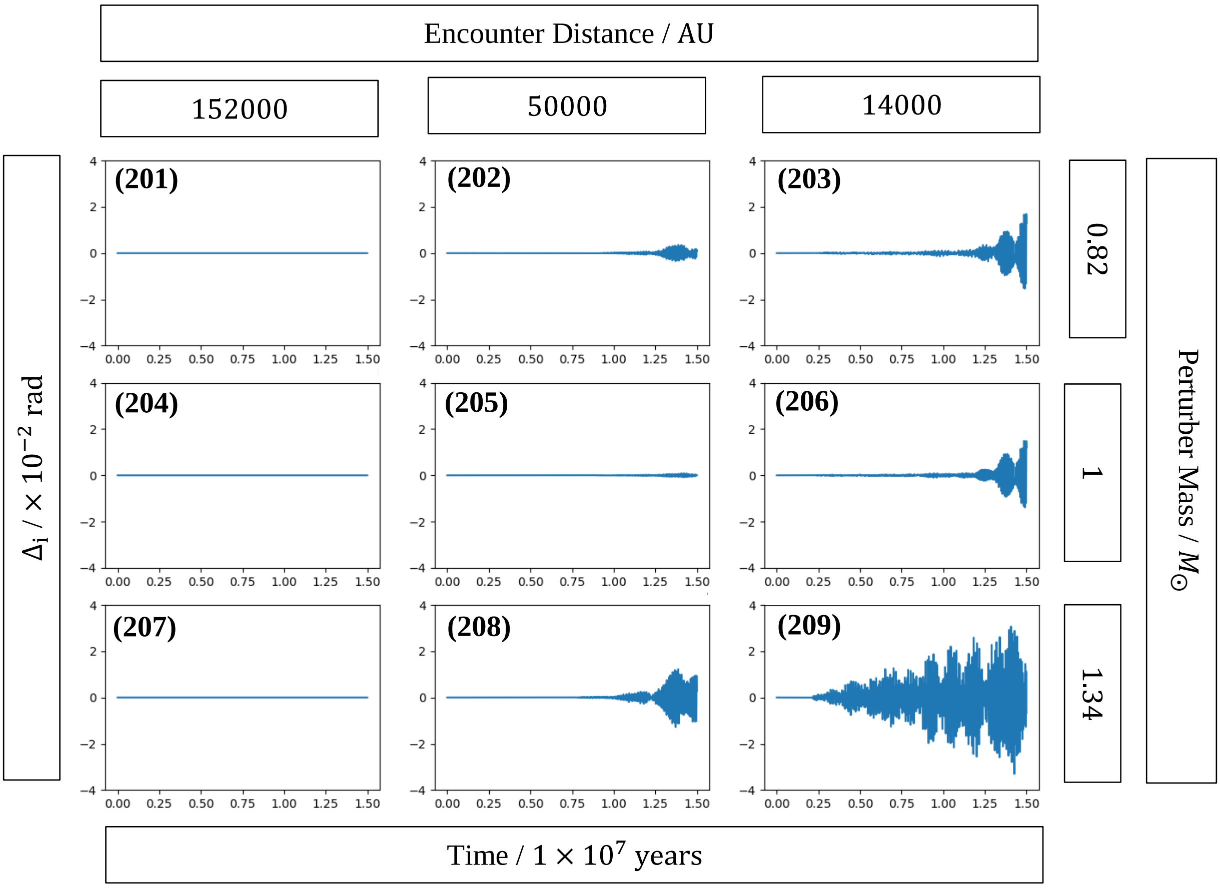


*Figure 55: Graphs of cases 201-209 showing the change in Earth's inclination $\Delta_i$ compared to the full-system baseline model.*

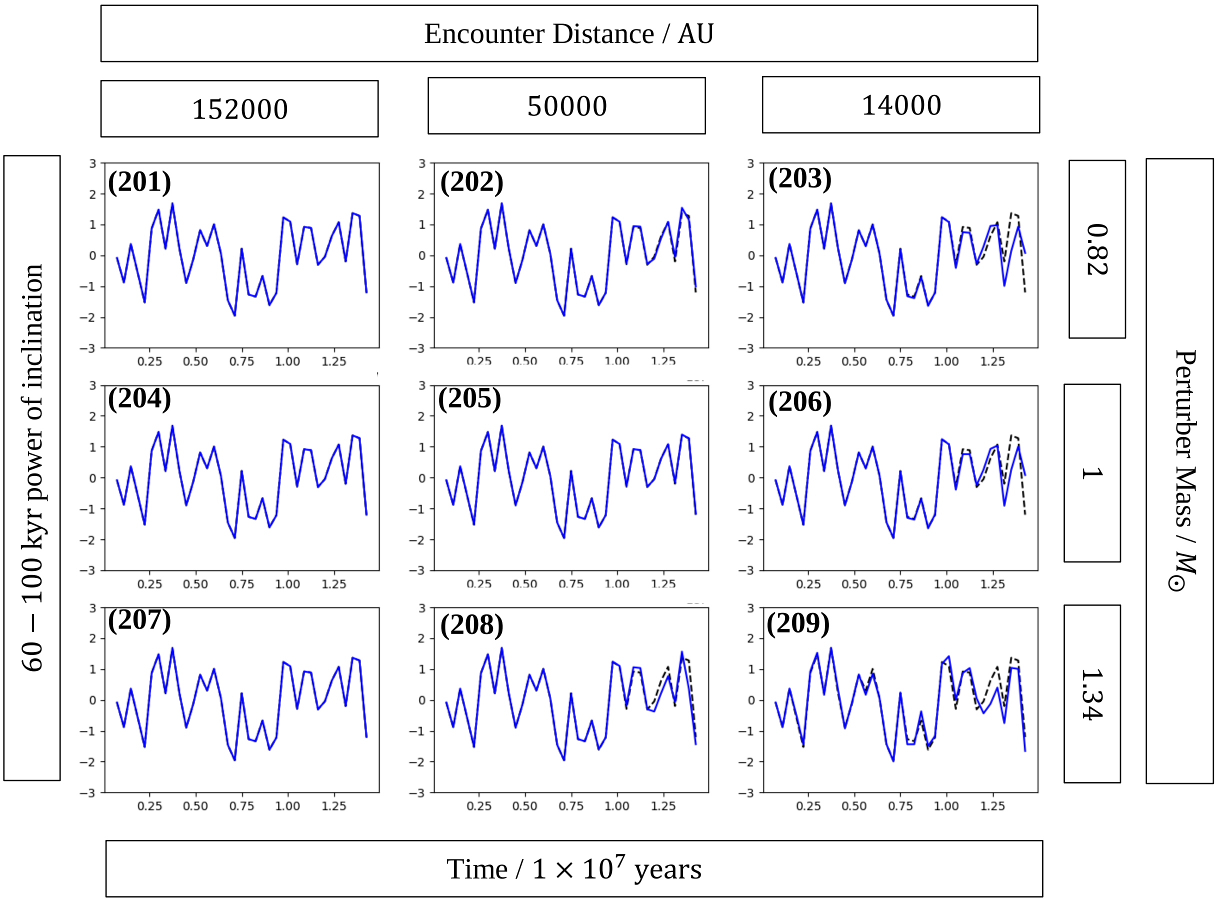


*Figure 56 Graphs of the FFT performed on a rolling boxcar of* $1.5$ *Myr on Earth's inclination for periods* $60-100$ *kyr normalised to have a mean value of* $0$ *and a standard deviation of* $1$*. The dashed line is the result from the baseline data, and the blue is the result from the respective case 201-209*

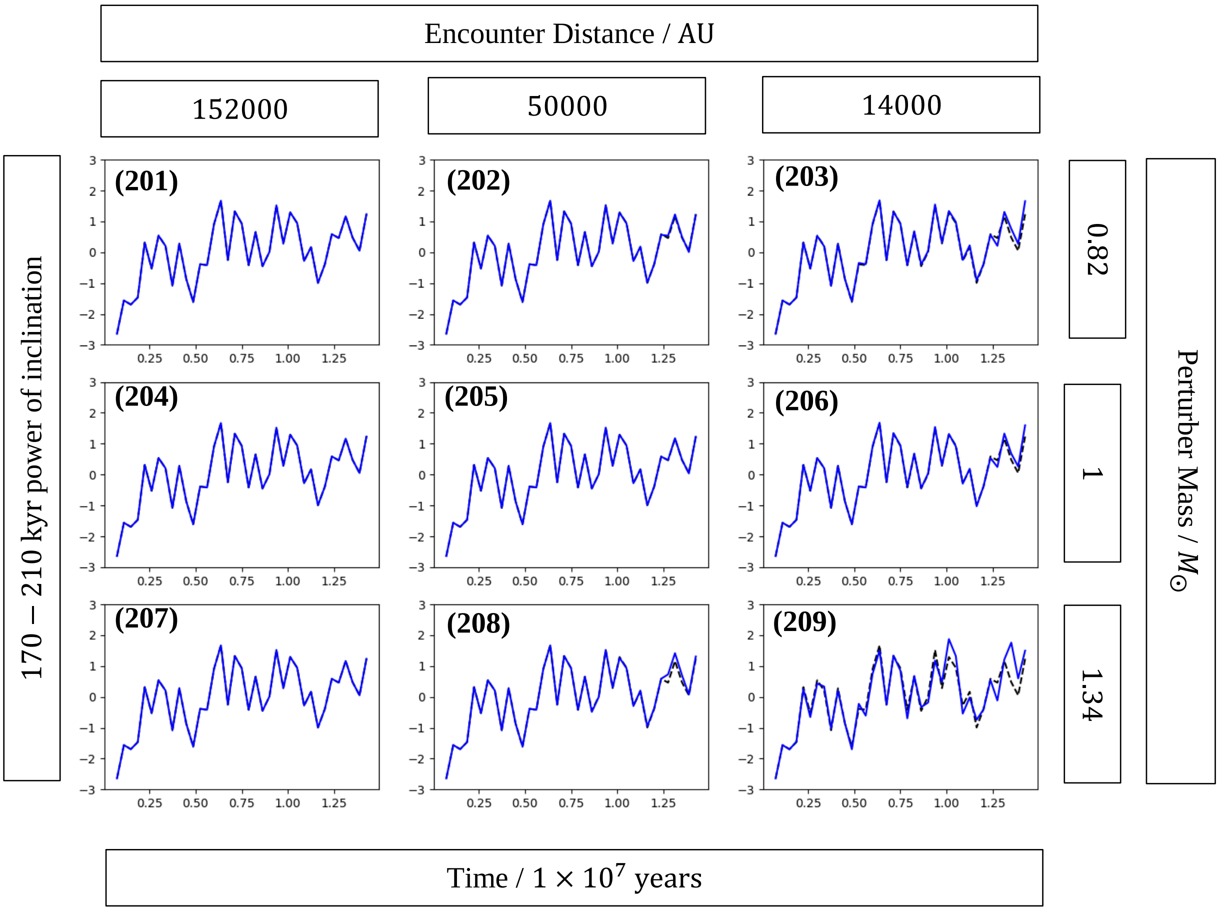


*Figure 57: Graphs of the FFT performed on a rolling boxcar of* 1.5 *Myr on Earth's inclination for periods* 170 − 210 *kyr normalised to have a mean value of* 0 *and a standard deviation of* 1*. The dashed line is the result from the baseline data, and the blue is the result from the respective case 201-209*

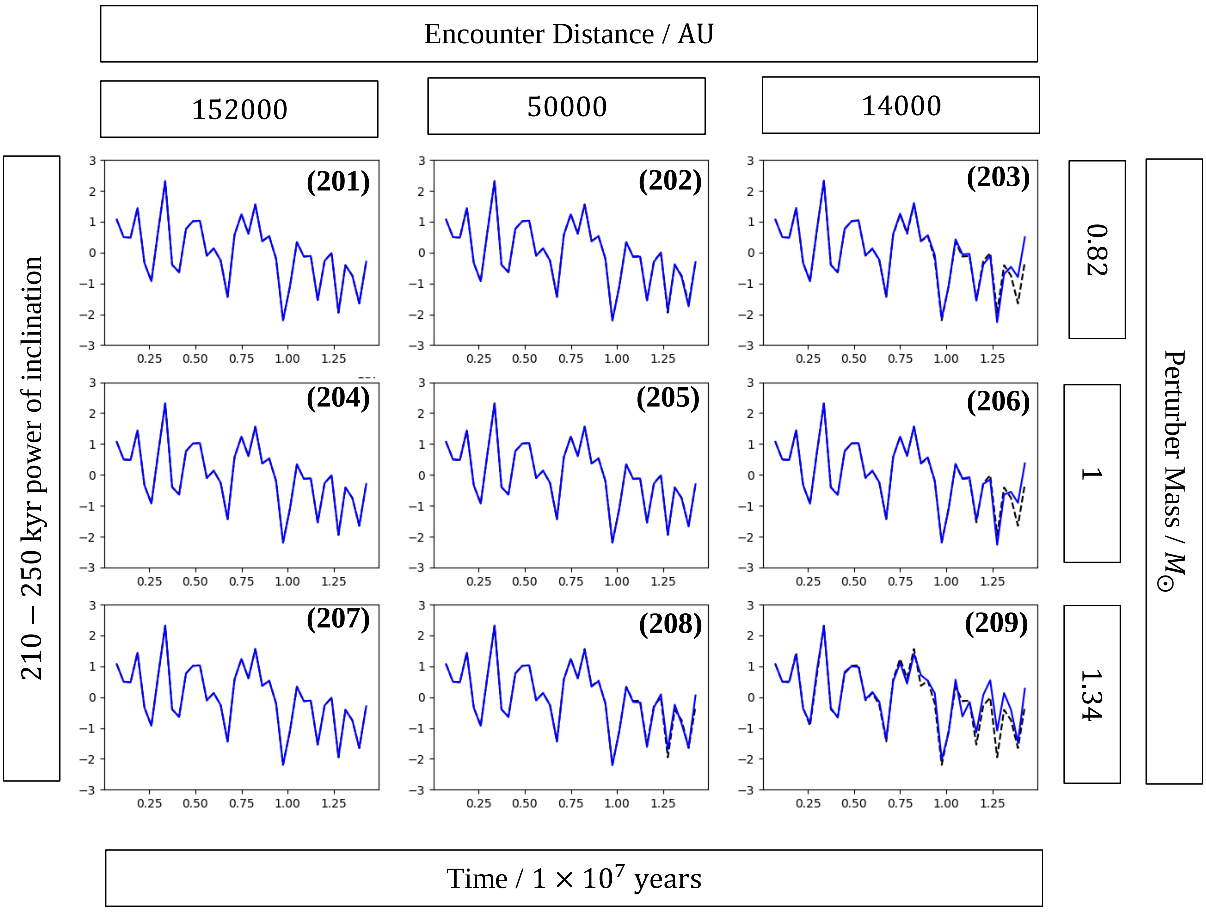


*Figure 58: Graphs of the FFT performed on a rolling boxcar of* 1.5 Myr *on Earth's inclination for periods* 210-250 kyr *normalised to have a mean value of 0 and a standard deviation of 1. The dashed line is the result from the baseline data, and the blue is the result from the respective*

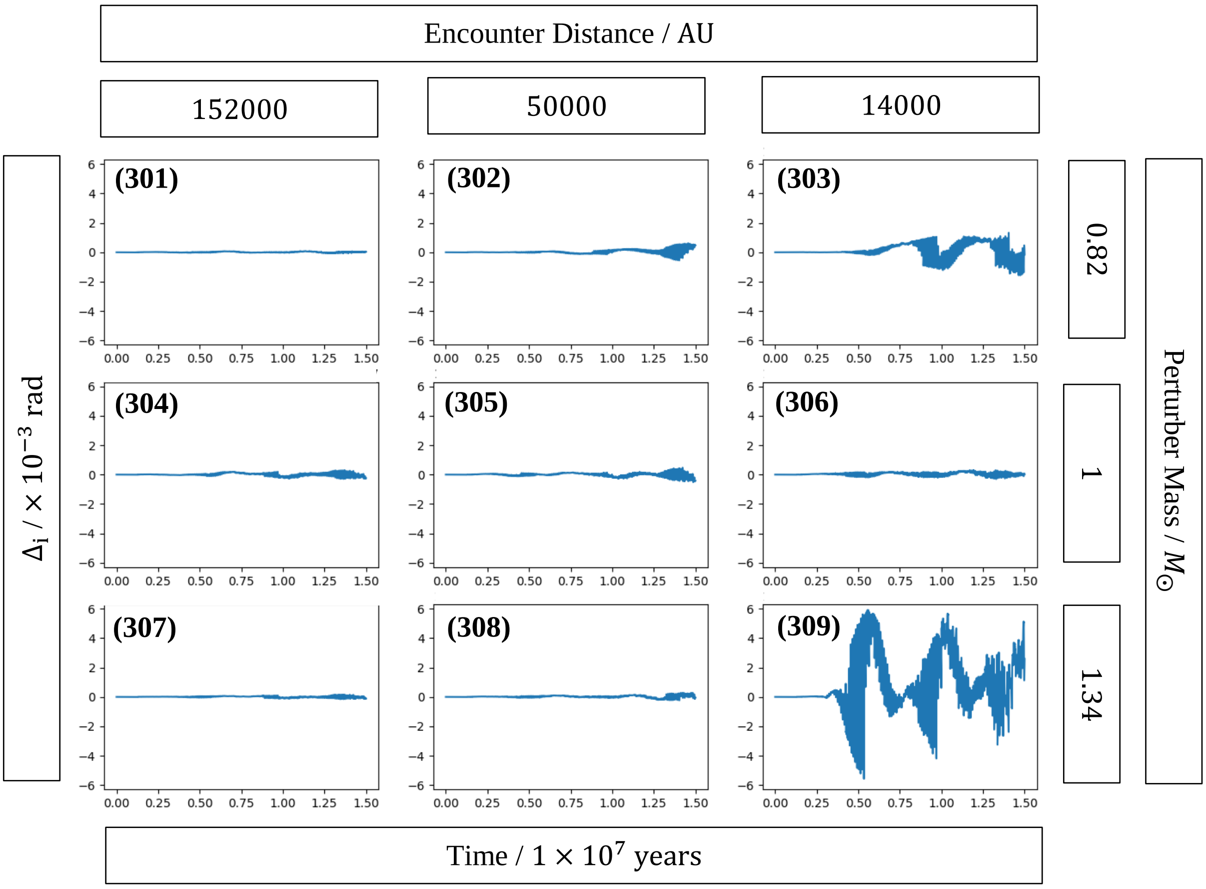


*Figure 59: Graphs of cases 301-309 showing the change in Earth's inclination $\Delta_i$ compared to the Jupiter-less baseline model.*

The FFT boxcars for the ~70 kyr, (figure 56) ~190 kyr (figure 57)and ~230 kyr (figure 58) cycles show that in the cases 202, 203, 206, 208 and 209 where the values of $\Delta_i$ are observed, that noticeable changes to the power of the cycles occur too. Comparing the changes inclination in cases 201-209 (figure 55) this with the changes in the Jupiter-less models 301-309 (figure 59), it can be seen that an effect one order of magnitude lower is shown in the Jupiter-less model. This suggests that Jupiter exacerbates the effect of passing perturbers, in the same way that was observed in the eccentricity investigation. However, unlike in the eccentricity investigation, the points at which the changes to Earth's inclination cycles become noticeable within the FFT boxcar do not match up with a particular amount of perturbations of Jupiter's inclination. This may be because that four of the five resonances that influence Earth's inclination evolution do not include Jupiter in the terms (Berger et al. 2005). The planets Mars, Venus and Mercury are present in the top five terms for the ~70 kyr, ~190 kyr and ~230 kyr cycles respectively (Berger et al., 2005). Despite this, no value for $\Delta_i$ corresponds to the changes in the periodicities of Earth's inclination. Figure 60, figure 61 and figure 62 show these changes for Mars, Venus and Mercury respectively. This suggests that the changes in Earth's inclination are the result of several factors and potentially more complex resonances. Yet the results do show that without Jupiter, the effects observed would be smaller. Therefore, Jupiter does play some role in promoting the changes to Earth's inclination when flybys are coplanar to the solar system.

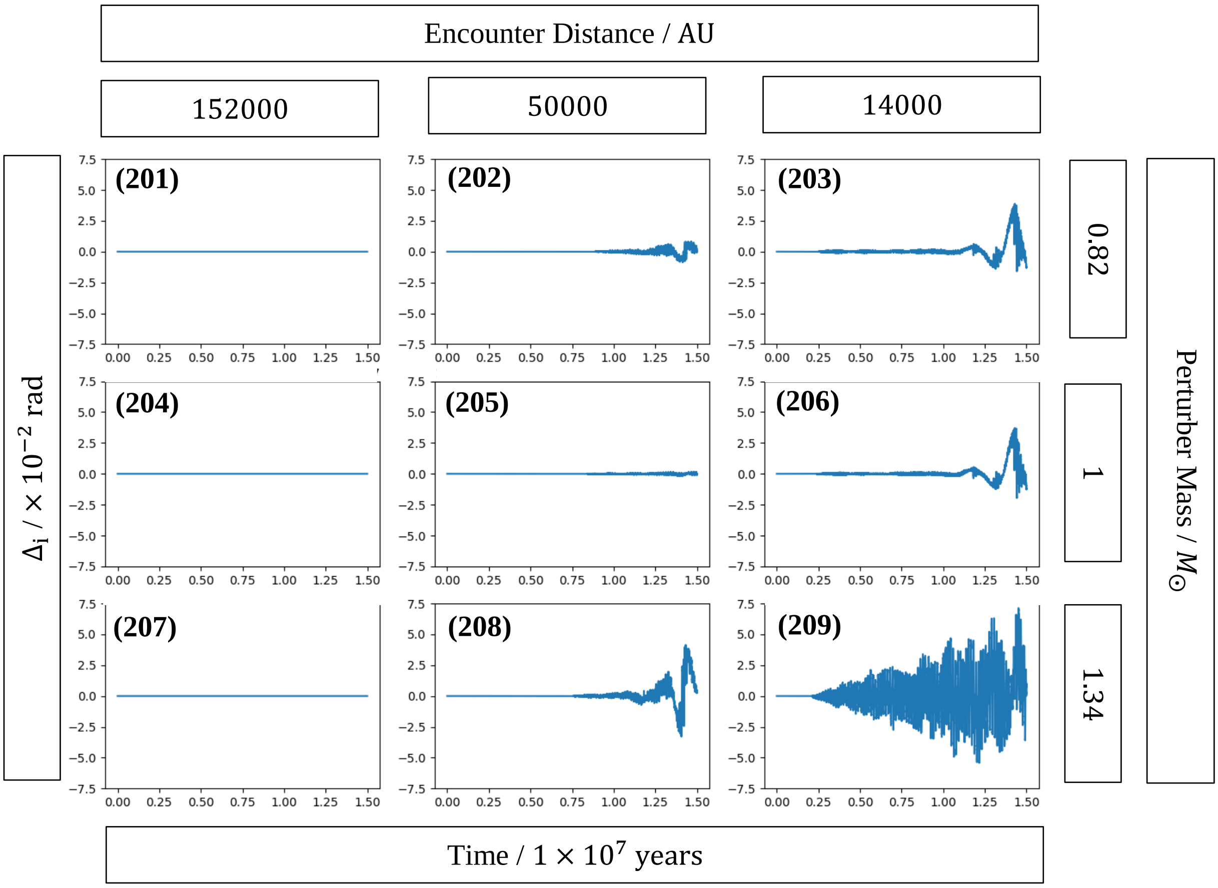


*Figure 60: Graphs of cases 201-209 showing the change in Mar's inclination $\Delta_i$ compared to the full-system baseline model.*

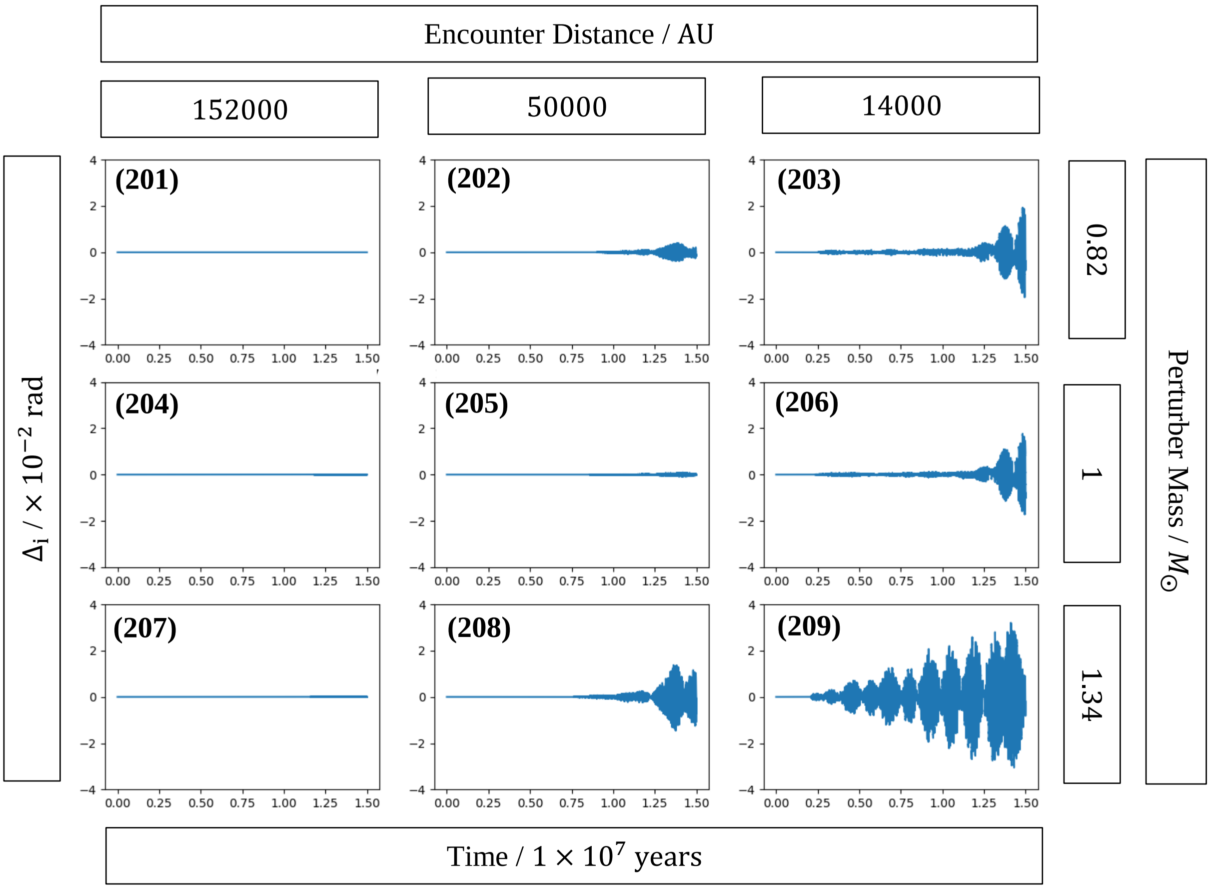


*Figure 61: Graphs of cases 201-209 showing the change in Venus's inclination $\Delta_i$ compared to the full-system baseline model.*

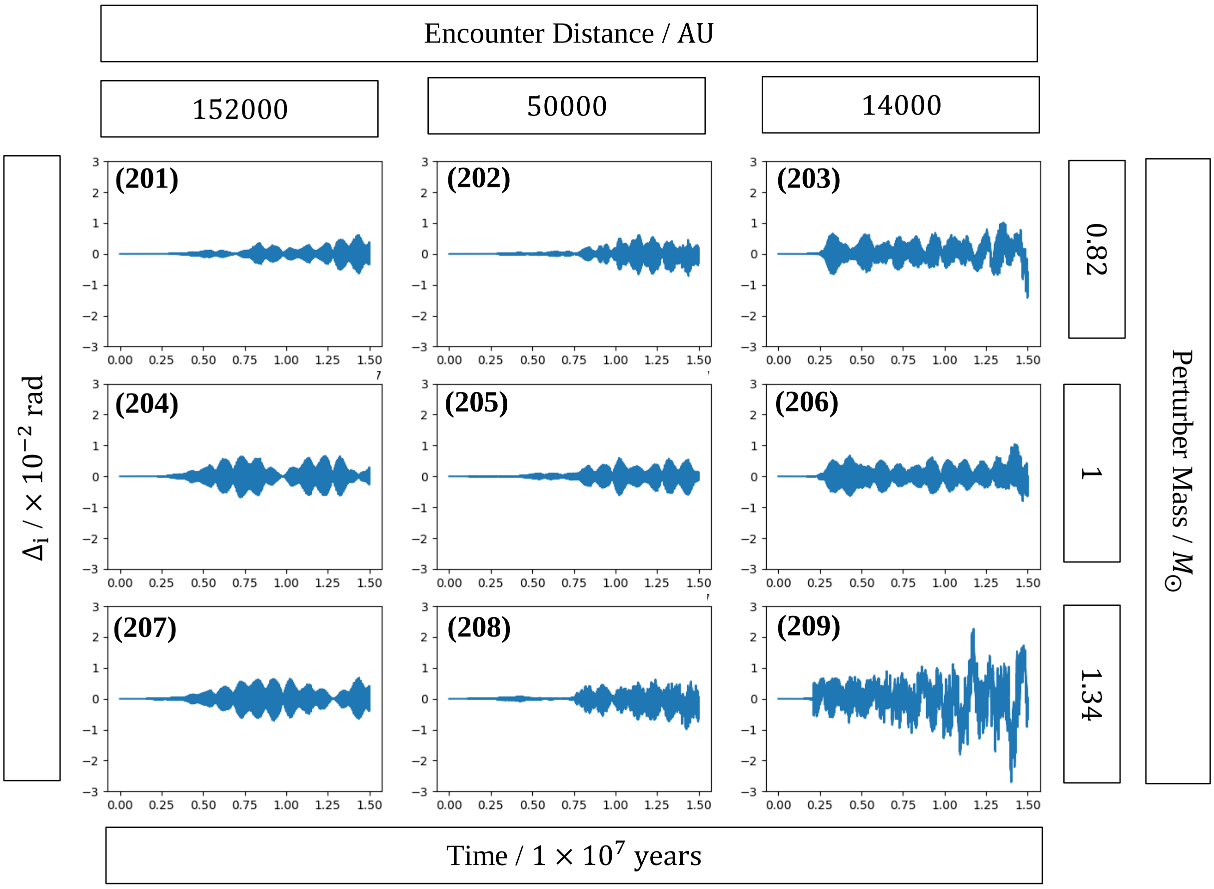


*Figure 62: Graphs of cases 201-209 showing the change in Mercury's inclination $\Delta_i$ compared to the full-system baseline model.*

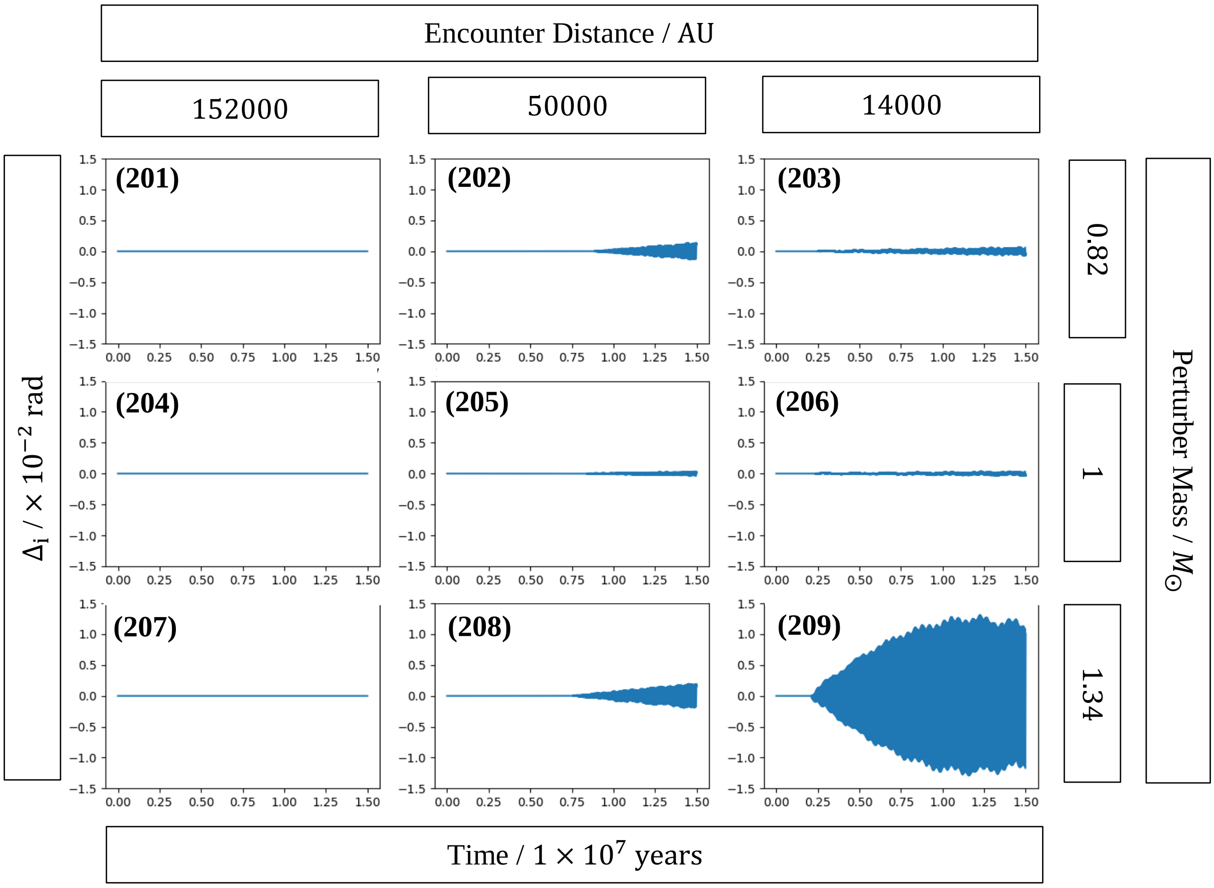


*Figure 63: Graphs of cases 201-209 showing the change in Jupiter's inclination $\Delta_i$ compared to the full-system baseline model.*

## 3.2.4 Non-coplanar flybys: Cases 210-227 & 310-327

When reviewing the results for cases 210-227 in figure 64, it can be seen that the changes to Earth's inclination are two orders of magnitude below those seen in the coplanar flybys. A greater effect is observed in the 60° inclined flybys (cases 210-218) than in the 90° inclined flybys. Yet, neither show are large enough perturbation to impact the periodicities of the inclination cycles to any noticeable level.

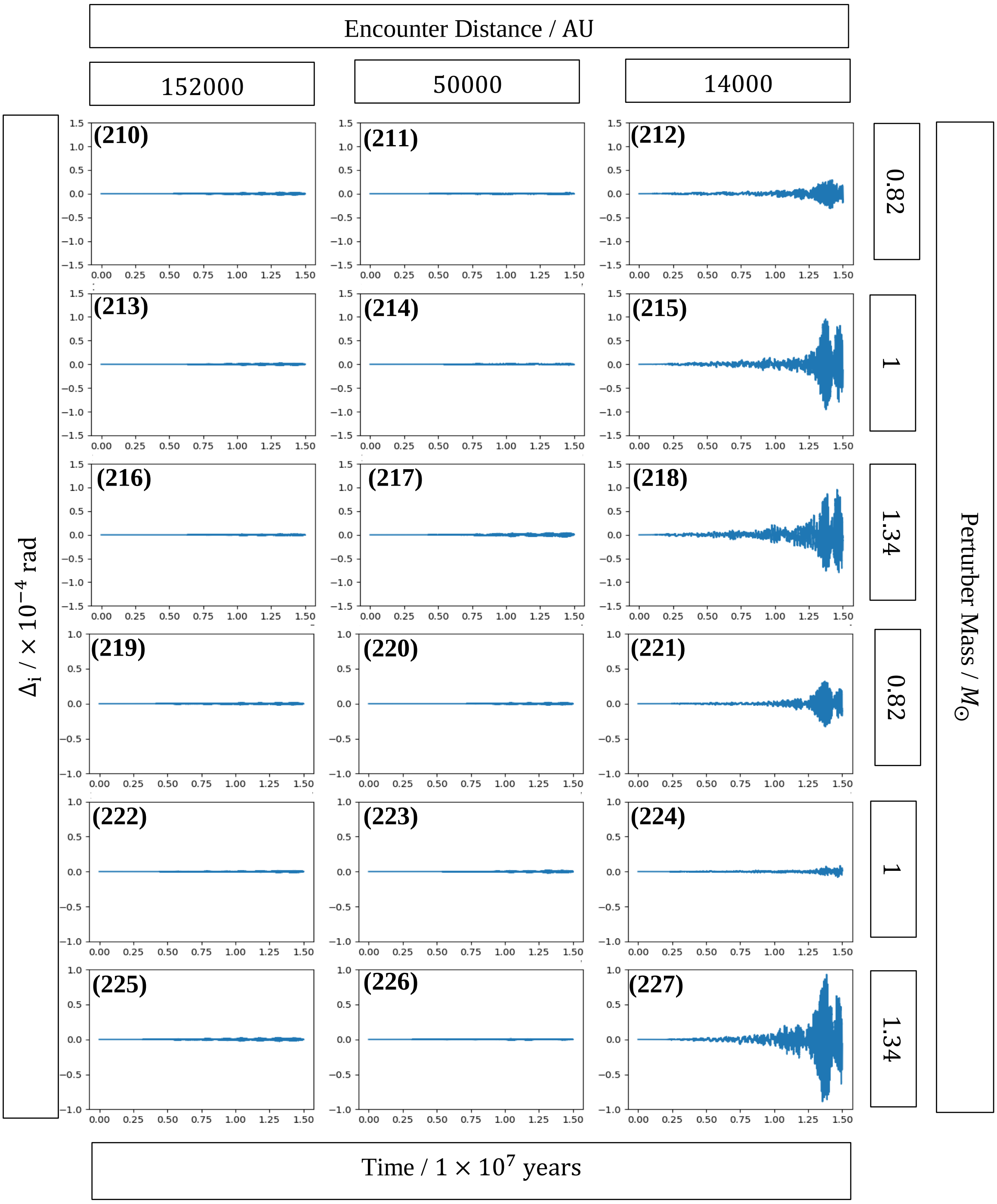


*Figure 64: Graphs of cases 210-218 (at an inclination of 60°) and cases 219-227 (at an inclination of 90°) showing the change in Earth's inclination $\Delta_i$ compared to the full-system baseline model.*

Figure 65 shows that Jupiter's orbit is perturbed only in the order of $10^{-5}$. Cases 201-209 suggested that Jupiter's perturbation is a driving factor in the perturbation of Earth's inclination. The smaller perturbations to both Earth's and Jupiter's orbital inclination in cases 210-227 support this finding. This relationship was also shown in the eccentricity investigation suggesting Jupiter plays a substantial role in the effect passing perturbers have on Earth's orbit.

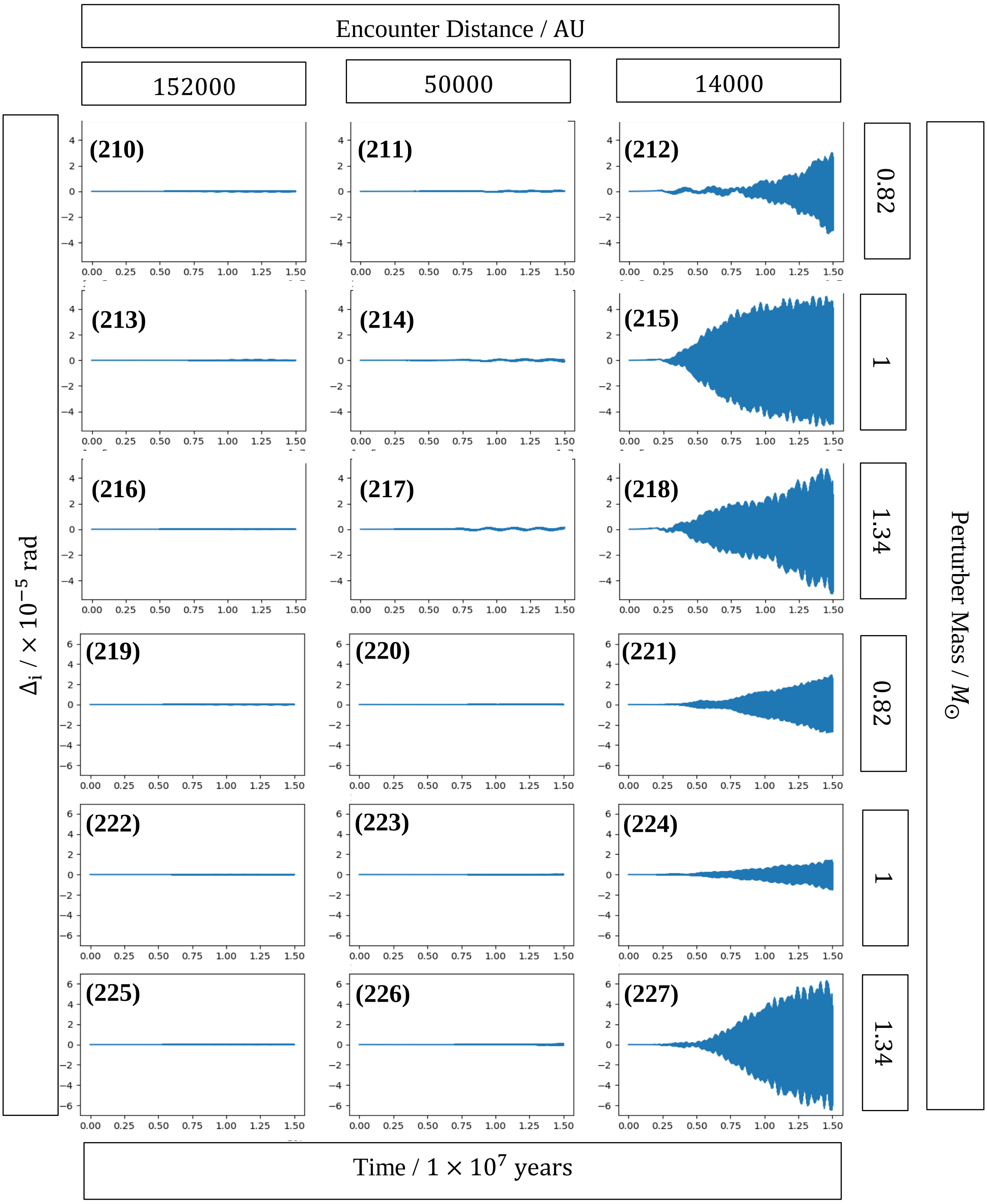


*Figure 65: Graphs of cases 210-218 (at an inclination of 60°) and cases 219-227 (at an inclination of 90°) showing the change in Jupiter's inclination $\Delta_i$ compared to the full-system baseline model.*

When Jupiter is removed from the system, the impact stellar flybys have on Earth's orbit is increased by two orders of magnitude, to the same magnitude as the coplanar flyby model where Jupiter is absent. This demonstrates that Jupiter not only exacerbates effect when flybys are coplanar, but that it inhibits effects when the perturbers are inclined out of the solar plane.

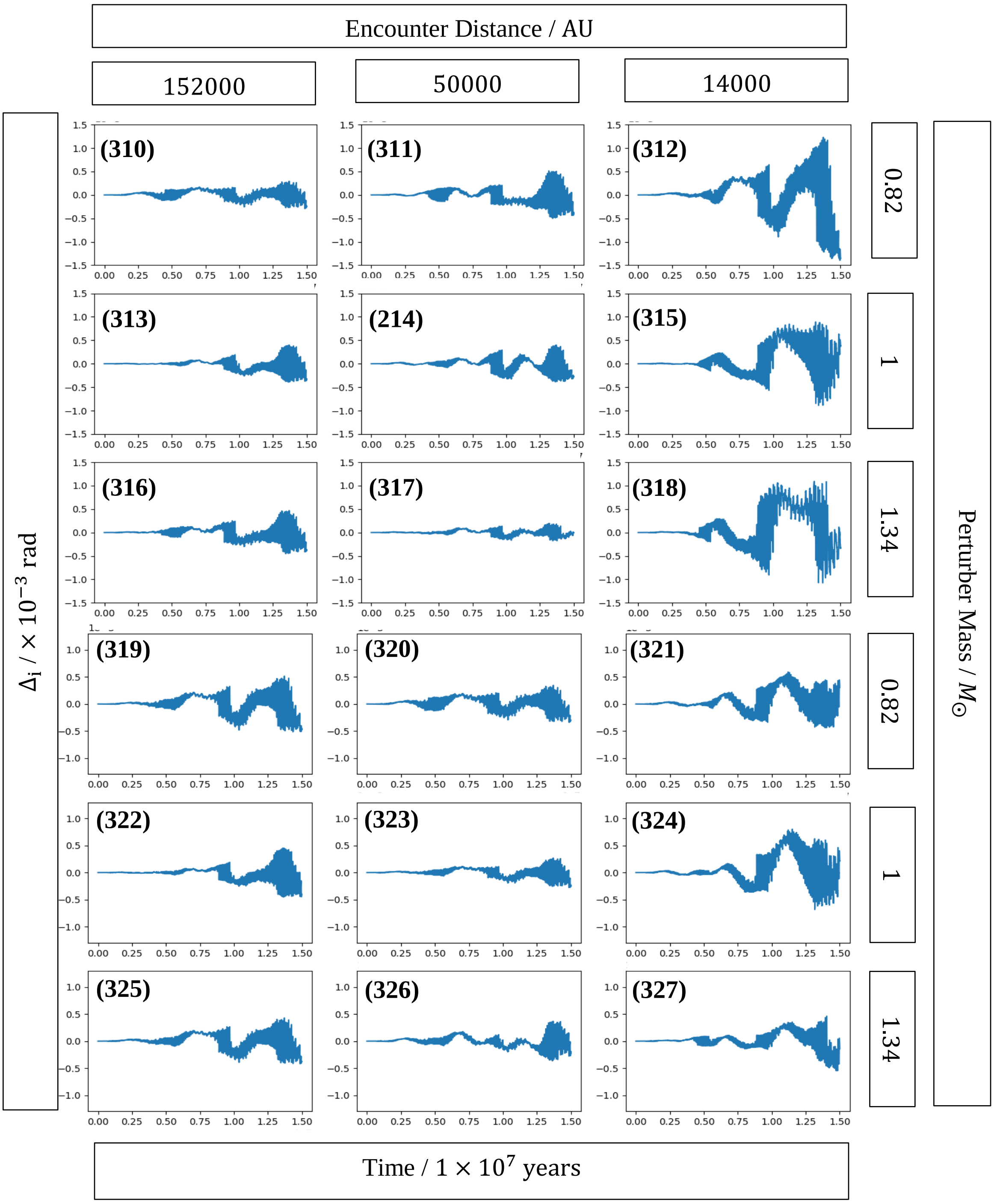


*Figure 66: Graphs of cases 310-318 (at an inclination of 60°) and cases 319-327 (at an inclination of 90°) showing the change in Earth's inclination $\Delta_i$ compared to the Jupiter-less baseline model.*

### 3.2.5 Summary

The results from the inclination investigation show many similarities with the eccentricity investigation. It shows again that the greatest effects are from perturbers that pass in the same plane as the solar system and have encounter distances $< 50{,}000$ AU. The perturbers with the greatest mass showed the greatest affect at each inclination, but that some randomness in the system causes $0.82\ M_{\odot}$ stars to show a greater difference from the baseline model than $1\ M_{\odot}$ stars. The figure below summarises cases 201-227:

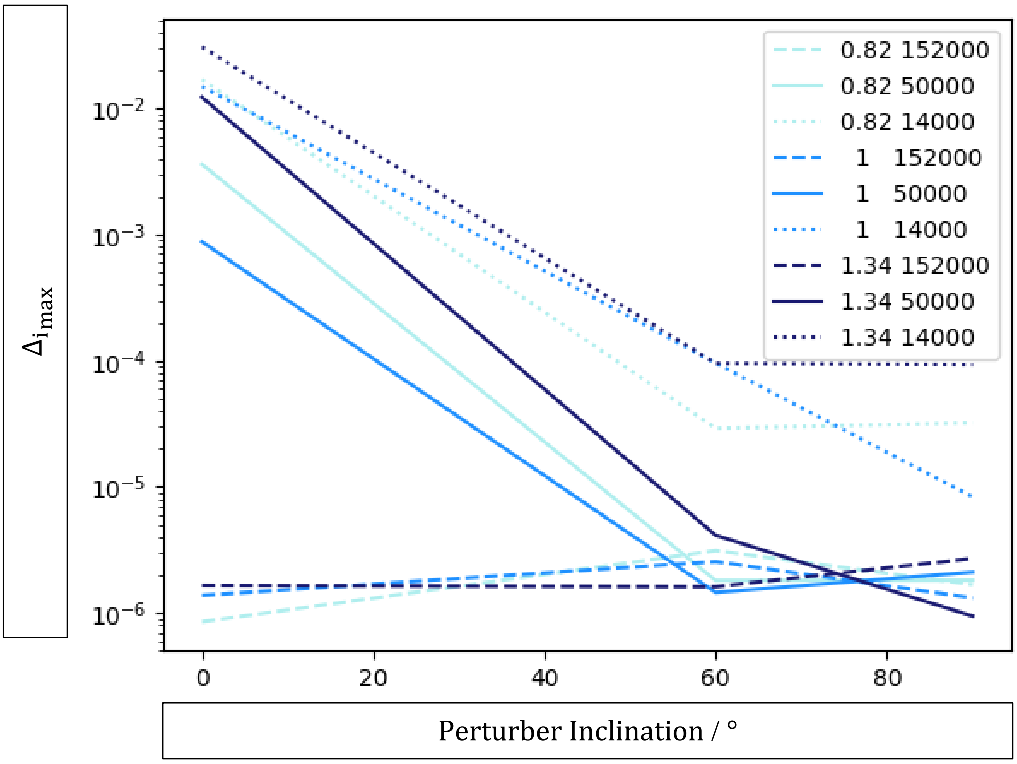


*Figure 67: Graph of the maximum $\Delta_i$ recorded plotted against encounter inclination for 9 combinations of perturber mass ($0.82\ M_{\odot}$, $1\ M_{\odot}$ and $1.34\ M_{\odot}$) and perturber encounter distance ($152000\ AU$, $50000\ AU$ and $14000\ AU$).*

The analysis suggests that Jupiter plays a key role in how the passing perturbers effect Earth's inclination. During consecutive coplanar flybys, Jupiter exacerbates the impact, causing noticeable changes to the power of the inclination cycles at $\sim$70 kyr, $\sim$190 kyr and $\sim$230 kyr (Berger et al, 2005). However, when the perturbers move out of this plane, Jupiter provides stability to these cycles. Unlike with some of the eccentricity cycles, a direct association between the point of change in the power of an inclination cycle and another planetary perturbation cannot be found. This is likely due to the number of planets in the resonance terms that modulate the inclination cycles (Berger et al, 2005; Brentagon, 1997).

Inclination has been suggested as a solution to the 100,000-year problem (Muller and MacDonald, 1997). It is argued that the inclination of Earth's orbit may move it into regions of increased cosmic material, such as dust, resulting in changes to the amount of solar radiation reaching Earth (Muller and MacDonald, 1997). Changes to the periodicities of Earth's inclination would change the time Earth passes through areas of higher or lower cosmic material. Therefore, if orbital inclination does affect the cycles of glaciation (Muller and MacDonald, 1997), then when passing perturbers alter Earth's inclination, the subsequent result would be changes to Earth's climate.

Some argue that there is insufficient evidence to suggest inclination is a driver of glacial cycles (Winckler et al, 2004; Berger, 1999). If this was shown to be the case, then perturbers may not be able to affect climate cycles through inclination perturbation. However, changes to Earth's eccentricity are still present, and thus may alter climate through this mechanism instead.

# CHAPTER 4

# CONCLUSIONS AND FUTURE WORK

The ideas that Milankovitch put forward in the 1920's redeveloped the field of climatology (Macdougall, 2011). With the evidence provided by Hays et al. (1976) the scientific community began to look to the solar system for the mechanisms and drivers of climate change here on Earth. The Milankovitch cycles are now a field that has been well studied, and their impact far reaching (Kostadinov and Gilb, 2014; Bennett, 1990; Forgan, 2016; Galet et al., 2002). However, not all the mechanisms associated with Milankovitch cycles are well understood (Muller and MacDonald, 1997; Raymo and Nisancioglu, 2003; Berger et al., 2005) and given the role that the Milankovitch cycles may play in mass extinction events (Bond and Grasby, 2017; van Dam, 2006), investigation is still needed.

Stellar flybys have been shown to have a variety of effects on the celestial bodies and systems that they pass (De Rosa and Kalas, 2019; Picogna and Marzari, 2014). Studies into flybys passing our own system have found evidence for encounter rates of these flybys (Bailer-Jones et al., 2018), their proximity to the Sun (Bailer-Jones et al, 2018; Bailer-Jones, 2015; Mamajek et al. 2015), and even their effect on our solar systems Oort cloud (Bailey and Fabrycky, 2019). Yet the effect that flybys may have on the larger planetary bodies in our solar system has often been discounted as negligible and is poorly investigated (Berski and Dybczynski, 2016). With encounter rates now estimated at around every 50 kyr (Bailer-Jones, 2018), there is potential for larger effects to be observed as the result of consecutive smaller perturbations.

It is hypothesised that during the passing of the solar system through the spiral arms, the effect of the Milankovitch cycles may be heightened (Gillman et al., 2018), and that this may be one of the reasons extinction events are associated with Galactic processes (Gillman and Erenler, 2008; Gillman et al, 2018). The passing of the solar system through regions of increased density may make stellar flybys more frequent (Gillman et al, 2018). Investigating whether flybys have the potential to alter the Milankovitch cycles will determine whether this is an area for further exploration.

A total of 34 scenarios were investigated, with additional ancillary models (such as Jupiter-less systems) run to determine the cause of the effects observed within these scenarios. Many cases showed little effect from the passing of stars at distances of $152{,}000$ AU, showing the system is stable over a $15$ Myr timeframe for average encounter distance flybys. The evidence presented in cases 201-209 and 301-309 suggest that consecutive flybys coplanar to the solar system have the potential to perturb Earth's eccentricity and inclination cycles when encounter distances are $< 50{,}000$ AU. The results suggest that changes to the $\sim 95$ kyr and $\sim 125$ kyr cycles of eccentricity are the result of perturbations to both Jupiter and Venus's orbits (Pälike, 2005). An effect on the $\sim 400$ kyr cycle is also observed; however, this is likely to be the result of more complex non-linear resonances (Pälike, 2005; Carruba et al., 2005). Similarly, non-linear resonances may be the cause of effects seen in the perturbations of the $\sim 70$ kyr, $\sim 190$ kyr and $\sim 230$ kyr cycles of inclination (Berger et al., 2005). Non-coplanar flybys are shown to have a substantially smaller effect on both eccentricity and inclination. The evidence suggests that Jupiter, while exacerbating coplanar flybys, offers stability when the path of perturbers is inclined out of the solar plane. Ultimately, the results imply, that in many cases, the passing of perturbers does have little effect on the planets in the solar system as suggested by Berski and Dybczynski, (2016), however that certain regimes can significantly alter the cycles of eccentricity and inclination.

Eccentricity and inclination have both been cited as solutions to the dubbed '$100$ kyr problem'; the change from a $\sim 41$ kyr cycle in glaciations to a $\sim 100$ kyr cycle approximately $800$ kyr ago. (Lisiekci, 2010; Muller and MacDonald, 1997; Davis and Brewer, 2008). If either were to be the case, then changes to the periodicity of these cycles would have an impact on the glacial cycles, and ultimately climate change. Changes in climate are associated with extinction events (Bond and Grasby, 2017). Therefore, the passing of stars that perturb Earths orbital cycles, may subsequently exacerbate or inhibit the orbital forcing of climate change, and play a role in the scale and appearance of extinction events. This suggests that the claims from Gillman et al. (2018) that the passing of the solar system through the spiral arms resulting in enhanced Milankovitch cycles may have some validity and is worth further investigation.

The results show that passing perturbers have the potential to effect Earth's eccentricity and inclination over a 15 Myr timeframe. The effect after this point is unknown and potentially over longer timeframes some regimes may show a greater or delayed effect. It is possible that the cases with the greatest effect may either continue to differ with the baseline or resume some form of stability. Additional testing would be required to determine the effect over longer timeframes.

A variety of cases were tested to determine whether any regimes had the potential to cause significant perturbations to Earth's orbit. Having shown that this is possible, more fine-grained testing with additional parameter values for perturber mass, inclination and encounter distance would disclose the limits of what parameter values are required to result in significant changes to Earth's orbit. Additionally, the effect of velocity is not an investigated parameter and may be another possible area of exploration.

The Milankovitch cycles also include obliquity (axial tilt) and climatic precession (Pälike, 2005). Neither of these are investigated explicitly, although a link between eccentricity and precession is noted, and therefore the effects that stellar flybys have on these orbital cycles is unknown. To fully explore the potential for enhanced Milankovitch cycles as the solar system passes through the spiral arms (Gillman et al., 2018), investigation would be required into whether passing stars could perturb these cycles, in a similar way to the perturbations of eccentricity and inclination.

The passing of stellar flybys has been shown, under some regimes, to alter Earth's eccentricity and inclination cycles significantly over a 15 Myr period. Changes in these cycles are linked with climate change and mass extinction events (Bond and Grasby, 2017). Therefore, stellar flybys have the potential not only to be a factor in the evolution of the Earth' orbit, but also factor in the evolution of the life on our planet.

# BIBLIOGRAPHY


Adhémar, J. (1842) *Revolutions de la mer*. Paris (France): Carilian-Goeury

Bailer-Jones, C.A.L. (2015) Close encounters of the stellar kind. *Astronomy & Astrophysics*, 575, A35

Bailer-Jones, C.A.L., Rybizki, J., Andrae, R., and Fouesneau, M. (2018) New stellar encounters discovered in the second Gaia data release. *Astronomy & Astrophysics*, 616, A37

Bailey, N., and Fabrycky, D. (2019) Stellar Flybys Interrupting Planet-Planet Scattering Generates Oort Planets. *The Astronomical Journal*, 158(2) 94

Bennett, K. (1990) Milankovitch cycles and their effects on species in ecological and evolutionary time. *Paleobiology*, 16(1) 11-21

Berger, A., and Loutre, M.F. (1991) Insolation values for the climate of the last 10 million years. *Quaternary Science Reviews*, 10(4) 297-317

Berger, A., Mélice, J. L., and Loutre, M.F. (2005) On the origin of the 100-kyr cycles in the astronomical forcing. *Paleoceanography*, 20, PA4019

Berger, W. H. (1999) The 100-kyr ice-age cycle: internal oscillation or inclinational forcing. *International Journal of Earth Sciences*, 88, 305-316

Hausler, B. (1999) *Microsatellites as Research Tools*. Oxford: Pergamon Press

Berski, F., and Dybczyński, P.A. (2016) Gliese 710 will pass the sun even closer: Close approach parameters recalculated based on the first Gaia data release. *Astronomy & Astrophysics*, 595, L10

Bond, D., and Grasby, S. (2017) On the causes of mass extinctions. *Palaeogeography, Palaeoclimatology, Palaeoecology*, 478, 3-29

Bordovitsyna, T. , Tomilova, I., and Chuvashov, Ivan. (2014) Secular resonances as a source of dynamic chaoticity in the long-term orbital evolution of uncontrolled satellites. *Solar System Research*, 48, 259-268

Calkin, M. (1996) *Lagrangian and Hamiltonian Mechanics*. Singapore: World Scientific Publishing Company

Canuto, E. (2018) *Spacecraft Dynamics and Control: The Embedded Model Control Approach*. Oxford: Butterworth-Heinemann,

Carruba, V., Michtchenko, T., Roig, F.,Ferraz-Mello, S. and Nesvorny, D. (2005) On the V-type asteroids outside the Vesta family. I. Interplay of nonlinear secular resonances and the Yarkovsky effect: the cases of 956 Elisa and 809 Lundia. *Astronomy & Astrophysics*, 441(2) 819-8129

Carusi, A., Valsechi, G., and Greenberg, R. (1990) Planetary close encounters: geometry of approach and post-encounter orbital parameters. *Celestial Mechanics and Dynamcial Astronomy*, 49, 111-131

Chiarenza, A., Farnsworth, A., Mannion, P., Lunt, D., Valdes, P., Morgan, J., and Allison, P. (2020) Asteroid impact, not volcanism, caused the end-Cretaceous dinosaur extinction. *Proceeding of the National Academy of Sciences of the United States of America*, 117(29) 17084-17093

Collins, B., and Sari, R. (2010) A unified theory for the effects of stellar perturbations and galactic tides on Oort cloud comets. *The Astronomical Journal*, 140, 1306-1312

Croll, J. (1864) XIII. On the physical cause of the change of climate during geological epochs. *The London, Edinburgh, and Dublin Philosophical Magazine and Journal of Science*, 28(187) 121-137

Curtis, H. (2020) *Orbital Mechanics for Engineering Students*. Oxford: Butterworth-Heinemann

Davis, B., and Brewer, S. (2008) Orbital forcing and role of the latitudinal insolation/temperature gradient. *Climate Dynamics*, 32(2) 143-165

De Rosa, R., and Kalas, P. (2019) A Near-coplanar Stellar Flyby of the Planet Host Star HD 10690. *The Astronomical Journal*, 157(3) 125

D'Onghia, E., Vogelsberger, M., Faucher-Giguere, C.-A., and Hernquist, L. (2010) Quasi-Resonant Theory of Tidal Interactions. *The Astronomical Journal*, 725(1) 353-368

Dvorak, R., and Lhotka, C. (2013) *Celestial Dynamics: Chaoticity and Dynamics of Celestial Systems*. New Jersey (USA): Wiley and Sons

Fisher, D., and Erickson, R. (2010) *The Solar System*. Pasadena (USA): Salem Press

Forgan, D. (2016) Milankovitch Cycles of Terrestrial Planets in Binary Star Systems. *Monthly Notices of the Royal Astronomical Society*, 463(3) stw2098

Franklin, F., and Soper, P. (2003) Some effects of mean motion resonance passage on the relative migration of Jupiter and Saturn. *The Astronomical Journal*, 125, 2678-2691

Froeschle, C., and Morbidelli, A. (1993) The Secular Resonances in the Solar System. In: *Asteroids, Comets, Meteors 1993 - Proceedings of the 160th Symposium of the International Astronomical Union*, Belgirate, Italy, 14-18 June. Dordrecht (Netherlands): Springer, 189-204. Available from https://link.springer.com/chapter/10.1007/978-94-011-1148-5_14#citeas [accessed 03/07/2020].

Gale, A., Hardenbol, J., Hathway, B., Kennedy, W., Young, J., and Phansalkar, V. (2002) Global correlation of Cenomanian (Upper Cretaceous) sequences: Evidence for Milankovitch control on sea level. *Geology*, 30(4) 291-294

García-Sánchez, J., Weissman, P., Preston, R., Jones, D., Lestrade, J., Latham, D., Stefanik, R. and Paredes, J. (2001) Stellar encounters with the solar system. *Astronomy & Astrophysics*, 379, 634-659

Gillman, M., and Erenler, H. (2008) The galactic cycle of extinction. *International Journal of Astrobiology*, 7(1) 17-26

Gillman, M., Erenler, H. and Sutton, P. (2018) Mapping the location of terrestrial impacts and extinctions onto the spiral arm structure of the Milky Way. *International Journal of Astrobiology*, 18(4) 323-328

Giorgini, J. D., and JPL Solar Systems Dynamic Group (2020) *NASA/JPL Horizons On-Line Ephemeris System*. California (USA): NASA. Available from https://ssd.jpl.nasa.gov/?horizons_doc#acknowledge [accessed 21/05/2020].

Giorgini, J. D. (2015) *Adding particles using NASA JPL Horizons system (iPython)*. California (USA): NASA. Available from https://rebound.readthedocs.io/en/latest/ipython/Horizons.html [accessed 21/05/2020].

Gurfil, P. (2006) *Modern Astrodynamics*. Oxford: Butterworth-Heinemann

Hamilton, W. (1834) On a general method in dynamics. *Philosophical Transactions of the Royal Society*, 2, 247-308

Hays, J., Imbrie, J., and Shackleton, N. (1976) Variations in the Earth's Orbit: Pacemaker of the Ice Ages. *Science*, 194, 1121-1132

Heller, R., and Pudritz, R. (2015) The search for extraterrestrial intelligence in Earth's solar transit zone. *Astrobiology*, 16(4) 259-270

Hipparchus (130 BC) *On the displacement of the Solsticial and Equinoctial Points*. Greece: Hipparchus

Horner, J., Gilmore, J., and Waltham, D. (2017) The influence of Jupiter, Mars and Venus on Earth's orbital evolution. In: *Proceeding of the 15th Australian Space Research conference*, Canberra (Austrailia), 29 September - 01 October. : , 81-100. Available from https://arxiv.org/abs/1708.03448 [accessed 13/07/2020].

Huybers, P., and Aharonson, O. (2010) Orbital tuning, eccentricity, and the frequency modulation of climatic precession. *Paleoceanography and Paleoclimatology*, 25(4) PA4228

Hyde, G., and Bargellini, P. (2002) *Reference Data for Engineers*. Oxford: Butterworth-Heinemann

Imbrie, J., Berger, A., Boyle, E., Clemens, S., Duffy, A., Howard, W., Kukla, G., Kutzbach, J., Martinson, D., McIntyre, A., Mix, A., Molfino, B., Morley, J., Peterson, L., Pisias, N., Prell, W., Raymo, M., Shackleton, N., and Toggweiler, J. (1992) On the structure and origin of major glaciation cycles. *Paleoceanography and Paleoclimatology*, 8(6) 699-735

Iyengar, S., and Jain, R. (2009) *Numerical Methods*. New Delhi (India): New Age International

Kaiho, K., and Oshima, N. (2007) Site of asteroid impact changed the history of life on Earth: the low probability of mass extinction. *Scientific Reports*, 7, 14855

Jiménez-Torres, J. J., Pichardo, B., Lake, G., and Throop, H. (2011) Effect of different stellar galactic environments on planetary discs – I. The solar neighbourhood and the birth cloud of the Sun. *Monthly Notices of the Royal Astronomical Society*, 418(2) 1272-1284

Kent, D., Olsen, P., Rasmussen, C., Lepre, C., Mundil, R., Irmis, R., Gehrels, G., Giesler, D., Geissman, J., and Parker, W. (2018) Empirical evidence for a stable 405 kiloyear Jupiter-Venus eccentricity climate cycle as a framework for an accurate chronostratigraphy for the Mesozoic and Cenozoic. *Proceeding of the National Academy of Sciences of the United States of America*, 115(24) 6153-6158

Kepler, J. (1609) *Astronomia nova*. Prague: Pragae

Kepler, J. (1619) *Harmonices Mundi*. Prague (Czech Republic): Pragae

Kingston, J., Deino, A., Edgar, R., and Hill, A. (2007) Astronomically forced climate change in the Kenyan Rift Valley 2.7-2.55 Ma: implications for the evolution of early hominin ecosystems. *Journal of Human Evolution*, 53, 487-503

Kostadinov, T., and Gilb, R. (2014) Earth Orbit v2.1: a 3-D visualization and analysis model of Earth's orbit, Milankovitch cycles and insolation. *Geoscientific Model Development Discussions*, 6(4) 5947-5980

Kutterolf, S., Jegen, M., Mitrovica, J., Kwasnitschka, T., Freundt, A., and Huybers, P. (2013) A detection of Milankovitch frequencies in global volcanic activity. *Geology*, 41(2) 227-230

Laplace, P. (1798) Traité de mécanique céleste. Paris (France): De L'Imprimerie de Crapelet : Chez J.B.M. Duprat

Lari, G., Saillenfest, M., and Fenucci, M. (2020) Long-term evolution of the Galilean satellites: the capture of Callisto into resonance. *Astronomy & Astrophysics*, 639, A40

Laskar, J. (1990) The chaotic motion of the solar system: A numerical estimate of the size of the chaotic zones. *Icarus*, 88(2) 266-291

Laskar, J., Fienga, A., Gastineau, M., and Manche, H. (2010) La2010: a new orbital solution for the long-term motion of the Earth. *Astronomy & Astrophysics*, 532, A89

Laskar, J., Robutel P., Joutel, F., Gastineau, M., Correia, A., and Levrard, B. (2004) A long-term numerical solution for the insolation quantities of the Earth. *Astronomy & Astrophysics*, 428(1) 261-285

Laughlin, G., and Adams, F. (1999) Stability and Chaos in the υ Andromedae Planetary System. *The Astrophysical Journal*, 526(2) 881-889

Lin, C., and Shu, F. (1964) On the Spiral Structure of Disk Galaxies. *Astrophysical Journal*, 140, 646

Lisiecki, L. (2010) Links between eccentricity forcing and the 100,000-year glacial cycle. *Nature Geoscience*, 3, 349-352

Macdougall, D. (2011) *Milutin Milankovitch*. London: Encyclopedia Britannca. Available from https://www.britannica.com/biography/Milutin-Milankovitch [accessed 02/03/2020].

MacLeod, N. (2003) The causes of Phanerozoic extinctions. In: Rothschild, L., and Lister, A. (eds.) *Evolution of Planet Earth*. Oxford: Elsevier 253-277.

Malmberg, D., Davies, M., and Heggie, D. (2010) The effects of fly-bys on planetary systems. *Monthly Notices of the Royal Astronomical Society*, 411, 859-877

Mamajek, E., Barenfeld, S., Ivanov, V., Kniazev, A., Vaisanen, P., Beletsky, Y., and Boffin, H. (2015) The closest known flyby of a star to the solar system. *The Astrophysical Journal Letters*, 800(1) L17

Matthews, R., and Frohlich, C. (2002) Maximum flooding surfaces and sequence boundaries: comparisons between observations and orbital forcing in the Cretaceous and Jurassic (65-190 Ma). *GeoArabia*, 7(3) 503-538

Melott, A. L., Lieberman, B. S., Laird, C. M., Martin, L. D., Medvedev, M. V., Thomas, B. C., Cannizzo, J. K., Gehrels, N., and Jackman, C. H. (2004) Did a gamma-ray burst initiate the late Ordovician mass extinction?. *International Journal of Astrobiology*, 3(1) 55-61

Michtcheno, T., and Feraz-Mello, S. (2001) Resonant structures of the outer solar system in the neighbourhood of the planets. *The Astronomical Journal*, 122, 474-481

Mitrovica, J. X., and Forte, A. M. (1994) Pleistocene glaciation and the Earth's precession constant. *Geophysical Journal International*, 121(1) 21-32

Muller, R., and MacDonald, G. (1995) Glacial cycles and orbital inclination. *Nature*, 377, 107-108

Muller, R., and MacDonald, G. (1997) Spectrum of 100-kyr glacial cycle: Orbital inclination, not eccentricity. *Proceeding of the National Academy of Sciences of the United States of America*, 94(16) 8329-8334

Mustill, A. J., and Wyatt, M. C., (2010) A general model of resonance capture in planetary systems: first and second-order resonance. *Monthly Notices of the Royal Astronomical Society*, 413(1) 554-572

Newton, I. (1687) *Philosophiae Naturalis Pricipia Mathematica*. London: Benjamin Motte

Pälike, H. (2005) Orbital Variation (Including Milankovitch Cycles). In: Selley, R. C., Cocks, L. R. M., and Plimer, I. R. (eds.) *Encyclopedia of Geology*. Oxford: Elsevier 410-421.

Parker, M. (2017) *Digital signal processing 101*. Oxford: Newnes

Peters, S. (2008) Environmental determinants of extinction selectivity in the fossil record. *Nature*, 454, 626-629

Picogna, G., and Marzari, F. (2014) Effects of stellar flybys on planetary systems: 3D modeling of the circumstellar disk’s damping effects. *Astronomy & Astrophysics*, 564, A28

Puetz, S. J., Prokoph, A., and Borchardt, G. (2016) Evaluating alternatives to the Milankovicth theory. *Journal of Statistical Planning and Inference*, 170, 158-165

Rampino, M. (1998) The Galactic Theory of Mass Extinctions: An Update. *Celestial Mechanics and Dynamcial Astronomy*, 69, 49-58

Raymo, M., and Huyber, P. (2008) Unlocking the mysteries of the ice ages. *Nature*, 451, 284-285

Raymo, M., and Nisancioglu, K. (2003) The 41 kyr world: Milankovitch's other unsolved mystery. *Paleoceanography*, 18(1) 1011

Rein, H., and Liu, S.-F. (2012) REBOUND: an open-source multi-purpose N-body code for collisional dynamics. *Astronomy & Astrophysics*, 537, A128

Rein, H., and Spiegel, D. (2014) IAS15: A fast, adaptive, high-order integrator for gravitational dynamics, accurate to machine precision over a billion orbits. *Monthly Notices of the Royal Astronomical Society*, 446(2) 1424-1437

Rein, H., and Tamayo, D. (2015) WHFAST: a fast and unbiased implementation of a symplectic Wisdom–Holman integrator for long-term gravitational simulations. *Monthly Notices of the Royal Astronomical Society*, 452(1) 376-388

Rial, J., Oh, J., and Reischmann, E. (2013) Synchronization of the climate system to eccentricity forcing and the 100,000-year problem. *Nature Geoscience*, 6(4) 289-293

Roe, G. (2006) In defense of Milankovitch. *Geophysical Research Letters*, 33(24) L24703

Schorghofer, N. (2008) Temperature response of Mars to Milankovitch cycles. *Geophysical Research Letters*, 35(18) L18201

Šidlichovskỳ, M., and Nesornỳ, D. (1997) Frequency Modified Fourier Transform and its Application to Asteroids. *Celestial Mechanics and Dynamical Astronomy*, 65, 137-148.

Silburt, A., Rein, H., and Tamayo, D. (2016) HERMES: a hybrid for simulating close encounters and planetesimal migration [pre-print]. Available from https://silburt.github.io/files/HERMES.pdf [accessed 6 February 2020]

Souami, D., and Souchay, J. (2012) The solar system's invariable plane. *Astronomy & Astrophysics*, 543, A133

Sugden, D. (2013) James Croll (1821–1890): ice, ice ages and the Antarctic connection. *Antarctic Science*, 26(6) 604-613

Tesink, R. J. (2019) *Perturbation of the Oort Cloud by Close Stellar Encounter with Gliese 710*. Bachelors. University of Groningen. Available from http://fse.studenttheses.ub.rug.nl/20609/1/Oort_Cloud_disruption_by_close_stellar_encounters.pdf [accessed 23/03/2020].

van Dam, J. A., Aziz, H. A., Sierra, M. A. A., Hilgen, F. J., van den Hoek Ostende, L. W., Lourens, L. J., Mein, P., van der Meulen, A. J., and Pelaez-Campomanes, P. (2006) Long-period astronomical forcing of mammal turnover. *Nature*, 443, 687-691

Varadi, F. (1999) Periodic orbits in the 3:2 orbital resonance and their stability. *The Astronomical Journal*, 118, 2526-2531

Virtanen, P., Gommers, R., Oliphant, T. E., Haberland, M., Reddy, T., Cournapeau, D., Burovski, E., Peterson, P., Weckesser, W., Bright, J., van der Walt, S. J., Brett, M., Wilson, J., Millman, K. J., Mayorov, N., Nelson, A. R. J., Jones, E., Kern, R., Larson, E., Carey, CJ., Polat, İ., Feng, Y., Moore, E. W., VanderPlas, J., Laxalde, D., Perktold, J., Cimrman, R., Henriksen, I., Quintero, E. A., Harris, C. R., Archibald, A. M., Ribeiro, A. H., Pedregosa, F., van Mulbregt, P. and SciPy 1.0 Contributors. (2020) SciPy 1.0: Fundamental Algorithms for Scientific Computing in Python. *Nature Methods*, 17, 261-272

Winckler, G., Anderson, R. F., Stute, M., and Schlosser, P. (2004) Does interplanetary dust control 100 kyr glacial cycles? *Quaternary Science Reviews*, 23(18-19) 1873-1878

Wisdom, J., and Holman, M. (1991) Symplectic maps for the N-body problem. *The Astronomical Journal*, 102, 1528-1538

Yoshida, H. (1990) Construction of higher order symplectic integrators. *Physics Letter A*, 150(5-7) 262-268